

Pricing in Transition and Physical Risks: Carbon Premiums and Stranded Assets

Christoph Hambel^a Frederick van der Ploeg^b

Current version: June 2024

Abstract: We analyze asset pricing and climate policy in the face of transition and physical risks using a global two-sector, DSGE model of climate and the economy. Physical risks consist of temperature-related risks of recurring climate-related disasters and the risks of irreversible climate tipping. Transition risks consist of changes in policy regime with three states (no, modest, or aggressive carbon pricing) and of technological breakthroughs in negative emissions technologies. Both these type of risks affect the carbon price, the risk-free rate, and the risk premiums of green and brown assets. We find that carbon premiums result from policy transition risks, especially if the economy is still quite carbon-intensive and close to the temperature cap, and give a signal to accelerate the green transition. We also show that transition risks trigger asset stranding. The risks of asset stranding are also priced in and lead to more sizable carbon risk premiums and a more rapid green transition.

Keywords: carbon premium, stranded assets, transition risks, physical risks

JEL subject codes: D81, G01, G12, Q5, Q54

^a Tilburg University, Tilburg School of Economics and Management (TiSEM), Department of Econometrics and Operations Research, P.O. Box 90153, 5000 LE Tilburg, The Netherlands. E-mail: C.Hambel@tilburguniversity.edu. Also affiliated with Netspar.

^b University of Oxford, Department of Economics, OXCARRE, Manor Road Building, Oxford OX1 3UQ, U.K. Phone: +44 (0) 1865 281285. E-mail: rick.vanderploeg@economics.ox.ac.uk. Also affiliated with University of Amsterdam, P.O. Box 15551, 1001 NB Amsterdam, the Netherlands, CEPR, and CESifo.

Declarations of interest: none

Pricing in Transition and Physical Risks: Carbon Premiums and Stranded Assets

Current version: June 2024

Abstract: We analyze asset pricing and climate policy in the face of transition and physical risks using a global two-sector, DSGE model of climate and the economy. Physical risks consist of temperature-related risks of recurring climate-related disasters and the risks of irreversible climate tipping. Transition risks consist of changes in policy regime with three states (no, modest, or aggressive carbon pricing) and of technological breakthroughs in negative emissions technologies. Both these type of risks affect the carbon price, the risk-free rate, and the risk premiums of green and brown assets. We find that carbon premiums result from policy transition risks, especially if the economy is still quite carbon-intensive and close to the temperature cap, and give a signal to accelerate the green transition. We also show that transition risks trigger asset stranding. The risks of asset stranding are also priced in and lead to more sizable carbon risk premiums and a more rapid green transition.

Keywords: carbon premium, stranded assets, transition risks, physical risks

JEL subject codes: D81, G01, G12, Q5, Q54

1 Introduction

Central bankers, other policy makers, and investors are increasingly concerned about transition risks and physical risks related to global warming highlighted by the former Governor of the Bank of England on breaking the tragedy of the horizon (Carney, 2015).¹ Transition risks can originate from a sudden stepping up of climate policies, a breakthrough in green technologies, or a sudden shifts towards green consumer preferences (e.g. Campiglio and van der Ploeg, 2022).² Physical risks include the risks of extreme weather events (hurricanes, floods, droughts, etc.) and the risks of tipping the climate system (e.g., melting of the Greenland or Antarctic Ice Sheets, or melting of the Siberian permafrost).

Central bankers use scenarios developed by the Network for Greening the Financial System (NGFS) and conduct stress tests to see how robust the economy is to transition and physical risks.³ In contrast, we analyze the effects of transition and physical risks in a calibrated two-sector DSGE model of the economy and the climate, and allow for the effects of these risks on asset prices, carbon prices and the rest of the economy. We do not use ad hoc scenarios to capture transition and physical risks.⁴ Instead, we model transition risk by stochastic transitions between three different climate policy states (no, modest, and ambitious climate policies) and two technology states (competitive negative emissions technology or not) and model physical risk by stochastic transitions between three different climate tipping states and by the risk of climate-related extreme weather events.

Our objective is to investigate the implications of transition and physical risks on climate policies and financial markets, in particular on carbon premiums and the risk of stranded financial assets, and on the speed of the green transition. Our contributions are threefold.

First, we show that both types of physical risk significantly increase carbon pricing and the ambition of climate policies. If financial markets price in these risks, they increase the equity premium and curb the risk-free interest rate in line with the empirical findings of Bansal et al. (2017) and Donadelli et al. (2017). In contrast, transition risks (both political and the possibility of a technological breakthrough in negative emission technologies) imply that climate policies are on average less ambitious than the first-best optimal policies.

¹Witness the large number of central banks that have joined the Network for Greening the Financial System.

²Companies, investors, and regulators increasingly have to take account of how climate litigation, regulatory enforcement, and other legal action shifts or amplifies exposure to transition and physical risks, and thus leads to additional climate risk exposures (Wetzer et al., 2024). We abstract from such issues here.

³See <https://www.ngfs.net/ngfs-scenarios-portal/explore>.

⁴The NFGS has designed 7 scenarios: an ambitious net-zero by 2050 scenario that limits global warming to 1.5 °C through stringent climate policies and innovation; (ii) as (i) but through behavioral changes that lower energy demand; (iii) a scenario with a 67% change of keep temperature below °C; (iv) delayed transition so mitigation policies have to be much more aggressive from 2030 onwards to reach net-zero in 2050; (v) a scenario with all pledged policies even if not implemented; (vi) current policies with high physical risks; (vii) a fragmented world scenario.

Second, we show that these transition risks are at the root of positive carbon premiums. This might explain the empirical evidence for such premiums since 2015 by Bolton and Kacperczyk (2021, 2023).⁵ and for a wider set of pollutants by Hsu et al. (2023).⁶ We thus provide an explanation why risk premiums on carbon-intensive assets have been consistently higher than those on greener, more climate-friendly assets, and why the resulting carbon premiums speed up the green transition. Moreover, we provide a mechanism of how the risk of tightening climate policy affects the pricing of brown assets as documented by Bouman (2023) and Campos-Martins and Hendry (2023).⁷ The same mechanism leads political transition risk to increase the demand for precautionary savings and reduce the risk-free interest rate considerably if temperatures are close to two degrees.

Third, we show that if the carbon-intensive sector operates with only fossil fuel, the possibility of a long wait before existing policies switch to greener policies implies the risk of stranded financial assets.⁸ This occurs, since it is costly or impossible to shift around capital from brown industries to productive use elsewhere after the green transition. However, the brown sector will never disappear completely, because with negative emissions technology there is always the possibility that policy makers tip and become brown again. In fact, negative emissions counteract the risk of stranded assets. The risk of stranded assets leads to higher carbon prices, boosts the risk premiums of risky assets, and accelerates the green transition. The risk of stranding coal-related and other carbon-intensive assets is a real possibility if climate policy is stepped up or sudden technological or regulatory change takes place (e.g. Caldecott et al., 2016, 2021; Caldecott, 2018).

To establish these results, we specify a two-sector DSGE model of climate and the economy with fossil fuel, renewable energy, and a wide array of economic, climate, and damage risks (cf. Hambel et al., 2024). There is limited substitutability between the two types of energy. Investments and capital reallocation from the brown to the green capital stock are subject to intertemporal and intrasectoral adjustment costs. We abstract from directed technical change towards green technologies (e.g. Bovenberg and Smulders, 1996; Acemoglu et al., 2012; Casey, 2023), but instead we have learning by doing in renewables production which captures some features of directed technical change. Temperature is

⁵Similarly, Delis et al. (2019) have found that banks price in climate policy exposure, especially after 2015, and also charge higher loan rates to fossil fuel firms. Ivanov et al. (2023) show that high-emission firms face shorter loan maturities, lower access to permanent forms of bank financing, and higher interest rates. Others have found mixed or even contrary evidence and thus challenge the existence of carbon and pollution premiums (e.g. Pastor et al., 2021, 2022; Bauer et al., 2022; Ardia et al., 2023; Aswani et al., 2024; Zhang, 2024; Hambel and van der Sanden, 2024 among others). Bolton and Kacperczyk (2024) have given a robust defense of their results in response to Aswani et al. (2024). However, Zhang (2024) argue that emissions grow linearly with firm sales, data is only available to investors with significant lags, and the positive carbon premium arises from the forward-looking firm performance information contained in emissions rather than from risk premiums. They show that, after accounting for the data release lag, the carbon premium turns negative in the U.S. and is insignificant globally.

⁶Hsu et al. (2023) find an annual pollution premium of 4.42% and suggest that this may stem from environmental litigation.

⁷These studies extract climate news from newspapers using textual analysis and show how these news affect risk premiums in the U.S. equity and corporate bond markets.

⁸For a further discussion of the risk of stranded assets during the green transition, see, e.g., van der Ploeg and Rezai (2020), Campiglio and van der Ploeg (2022) and the references therein.

driven by cumulative emissions.⁹ We allow global warming to adversely affect output as in the seminal DICE model (e.g., Nordhaus, 2017), to increase the risk of recurring climate-related disasters (cf. Karydas and Xepapadeas, 2022; Hambel et al., 2024), and to increase the risk of (repeated) climate tipping (cf. Lemoine and Traeger, 2014, 2016; van der Ploeg and de Zeeuw, 2018; Cai and Lontzek, 2019). If policy makers undertake climate policies, they internalize these three externalities.

Our key novel feature is to allow for two types of *transition* risks and two types of *physical* risks. The first transition risk is technological and comes from the emergence of a negative emissions technology at an uncertain future date, and thus corresponds to 2 states.¹⁰ The second transition risk is due to changing policy regimes as we allow for the repeated tipping between three policy states corresponding to no, moderate, and strong carbon pricing, respectively. Our climate policy scenarios are calibrated to the range presented in Moore et al. (2022). We allow for the risk of climate tipping leading to upward jumps in the sensitivity of temperature to cumulative damages and in damages to aggregate production. This gives 3 climate states. We thus model technological, policy, and climate tipping by a three-dimensional Markov chain with $2 \times 3 \times 3 = 18$ states, where policy tipping is reversible as it can also go back from more ambitious to less ambitious policies, or to no climate policies. We also allow for a second type of physical risk, i.e. the temperature-related increase in extreme weather events. We extend Cai and Lontzek (2019), who focus on climate tipping only with a one-sector DSGE model, by allowing for brown and green capital stocks and for two types of transition risks as well as the recurring risk of extreme weather events in a two-sector DSGE model of climate and the economy.

While the effect of climate tipping points and feedback loops in the temperature dynamics on the social cost of carbon has been studied (e.g. Lemoine and Traeger, 2014, 2016, Cai et al., 2016; Cai and Lontzek, 2019; Hambel et al., 2021a), these studies are silent about the influence of physical climate risk on financial markets. We show how those risks are priced in by financial markets, and lead to higher risk premiums and an increased demand for precautionary savings curbing the risk-free interest rate.¹¹

Although Hsu et al. (2023) formulates a reduced-form model of transition risk, Barnett (2023) is perhaps most closely related. It investigates transition risk within the context of a DSGE model but we allow for a richer structure and interactions between climate tipping risk, political risk, and risk of a technological breakthrough, and the possibility of one tip setting in motion another, different type of tip ("cascading"). We have 18 Markov states rather than 2. We allow for the emergence of a negative

⁹See Matthews et al. (2009), Allen et al. (2009), IPCC (2014), van der Ploeg (2018), and Dietz and Venmans (2019), among others, for a discussion and justification of this approach.

¹⁰Negative emissions technologies such as direct air capture and storage are not yet competitive as their current marginal removal costs exceed by far current carbon prices (e.g., Rebonato et al., 2023). Technological breakthroughs can make those technologies competitive and allow removal of carbon dioxide from the atmosphere. Those technologies are essential for the target of net-zero emissions.

¹¹In contrast to Kelly and Kolstad (1999), Kelly and Tan (2015), and Gerlagh and Liski (2018), we abstract from learning about climate parameters.

emissions technology, essential for a serious story of the green transition, and for imperfect substitution between the energy types and intra-sectoral adjustment costs which allow us to study stranded assets. In contrast to Barnett (2023), we allow for repeated climate tipping points, temperature-related risks of recurring climate-related disasters, and exogenous risks of recurring Barro-style macro disasters.

Our model explains three types of climate-related risk premiums in equity markets. First, we provide a mechanism for a *temperature risk premium* in the spirit of Bansal et al. (2017), Donadelli et al. (2017), Hong et al. (2019), and Gregory (2024). In line with those empirical results, we find that global warming carries a positive risk premium that is rooted in physical climate risk and increases in the level of temperature. Second, our model can explain the existence of a *transition risk premium* in the spirit of Engle et al. (2020) and Faccini et al. (2023). In particular, we show how political risk drives the risk premiums of both green and brown assets. The effect of transition risk on asset markets is particularly pronounced when tightening climate policy could weight down the economy, i.e. when the share of brown capital is relatively high. Third, although both types of risky assets carry this risk premium, the brown asset is stronger affected than the green asset. This asymmetry is in line with Bolton and Kacperczyk (2021, 2023) and Hsu et al. (2023). Thus, our analysis also sheds light on the *carbon premium* or *pollution premium*.

Section 2 presents our DSGE model of climate and the economy. Section 3 explains how we solve and optimize our model. Section 4 presents the calibration. Section 5 provides our benchmark results on carbon pricing, carbon premiums, and the green transition. Section 6 show how transition risks might affect the risk of stranded assets. Section 7 concludes.¹²

2 A DSGE Model of Climate and the Economy

We present a stochastic, dynamic two-sector production economy with endogenous growth and recursive preferences. Global warming adversely affects production and increases the recurring risk of climate-related disasters and the risk of irreversible climate tipping. We also allow for the possibility of technological breakthroughs. We first discuss the economic part, then the climate part, and finally the various policy transition scenarios and disruptive changes resulting from climate, technological, and political tipping points. Those disruptive changes are modeled by a three-dimensional Markov chain \mathbf{X} , which is described in detail in Section 2.4.

¹²Proofs, the numerical solution algorithm, calibration details, and further simulation results and robustness checks are presented in the appendices.

2.1 Economic Part

Production of Green and Brown Goods Final goods are produced in two sectors. Total output is the sum of outputs produced in the two sectors, $Y = Y_1 + Y_2$.¹³ Outputs of both sectors $n \in \{1, 2\}$ follow from the Cobb-Douglas production functions

$$Y_n = A_n K_n^{1-\eta_n} E_n^{\eta_n} \Lambda_n(T, \mathbf{X}), \quad (2.1)$$

where K_n is the capital stock of sector n and E_n is an energy composite consisting of renewable energy and fossil fuel.¹⁴ The Cobb-Douglas weight $0 < \eta_n < 1$ and total factor productivity $A_n > 0$ are sector-specific constants. Here, T denotes global mean temperature relative to the beginning of the industrial revolution. Following Cai and Lontzek (2019), mean temperature and the climate tipping state affect the sectors of the economy negatively via

$$\Lambda_n(T, \mathbf{X}) = \frac{1 - d(\mathbf{X})}{1 + \theta_n T^2}, \quad (2.2)$$

where the function d increases in the climate tipping state. In line with Golosov et al. (2014), E_n is an energy composite modeled by a CES aggregate,

$$E_n = \left(\kappa_{1,n} G_n^{\rho_n} + \kappa_{2,n} F_n^{\rho_n} \right)^{\frac{1}{\rho_n}}, \quad (2.3)$$

where $\kappa_{i,n} \geq 0$ and $\rho_n < 1$ may be positive or negative. Here G_n and F_n denote renewable (or green) energy and fossil fuel use in sector n , respectively, and are imperfect substitutes. The elasticity of substitution between the two energy sources in sector n is $\zeta_n = \frac{1}{1-\rho_n}$. We suppose that the second sector relies significantly more on fossil fuel use than the first sector. We thus refer to the first sector ($n = 1$) as *green* and to the second sector ($n = 2$) as *brown*.

Dynamics of Green and Brown Capital Let I_n be the investment rate in sector n and R the rate at which brown capital can be converted into green capital. Investment is subject to quadratic intertemporal adjustment costs (cf. Pindyck and Wang, 2013). The conversion of brown into green capital incurs quadratic intrasectoral adjustment costs. One dollar of brown capital can thus be converted into less than one dollar of green capital where the wedge increases in the amount being converted. The depre-

¹³We have perfect substitution between the two outputs, but it is easy to have imperfect substitution (Hambel et al., 2024). This does not change the qualitative nature of the results much.

¹⁴There is an additional production factor, i.e. labour, which is subsumed in total factor productivity A_n . This production function allows for endogenous technical change, since the Cobb-Douglas weights add up to one.

ciation rates of the physical capital stocks are $\delta_n^k \geq 0$, $n \in \{1, 2\}$. The capital stock dynamics of the green and brown sector are then

$$\begin{aligned} dK_1 &= \left(I_1 - \frac{1}{2} \varphi_1 \frac{I_1^2}{K_1} + R - \frac{1}{2} \kappa \frac{R^2}{K_1} - \delta_1^k K_1 \right) dt + K_1 \sigma_1 dW_1 - \sum_{i=c,e} K_1 - \ell_i dN_i \\ dK_2 &= \left(I_2 - \frac{1}{2} \varphi_2 \frac{I_2^2}{K_2} - R - \delta_2^k K_2 \right) dt + K_2 \sigma_2 \left(\rho_{12} dW_1 + \sqrt{1 - \rho_{12}^2} dW_2 \right) - \sum_{i=c,e} K_2 - \ell_i dN_i \end{aligned} \quad (2.4)$$

where $\varphi_n > 0$, $n = 1, 2$, are the investment adjustment cost parameters, $\kappa > 0$ the capital reallocation cost parameter, and W_1 and W_2 two independent Brownian motions. The parameter ρ_{12} denotes the instantaneous diffusive correlation coefficient between the Brownian shocks of the two capital stocks. The processes N_i , $i \in \{c, e\}$ are independent point processes modeling macroeconomic disasters and climate-related disasters (e.g. extreme weather events), respectively. The disaster intensity of macroeconomic disasters λ_e is constant (Barro, 2006, 2009; Barro and Jin, 2011). The disaster intensity of climate-related disasters $\lambda_c(T)$ increases in temperature (Hambel et al., 2024). The probability for a jump to occur over a small time interval dt is $\lambda_i dt$ and the expected waiting time to the next jump is $1/\lambda_i$. The parameter ℓ_i denotes the corresponding jump size which is drawn from an i.i.d. process, but independent of the Brownian and Poisson shocks in the model. The corresponding recovery rate is denoted by $Z_i = 1 - \ell_i$. We suppose that the jump sizes are the same for both types of capital.¹⁵

The total stock of capital is defined by $K \equiv K_1 + K_2$ and the share of brown capital by $S \equiv \frac{K_2}{K_1 + K_2}$. The dynamics of K and S are discussed in Appendix A.3.

Equilibrium Conditions The amount of consumption goods provided by each sector is the cash flow net of investments, energy costs, and costs of negative emissions technology,

$$C_n = Y_n - I_n - b_g G_n - b_f F_n - \zeta_n b_d(S, \mathbf{X}, D, K), \quad (2.5)$$

where $b_g = b_g(S)$ denotes the real price of one unit of green energy and $b_f = b_f(S)$ the real price of one unit of fossil fuel. We suppose that over time green energy becomes more competitive, so that b_g decreases in the share of green capital $1 - S$.¹⁶ The technology for producing fossil fuel is more likely to be mature, so that b_f does not depend on S .

¹⁵Since this disaster shock affects both types of capital, it significantly increases the total correlation between the capital stocks; see Hambel et al. (2024). Besides, we can allow for different jump sizes for the sectors.

¹⁶One way of justifying this is Wright's law, which states that unit production costs of solar panels, wind mills, and batteries decline as more of these have been used in the past. This captures learning by doing.

Negative Emissions Rechnology A competitive negative emission technology, such as direct air carbon capture and storage (DACCS), that extracts CO₂ from the atmosphere at low marginal costs, may eventually emerge. We model such a technological breakthrough as an irreversible technological tipping point. The cost of removing an amount D of CO₂ from the atmosphere is $b_d = b_d(S, \mathbf{X}, D, K)$ and depends on the share of brown capital. These costs are homogeneous of degree one in capital and marginal removal costs $\frac{\partial b_d}{\partial D}$ are strictly positive for every level D (cf. Rebonato et al., 2023). The term $\varsigma_n = \varsigma_n(S)$ models a cost-sharing mechanism by which the total removal costs are divided between the two sectors, so that $\varsigma_1 + \varsigma_2 = 1$.¹⁷ Without a technological breakthrough modeled by the two-state Markov chain X^t , this technology is not yet competitive and plays only a negligible role and $D = 0$. We then have $X^t = 1$, while if the breakthrough in negative emissions technology has taken place we have $X^t = 2$.

Aggregate Consumption Consumption goods are perfect substitutes, so that aggregate consumption is $C = C_1 + C_2$. Our analysis would also work for imperfect substitutes (e.g., if aggregate consumption is a CES aggregate of the consumption goods produced in each sector). To focus on the novel implications of transition risks on carbon prices, asset prices, and the green transition, we keep the setting simple and consider the special case of perfect substitutes.

Recursive Preferences Our economy has identical agents with recursive preferences. As shown in Duffie and Epstein (1992b), these preferences are the continuous-time version of discrete-time recursive utility (Kreps and Porteus, 1978; Epstein and Zin, 1989). The coefficient γ of relative risk aversion (RRA) can be chosen independently of the elasticity of intertemporal substitution (EIS), ψ . The value function (or indirect utility function) of the representative household J is recursively defined by

$$J(t, K_1, K_2, T, \mathbf{X}) = \sup_{D, F_n, G_n, I_n, R} \mathbb{E}_t \left[\int_t^\infty f(C_s, J(s, K_{1s}, K_{2s}, T_s, \mathbf{X}_s)) ds \right], \quad (2.6)$$

where f is the aggregator function determining preferences. For relative risk aversion $\gamma \neq 1$ and elasticity of intertemporal substitution ψ , this aggregator function has the form

$$f(C, J) = \begin{cases} \delta \theta J \left[\frac{C^{1-1/\psi}}{[(1-\gamma)J]^{1/\theta}} - 1 \right], & \psi \neq 1, \\ \delta(1-\gamma)J \ln \left(\frac{C}{[(1-\gamma)J]^{1-\gamma}} \right), & \psi = 1, \end{cases}$$

where $\theta = \frac{1-\gamma}{1-1/\psi}$ and $\delta > 0$ is the rate of time impatience. Notice that f depends on the value function J , which reflects the recursive structure of the preferences. Relative risk aversion typically exceeds $1/\psi$,

¹⁷In our calibrated model, $\varsigma_1 = 1 - S$ and $\varsigma_2 = S$, but a more general case is given in Proposition A.1.

which reflects preference for early resolution of uncertainty. For $\gamma = 1/\psi$, i.e. $\theta = 1$, preferences collapse to time-additive CRRA utility with $J_t = \int_t^\infty e^{-\delta(s-t)} \frac{C_s^{1-\gamma}}{1-\gamma} ds$.

Dividends Empirically, dividends are more volatile than consumption (e.g. Bansal and Yaron, 2004) and much more so if a disaster hits the economy (Longstaff and Piazzesi, 2004; Wachter, 2013). This is because dividends are only a small part of household income, while labour income is the largest part of household income is much less volatile than dividends. Following Wachter (2013), among others, we thus model dividends as leveraged consumption, $\mathcal{D}_n = C_n^\phi$ with leverage parameter $\phi > 1$, common for both sectors.¹⁸

2.2 Climate Part

Following Allen et al. (2009), Matthews et al. (2009), and IPCC (2014), global mean temperature T rises in cumulative net emissions $\mathcal{E}_t = \int_0^t E_s^{net} ds$ measured in gigatons of carbon (GtCs),

$$dT = \vartheta E^{net} dt + \sigma_T dW_3, \quad (2.7)$$

where $\vartheta = \vartheta(\mathbf{X})$ denotes the transient climate response to cumulative emissions (TCRE) and W_3 denotes a third standard Wiener process that is independent of W_1, W_2, N^c, N^e , and \mathbf{X} to allow for regular shocks to the climate system. In line with Cai and Lontzek (2019), the Earth's climate system is also exposed to tipping risk modeled by the Markov chain X^c . These climate tipping points irreversibly affect the future evolution of the climate system by increasing the TCRE, $\vartheta(\mathbf{X})$, and also affect output damages from climate change.¹⁹ The temperature diffusion coefficient, σ_T , is constant and captures remaining uncertainty in the climate system.

Gross emissions are $\nu(F_1 + F_2)$, where F_n denotes fossil fuel use in sector n ,²⁰ and the emission intensity per unit of fossil fuel use, denoted by ν , evolves according to

$$d\nu = \nu_- \left[g_\nu dt - \frac{dK}{K_-} \right]. \quad (2.8)$$

¹⁸An alternative to this approach is modelling the consumption-dividend ratio as a stationary but persistent process (e.g. Longstaff and Piazzesi, 2004). In order to focus on the novel implications of climate transition risk on asset prices, we keep the setting simple although following this approach would also be feasible in our setting. A more rigorous approach where capital is owned by intermediaries who issue stocks and pay dividends to households is beyond the scope of this paper.

¹⁹An example is the melting of permafrost soils in the Siberian tundra, which is the largest methane reservoir in the Earth. Such a tipping event is irreversible because, for example, the methane cannot be restored once it has been released. Other examples are melting of the Greenland or Antarctic Ice Sheet or dieback of the Amazon rain forest (cf. Cai et al., 2016).

²⁰We model fossil fuel as an inexhaustible resource. To test whether exhaustibility matters for our policy simulations, we have studied a model variant that takes account of the constraint $\int_0^t E_s^{ind} ds \leq \bar{E}$, where \bar{E} denotes the maximum amount of total carbon emissions if all fossil fuel resources were to be exploited. We find that this constraint is not binding if \bar{E} is set in line with recent estimates on exhaustible fossil fuel resources, 11,000GtCO₂ or 3,000GtC (McGlade and Ekins, 2015).

If g_v is smaller than the expected economic growth rate, the emission intensity declines in expectation but it might be state-dependent. Net emissions are gross emissions reduced by the amount of CO₂ extracted from the atmosphere if the negative emission technology is available, $E^{net} = v(F_1 + F_2) - D$. Hence, the temperature dynamics becomes

$$dT = \vartheta[v(F_1 + F_2) - D]dt + \sigma_T dW_3. \quad (2.9)$$

2.3 Policy Tipping

The third Markov chain X^P models different policy scenarios. While climate tipping and technological breakthroughs are irreversible, policy shocks are reversible due to political regime changes. For example, the election of a new government that takes climate change less seriously than its predecessor can at a later time be replaced by a government with more climate ambition. We focus on three policy states of the Markov chain:

- (i) *No climate policies* (BAU): In this business-as-usual (BAU) state ($X^P = 1$), policy makers are climate change deniers and ignore the adverse impacts of climate change on the economy, so do not implement a carbon tax. Global warming damages are not internalized by policy makers but financial markets do price in physical and transitions risks.
- (ii) *Modest climate policies* (PIGOU): In this state ($X^P = 2$), policy makers levy an optimal carbon tax, which is set to the social cost of carbon or SCC and internalizes all three externalities resulting from the adverse effect of global warming on aggregate production, the risk of climate-related disasters, and the risks of climate tipping.
- (iii) *Ambitious climate policies* (CAP): In this state ($X^P = 3$), there is in addition a legally binding carbon budget constraint to ensure that temperature stays below a pre-specified cap T_{cap} of a two-degrees target, $T_{cap} = 2^\circ\text{C}$, in accordance with the Paris agreement (cf. United Nations, 2015). If the cap (CAP) is exceeded, a binding constraint comes into force so that fossil fuels cannot be burnt anymore: $F_{1,t} = F_{2,t} = 0$ if $T_t > T_{cap}$. If this constraint bites, carbon prices will exceed the Pigouvian carbon prices.

A transition from one policy regime to another arises when a policy maker changes its climate ambition or when there is a change of policy makers (e.g., due to an election). Financial markets anticipate transition risks as well as physical risks and technological risks. Asset prices reflect transition risks even if society is still in the BAU state. Starting in the BAU state also implies that society faces and internalizes the economic costs of delaying climate action, which lead to more stringent policies as soon

as the government starts internalizing global warming externalities or as a legally binding temperature cap comes into force. These costs of delaying climate policies are priced in and thus affect asset returns.

2.4 Full Markov Chain for Disruptive Changes

Our framework is rich enough to model disruptive changes to a broad range of input parameters and political scenarios, but we focus on three dimensions. First, the Earth’s climate system is affected by two irreversible climate tipping points and modeled by a directed Markov chain X^c with 3 states (cf. Cai et al., 2016). Second, an irreversible technological breakthrough in negative emission technologies (e.g. direct air capture and storage to remove CO₂ from the atmosphere) is modeled by X^t tipping from state 1 to state 2. Third, the political regime switches are modeled by the non-directed Markov chain X^p . The political regime can thus shift to and from each of three states: no, modest, or ambitious climate policies.²¹ The sudden shocks to the political landscape, the Earth’s climate system, and negative emissions technology are summarized by the 3-dimensional Markov chain $\mathbf{X} = (X^c, X^t, X^p)$ with 18 different states in $\mathcal{X} = \{1, 2, 3\} \times \{1, 2\} \times \{1, 2, 3\}$ as illustrated in Figure 1. The transition intensity of jumping from state $i \in \mathcal{X}$ to state $j \in \mathcal{X}$ is endogenous and modeled by the sufficiently smooth non-negative function $\lambda_x(\mathbf{S}, i, j)$, where \mathbf{S} denotes the vector of all state variables in the economy.²²

3 Carbon Taxes, Negative Emissions, and Asset Returns

In both the modest (PIGOU) and ambitious (CAP) policy scenarios, welfare (2.6) is optimized subject to the constraints of our DSGE model of the climate and the economy. The only difference between the modest and ambitious policy scenario is that in the latter there is an additional constraint on cumulative emissions to take account of. The no policy (BAU) scenario also requires solving a stochastic dynamic optimization problem where no account is taken of the adverse effects of temperature on the economy and on the risk of climate-related disasters or climate tipping points. Once this optimization is done, these adverse effects do impinge on the economy and private agents take account of this.

The numerical algorithm that we use to solve our dynamic programming problems is discussed in Appendix A. The value function must satisfy the Hamilton-Jacobi-Bellman equation (A.1). Under some very mild assumptions, it can be expressed as $J(t, K_1, K_2, T, \mathbf{X}) = \frac{1}{1-\gamma} K^{1-\gamma} V(t, T, S(K_1, K_2), \mathbf{X})$, where

²¹We can easily allow for more states in each of these layers. For instance, a model extension with more climate tipping elements or several intermediate states between BAU and PIGOU, in which an increasing proportion of carbon dioxide emissions is taxed, can be implemented, but we keep this simple structure for ease of exposition.

²²We also denote the transition intensities of X^ℓ by $\lambda_\ell(\mathbf{S}, i, j)$, where ℓ equals c , t , or p , respectively. To keep the mechanisms transparent, we assume that the jump intensity $\lambda_\ell(\mathbf{S}, i, j)$ of a component X^ℓ does not explicitly depend on the other components. We therefore have no direct domino effects of the entire chain, but we do have the indirect effect, since the jump intensities depend on the common factors S and T .

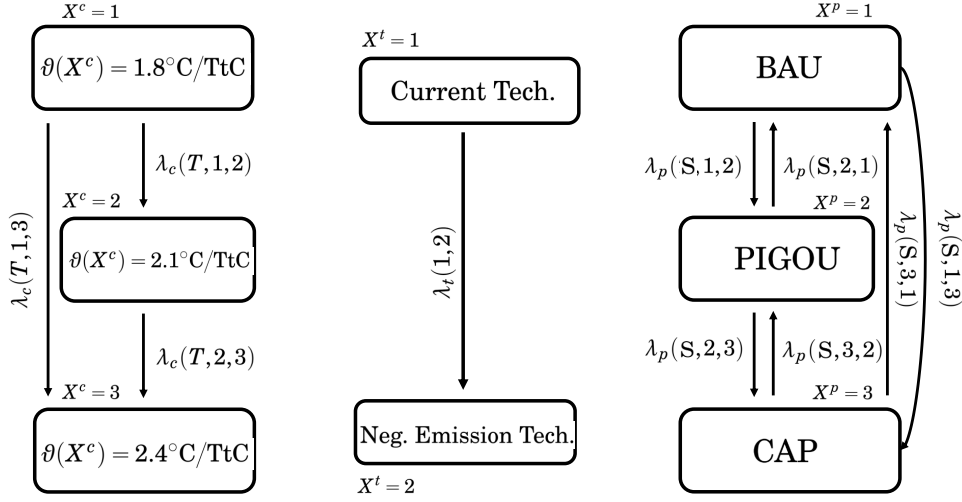


Figure 1: Structure of the Markov Chains. The Markov system consists of a three-dimensional Markov chain $\mathbf{X} = (X^c, X^t, X^p)$ with three states for climate tipping points $X^c \in \{1, 2, 3\}$, two technological states $X^t \in \{1, 2\}$ and three political states $X^p \in \{1, 2, 3\}$. Jump intensities between two states may explicitly depend on the share of brown capital and temperature. The states from the different chains can link together in 18 different combinations.

$S = S(K_1, K_2) \equiv \frac{K_2}{K_1 + K_2}$, $K \equiv K_1 + K_2$, and $V = V(t, T, S, \mathbf{X})$ satisfies the simpler and easier-to-solve Hamilton-Jacobi-Bellman equation (A.12).

Social Cost of Carbon The SCC, the expected present discounted value of all present and future negative effects of emitting one ton of CO_2 , is

$$\tau = -\frac{\partial(\mathbf{X})J_T}{f_c(C, J)} = \frac{\partial(\mathbf{X})c^{1/\psi}}{\delta(\gamma - 1)} \frac{V_T}{V^{1-1/\theta}} K > 0 \quad (3.1)$$

(see Appendix A.2). The SCC is proportional to the total stock of capital as marginal damages are proportional to aggregate economic activity (e.g., Nordhaus, 1991; Golosov et al., 2014; van den Bijgaart et al., 2016; Rezai and van der Ploeg, 2016; Hambel et al., 2021b). Notice that if the political state is BAU rather than PIGOU or CAP, the SCC can be computed too but there is no carbon price that is implemented by policy makers.

Negative Emissions The optimality condition for carbon removal is

$$\frac{\partial b_d(S, \mathbf{X}, D, K)}{\partial D} \geq \tau, \quad D \geq 0, \quad c.s. \quad (3.2)$$

(see Appendix A.2). The economy does not extract carbon from the atmosphere, $D = 0$, if the marginal cost of extraction exceeds the marginal benefit (i.e. the SCC). As soon as, negative emissions technology has become competitive, the marginal cost equals the SCC and $D > 0$.

Risk-free Rate and Precautionary Savings In equilibrium the risk-free rate r^f is²³

$$\begin{aligned}
r_t^f = & \underbrace{\delta}_{\text{Discounting}} + \underbrace{\frac{1}{\psi}\mu_C}_{\text{Smoothing}} - \underbrace{\frac{1}{2}\gamma\left(1 + \frac{1}{\psi}\right)\|\sigma_C\|^2}_{\text{Standard Diffusion Risk}} - \underbrace{\sum_{i=c,e} \lambda_i(T)\mathbb{E}\left[Z_i^{-\gamma} - 1 + \frac{\theta-1}{\theta}(1 - Z_i^{1-\gamma})\right]}_{\text{Macroeconomic and Climate-related Disaster Risk}} \\
& + \underbrace{\frac{\gamma\psi-1}{2\psi^2}\left(\|\sigma_C - \sigma_k\|^2 + \psi(\|\sigma_C\|^2 - \|\sigma_k\|^2)\right) + \frac{\theta-1}{\theta\psi}\sigma_g^\top(\sigma_C - \sigma_k)}_{\text{Temperature Interaction Risk}} \\
& - \underbrace{\sum_{x \neq \mathbf{X}} \lambda_x(\mathbf{S}, \mathbf{X}, x)\left[(1 - j_v^x)^{1-1/\theta}(1 - j_c^x)^{-1/\psi} - 1 + \frac{\theta-1}{\theta}j_v^x\right]}_{\text{Tipping and Transition Risk}}
\end{aligned} \tag{3.3}$$

Equation (3.3) decomposes the risk-free interest rate (cf. Barro, 2006, 2009; Pindyck and Wang, 2013; Wachter, 2013). It extends the results in Hambel et al. (2024) to various types of climate-related tipping and transition risks. The first two terms in equation (3.3) also arise in deterministic models. If the time preference rate δ is high, there are strong preferences for early consumption and one would like to borrow. Since, in equilibrium, the risk-free asset is in zero net supply, the risk-free rate must increase to counter this. The risk-free rate also increases in expected consumption growth μ_C due to the preference for smooth consumption streams. This effect is bigger if it is more difficult to substitute present for future consumption (if the elasticity of intertemporal substitution ψ is small).

The third term $-\frac{1}{2}\gamma\left(1 + \frac{1}{\psi}\right)\|\sigma_C\|^2$ in equation (3.3) is negative and represents the motive for precautionary savings in response to diffusion risk, which requires the interest rate to fall to keep the risk-free asset in zero net supply. Expected consumption growth and its volatility depend non-linearly on both temperature and the brown capital share, whereby the result is more involved and qualitatively different from one-tree endowment economies. While the effect of temperature on the precautionary-savings term $-\frac{1}{2}\gamma\left(1 + \frac{1}{\psi}\right)\|\sigma_C\|^2$ is negligible, the share of brown capital has a significant influence on the equilibrium risk-free rate. The latter result stems from a diversification argument (cf. Cochrane et al., 2007; Hambel et al., 2024). Diversifying across the green and brown capital stocks reduces the volatility of the total capital stock and aggregate consumption, so that the need for precautionary saving falls.

The fourth term $-\sum_{i=c,e} \lambda_i(T)\mathbb{E}\left[Z_i^{-\gamma} - 1 + \frac{\psi^{-1}-\gamma}{1-\gamma}(1 - Z_i^{1-\gamma})\right]$ in (3.3) reflects precautionary savings in response to both macroeconomic and climate-related recurring disaster risks (denoted by subscripts e

²³Details on the derivation are in Appendix B.1, where we also derive the dynamics of the pricing kernel (B.6).

and c , respectively. As for standard diffusion risk, these terms reduce the interest rate to keep the risk-free asset in zero net supply. The greater the coefficient of relative risk aversion γ , the greater is this effect, see also the extensive discussion in Wachter (2013).

The terms in the second row in equation (3.3) capture the interdependence between capital, consumption, temperature, and the value function. They represent precautionary savings for uninsurable temperature risk. These components depend on the relevant state variables, in particular on temperature, in a nonlinear manner, but have little effect on the risk-free rate because consumption volatility σ_C is close to capital volatility σ_k . In case of time-additive CRRA-utility ($\gamma = 1/\psi$, $\theta = 1$), these terms vanish.

The last term in (3.3) reflects precautionary savings in response to the disruptive changes resulting from climate, technological, and political tipping. These terms have a similar structure as the precautionary savings terms for standard disaster risk and also lead to higher precautionary savings and curb the risk-free rate. While disaster risk affects the capital stock via the loss ℓ , these shocks affect utility and consumption via state-dependent terms j_v^x and j_c^x that measure the relative change in the indirect utility function and consumption rate, respectively, when the Markov chain jumps to state x .²⁴

In contrast to the well-established decompositions in the aforementioned literature, the risk-free interest rate (3.3) is not a continuous process because it depends on the current state of the Markov chain \mathbf{X} and thus reacts abruptly to climate tipping and transition risks. This novel feature can be seen from the precautionary savings term $-\sum_{x \neq \mathbf{X}} \lambda_x(\mathbf{S}, \mathbf{X}, x) [(1 - j_v^x)^{1-1/\theta} (1 - j_c^x)^{-1/\psi} - 1 + \frac{\theta-1}{\theta} j_v^x]$, which depends on \mathbf{X} . Moreover, the expected consumption growth rate μ_C also depends on \mathbf{X} . We perform an extensive quantitative analysis on how transition risks affect the risk-free rate in Section 5.3.

Asset Prices For the dividend stream $\mathcal{D}_n = C_n^\varphi$, the time- t ex-dividend price of asset n equals

$$P_{nt} = \mathbb{E}_t \left[\int_t^\infty \frac{H_s}{H_t} \mathcal{D}_{ns} ds \right], \quad (3.4)$$

where H_s denotes the pricing kernel for discounting from time s to time t (see (B.6)). Its equilibrium expected excess return corresponds to the risk premium of the asset. It is the sum of its expected ex-dividend stock return, μ_n^p , and the dividend yield, $y_n^d = \mathcal{D}_n/P_n$, minus the risk-free interest rate, r^f , so that $r_n^p = \mu_n^p + y_n^d - r^f$.²⁵ Finally, we define the carbon premium as the difference between the brown and green risk premiums, i.e. $r_2^p - r_1^p$.

²⁴These are computed numerically and are given in equations (B.3) and (B.5) of Appendix B.1.

²⁵The price-dividend ratio $\Pi_n = P_n/\mathcal{D}_n$ satisfies the parabolic partial differential equation (B.11), which we solve numerically (see Appendices B.3 and B.4).

4 Calibration

We first calibrate the economic part of our model by disregarding climate damages and tipping points to closely match the historical evolution of interest rates, expected asset returns, GDP growth, and the consumption-GDP ratio. We then calibrate the climate part of our model and damages in the pre-tipping state. Finally, we calibrate the Markov chains, which model disruptive changes stemming from tipping points in the climate system, negative emission technologies, and the political landscape.

Table 1 summarizes our benchmark calibration. Appendix C.1 discusses the details (macroeconomic uncertainty, economic growth, asset returns, energy consumption, energy intensity, temperature dynamics, and damages). Our calibration is market-based. We have learning by doing in the production of renewables as the unit production cost drops by 20% for every doubling of cumulative installed volume of renewables. The green sector does not fuse fossil fuel. The elasticity of substitution between the two energy types in the brown sector is $\zeta_2 = 2 > 1$. It is thus possible to *fully* replace fossil fuel by renewables. The initial share of brown capital is 87.6%. The calibrated emission intensity ν_t is deterministic and declines over time. Our transient climate response to cumulative emissions is $1.8^\circ\text{C}/\text{TtC}$.

Damage Specification We have a level impact and a climate-related disaster risk component. We adapt the damage function (2.2) from Cai and Lontzek (2019) but modify our damage parameter $\theta_n = 0.00236$ in line with the DICE model in the pre-tipping state (Nordhaus, 2017). Following the median damage scenario in Cai and Lontzek (2019), we set a post-tipping permanent damage of 5% of global output and 2.5% in the intermediate state: $d(X^c = 0) = 0$, $d(X^c = 1) = 0.025$, $d(X^c = 2) = 0.05$. We assume that the intensity of climate-related disasters rises linearly in temperature, so $\lambda_c(T) = \hat{\lambda}_c T$ with $\hat{\lambda}_c = 0.096$ and $\lambda_c(T_0) = 0.122$. The expected loss is $\mathbb{E}[\ell_c] = 1.5\%$ (cf. Karydas and Xepapadeas, 2022; Hambel et al., 2024), compared to 25% for economic disasters. Fitting a power distribution, we obtain $\alpha_c = 65.7$.²⁶ Climate-related disasters thus occur about twice as often as economic disasters but are less severe.

Table 2 summarizes the calibration of our three Markov chains with details in Appendix C.1.

Climate tipping The tip from a TCRE of 1.8 to $2.1^\circ\text{C}/\text{TtC}$ has an expected duration of 309 years if temperature remains fixed at $T_0 = 1.27^\circ\text{C}$ while the expected tip from a TCRE of 2.1 to $2.4^\circ\text{C}/\text{TtC}$ has an expected duration of 50 years. We thus allow for both imminent and slow tips of the climate system.

²⁶The intensity of climate-related disasters or their damage distribution may depend on the climate tipping state X^c . This generalizes Cai et al. (2016) and Cai and Lontzek (2019), and leads to qualitatively similar results.

Preferences			
δ	time-preference rate	calibrated (Appendix C.1)	0.0346
γ	relative risk aversion	calibrated (Appendix C.1)	2.977
ψ	elasticity of intertemp. substitution	Bansal and Yaron (2004)	1.5
Economic Model			
Y_0	initial GDP (trillion US \$)	Nordhaus (2017)	116
S_0	initial share of brown capital	from World Bank data (Footnote 43)	0.876
$K_{1,0}$	initial green capital (trillion US \$)	calibrated (Appendix C.1)	74.3
$K_{2,0}$	initial brown capital (trillion US \$)	calibrated (Appendix C.1)	1353.9
A_1	green productivity	calibrated (Appendix C.1)	0.3323
A_2	brown productivity	calibrated (Appendix C.1)	0.3451
φ_n	investment adjustment cost parameter	calibrated (Appendix C.1)	13.61
κ	capital reallocation cost parameter	calibrated to modified RCP8.5 (Section 4)	2
$b_{f,0}$	initial fossil fuel costs (\$ per tC)	Hambel et al. (2024)	540
$b_{g,0}$	initial renewable energy costs (\$ per etC)	Hambel et al. (2024)	810
k_0	cost function parameter	from Swanson's law (Footnote 41)	0.5107
k_1	cost function parameter	from Swanson's law (Footnote 41)	0.3219
η_n	energy share in production	van den Bremer and van der Ploeg (2021)	0.043
ζ_2	elasticity of energy substitution	Golosov et al. (2014)	2
$\kappa_{1,2}$	renewable energy weight in brown sector	Golosov et al. (2014)	0.356
$\kappa_{2,2}$	fossil fuel weight in brown sector	Golosov et al. (2014)	0.644
$\kappa_{1,1}$	renewable energy weight in green sector	assumption	1
$\kappa_{2,1}$	fossil fuel weight in green sector	assumption	0
ϕ	leverage parameter	Wachter (2013)	2.6
σ_n	annual capital volatility	Wachter (2013)	0.02
ρ_{12}	instantaneous correlation	Cochrane et al. (2007)	0
α_e	macroeconomic jump size parameter	calibrated in line with Wachter (2013)	5
λ_e	macroeconomic disaster intensity	calibrated in line with Wachter (2013)	0.06
Climate Model and Damages			
T_0	initial temperature ($^{\circ}\text{C}$)	temperature data	1.27
$\vartheta(\mathbf{X}_0)$	TCRE ($^{\circ}\text{C}/\text{TtC}$)	Hambel et al. (2024)	1.8
σ_T	annual temperature volatility	RCP data (Footnote 45)	0.033
θ_n	damage function parameter	Nordhaus (2017)	0.00236
α_c	climate disaster jump size parameter	Hambel et al. (2024)	65.7
$\hat{\lambda}_c$	marginal climate disaster intensity	Hambel et al. (2024)	0.096

Table 1: Benchmark Calibration. Preferences, the economy, the climate, and damages.

Irreversible Climate Tipping Risk		
TCRE	$\vartheta(X^c = 1) = 1.8, \vartheta(X^c = 2) = 2.1, \vartheta(X^c = 3) = 2.4$ $^{\circ}\text{C}/\text{TtC}$	from Allen et al. (2009)
Damage parameters	$d(X^c = 1) = 0, d(X^c = 2) = 0.025, d(X^c = 3) = 0.05$	cf. Cai and Lontzek (2019)
Intensity parameters	$\hat{\lambda}_c^{1,2} = 0.012, \hat{\lambda}_c^{1,3} = 0.012, \hat{\lambda}_c^{2,3} = 0.02$	cf. Cai and Lontzek (2019)
Breakthrough of Negative Emission Technology		
Cost function	$b_1 = 1.77 \cdot 10^{-4}, b_2 = 1.19 \cdot 10^{-5}, b_3 = 1$ $c_1 = 0.34, c_2 = 0.03, c_3 = 0.34, \zeta = 0.1$	from Rebonato et al. (2023) Appendix C.2, Footnote 27
Intensity parameter	$\hat{\lambda}_t^{1,2} = 0.0224$	assumed
Political Transition Risks		
Intensity parameters	$\hat{\lambda}_p^{1,2} = 0.12, \hat{\lambda}_p^{1,3} = 0.05, \hat{\lambda}_p^{2,3} = 0.05, \hat{\mu} = 0.75$ $\hat{\lambda}_p^{2,1} = 0.12, \hat{\lambda}_p^{3,1} = 0.06, \hat{\lambda}_p^{3,2} = 0.10$	using Moore et al. (2022)

Table 2: Benchmark Calibration of the Markov chain $\mathbf{X} = (X^c, X^t, X^p)$.

Technological Tipping The cost of the negative emission technology once it has become available is proportional to the capital stock, $b_d(S, \mathbf{X}, D, K) = \tilde{b}_d(S, \mathbf{X}, D)K$ with

$$\tilde{b}_d(S, \mathbf{X}, D) = \mathbb{1}_{\{D > 0\}} [a_1(S)D + a_2(S) \exp(a_3(S)D)],$$

where a_j are truncated power functions of the form $a_j(S) = b_j \max(\zeta, S)^{c_j}$, $j \in \{1, 2, 3\}$. This mimics the exponential marginal cost structure of Rebonato et al. (2023) with some differences. First, the term $a_1(S)D$ ensures that even the first ton of carbon to be removed and stored has non-zero marginal costs. Second, carbon removal becomes cheaper as the green transition progresses via $a_j(S) = b_j \max(\zeta, S)^{c_j}$.²⁷ Third, carbon removal costs are stochastic as S is stochastic. Fourth, this technology operates at strictly positive but finite marginal costs $0 < \frac{\partial \tilde{b}_d(S, \mathbf{X}^t=2, D)}{\partial D} = a_1(S) + a_2(S)a_3(S) \exp(a_3(S)D) < \infty$. We have calibrated this cost function to the marginal cost curves in Figure 5 of Rebonato et al. (2023) for 2050 and 2100.²⁸ The calibration details are given in Appendix C.2 and the fit to the data is shown in Figure C.2. We assume that costs are shared according to the size of the two sectors, $\zeta_1 = 1 - S$ and $\zeta_2 = S$. We assume that the negative emission technology becomes competitive somewhere in the period up to the year 2050 with a probability of 50% corresponding to a jump intensity of $\hat{\lambda}_t^{1,2} = 0.0224$.²⁹

Political Transition Risks Ongoing global warming (exponentially) increases the likelihood of strengthening climate policy once temperature has crossed 1.5°C (Barnett, 2023). Although carbon taxes or cap-and-trade systems have never been completely abolished after they had been implemented, there is a significant hazard of climate change deniers coming (back) to power. To allow for transitions back to BAU, we model political transition intensities by

$$\begin{aligned} \lambda_p(\mathbf{S}, i, j) &= \hat{\lambda}_p^{i,j} \exp(\hat{\mu}[\max(T - 1.5, 0) - S]), & i < j \\ \lambda_p(\mathbf{S}, i, j) &= \hat{\lambda}_p^{i,j} \exp(\hat{\mu}[\min(1.5 - T, 0) + S]), & i > j \end{aligned}$$

with $\hat{\lambda}_p^{i,j} > 0$ for $i \neq j$ and $\hat{\mu} > 0$. The probability for jumps to a more ambitious climate policy ($j > i$) thus rises in temperature if $T > 1.5^\circ\text{C}$. It also falls in the share of brown capital as a result of lobbies

²⁷ We assume that carbon removal costs no longer fall once the share of green capital reaches 90%, so set $\zeta = 0.1$. The truncation parameter ensures that costs for carbon removal does not fall to zero when the share of green capital approaches 100%. Alternative parametrizations with different truncation parameters or alternative functional forms do not significantly affect the qualitative nature of our results.

²⁸ These marginal cost curves build upon cost estimates for negative emission technologies of Fuss et al. (2018) and the comprehensive review in the of the Sixth Assessment Report of the IPCC (2022), which has shown the important role for negative emissions technologies in limiting global warming to 2°C .

²⁹ Alternative calibrations for when the jump intensity depends on the political state or the share of brown capital do not significantly affect our results. Moreover, our main asset pricing implications are hardly affected if we exclude the possibility of a competitive negative emissions technology (see Appendix D.3).

to slow down the green transition;³⁰ also, as the green sector grows in size, green lobbies increase the chance of more stringent climate policies. Conversely, the probability for jumps back to a less ambitious climate policy ($j < i$), falls in temperature if $T > 1.5^\circ\text{C}$ and rises in the share of brown capital due to stronger brown and weaker green lobbies.

We choose parameters to roughly match the likelihood and resulting temperature increase of the various transition scenarios in Moore et al. (2022): about 48% of their simulations are in their modal scenario, which leads to an average temperature increase of 2.3°C . About 28% of their simulations lead to aggressive climate action limiting global warming to up to 1.8°C . There is less ambitious or less effective climate action in the remaining scenarios (about 24%) with average temperature increases of around 3°C , of which less than two percent of the simulations lead to significantly higher temperatures. To replicate those figures with our model, we use the parameterization in Table 2. We thus find that the jump intensity from BAU to modest (PIGOU) or ambitious (CAP) climate policies at $T_0 = 1.27^\circ\text{C}$ and $S_0 = 0.876$ is 6.22% and 2.59%, respectively, which correspond to an expected duration of 16.08 or 38.56 years. The average time until the government takes climate action is half the harmonic mean of those average durations: 11.35 years. Compared to technological or climate tips, these are quick transitions. If BAU continues and temperature rises to say 2°C , expected durations shorten to 11.05 and 26.52 years, respectively. This cuts the average time until the government takes climate action to 7.80 years. Hence, we assume that ongoing global warming and a smaller share of brown capital make it more likely that policy makers start taking the climate serious.

5 Benchmark Results

Here we present our policy optimization and simulation results using the calibration discussed in Section 4. We solve our model numerically with the grid-based finite-differences method outlined in Appendix A.5, and use 200,000 sample paths until the year 2100 to calculate means, medians, and quantiles of all relevant decision and state variables.

5.1 Business-as-usual Scenario without Policy Transition Risks

First, we discuss the results for a pure BAU scenario, which excludes policy transitions to active climate policies (PIGOU or CAP) and with the political and technological Markov chains switched off. This aids comparison with transition risk scenarios. Figure 2 shows the simulation of key variables until the year 2100. The average values of a variable are depicted by solid lines (—) and referred to as the mean

³⁰For instance, more than 2400 lobbyists affiliated with oil and gas industries attended the recent climate summit COP28, e.g. <https://www.theguardian.com/environment/2023/dec/05/record-number-of-fossil-fuel-lobbyists-get-access-to-cop28-climate-talks>.

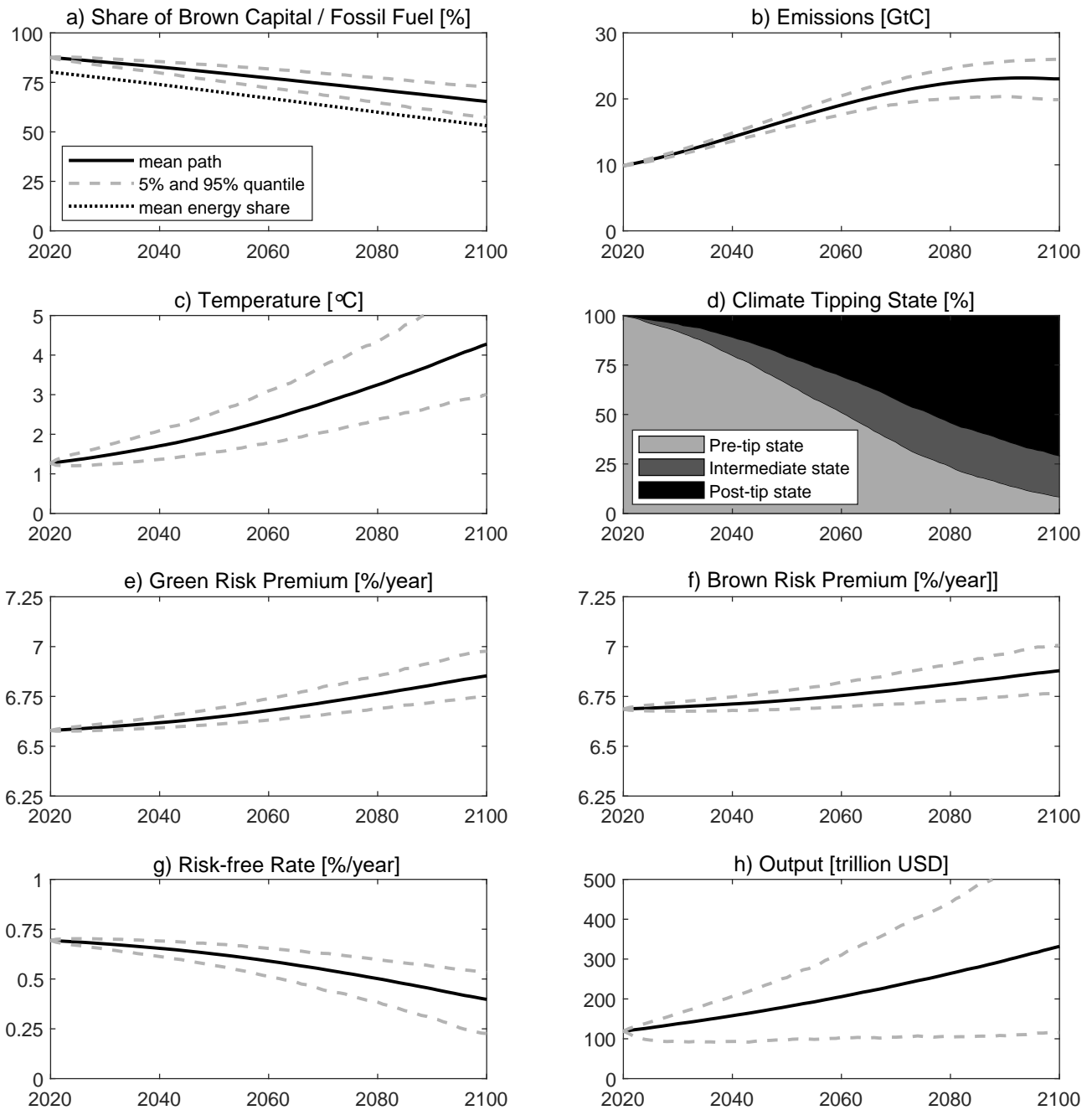


Figure 2: Business-as-usual Scenario With No Transition Risks. Average values are depicted by solid lines (—) and 5% and 95% quantiles by dashed lines (- - -). The dotted line (· · · · ·) in Panel a) depicts the mean path of the share of fossil fuel in the global energy mix. The light (■), dark gray (■), and black (■) areas in Panel d) depict the proportion of simulations in the pre-tip ($X^c = 1$), intermediate ($X^c = 2$), and post-tip ($X^c = 3$) climate state, respectively.

path. Dashed lines (- - -) show 5% and 95% quantiles. In this scenario, policy makers never take account of negative global warming externalities, and thus the green transition takes place at a slow

pace (Panel a)). The transition is solely driven by the desire to diversify assets and the falling cost of green energy as the share of green capital rises (Hambel et al., 2024). The share of fossil fuel in the energy mix is always a bit below the share of brown capital, since the brown sector can be operated with both fossil fuel and renewable energy. Emissions are high (Panel b)) and global average temperatures reach on average 4.2°C (3.8°C disregarding climate tipping) above the pre-industrial average by the end of this century (Panel c)). The latter is thus partly due to climate tipping.

The light area (■) in Panel d) represents the proportion of paths in the pre-tip state ($X^c = 1$), the dark gray area (■) in the intermediate state ($X^c = 2$), and the black area (■) in the post-tip state ($X^c = 3$). Climate tipping points occurs in almost 90% of the paths. These events further fuel global warming and lead to additional economic damages.

In contrast to policy makers, financial markets do anticipate the negative effects of emissions on output, the intensity of recurring climate-related disasters, and the risk of climate tipping, and price these risks in. This leads to an additional risk premium for both green and brown assets (Panels e) and f)). These premiums show a slight upward-trend because of growing climate risks. There is a tiny carbon premium (the difference between the brown and green risk premium) of 0.1% per year as in this scenario we have no policy tipping. As discussed in Section 3, the risk-free rate falls over time as growing temperatures and tipping risks increase demand for precautionary savings (Panel g)). The effect of physical climate risks on interest rates is slightly more pronounced than those on risk premiums. Global output appears quite volatile as it is plagued by many types of economic uncertainty (Panel h)).

5.2 Business-as-Usual Scenario with Transition Risks

Now, we turn to our benchmark scenario for which we switch on the political Markov chain and start in the year 2020 with the BAU state.

Markov Chains and Temperature Scenarios By 2060, society has implemented a carbon tax (■) or temperature cap (■) in about half of the simulated pathways (see Panel a) of Figure 3). This figure rises to 80% by the end of the century and stabilizes there. The gradual increase in paths with active climate policies is due to the dependence of transition intensities on temperature and the share of brown capital. Even the paths that are in the BAU state in 2100 often had carbon taxes implemented in the past and thus emissions in 2100 are lower than in the pure BAU simulation. The evolution of the climate tipping state (see Panel b)) looks similar to the pure BAU simulation, but the tipping loop is slowed down somewhat because society is mitigating climate change in many paths and thus delaying climate tipping. In about two-thirds of the simulated paths, there is a technological breakthrough by 2100 that makes negative emission technologies competitive (see Panel c)).

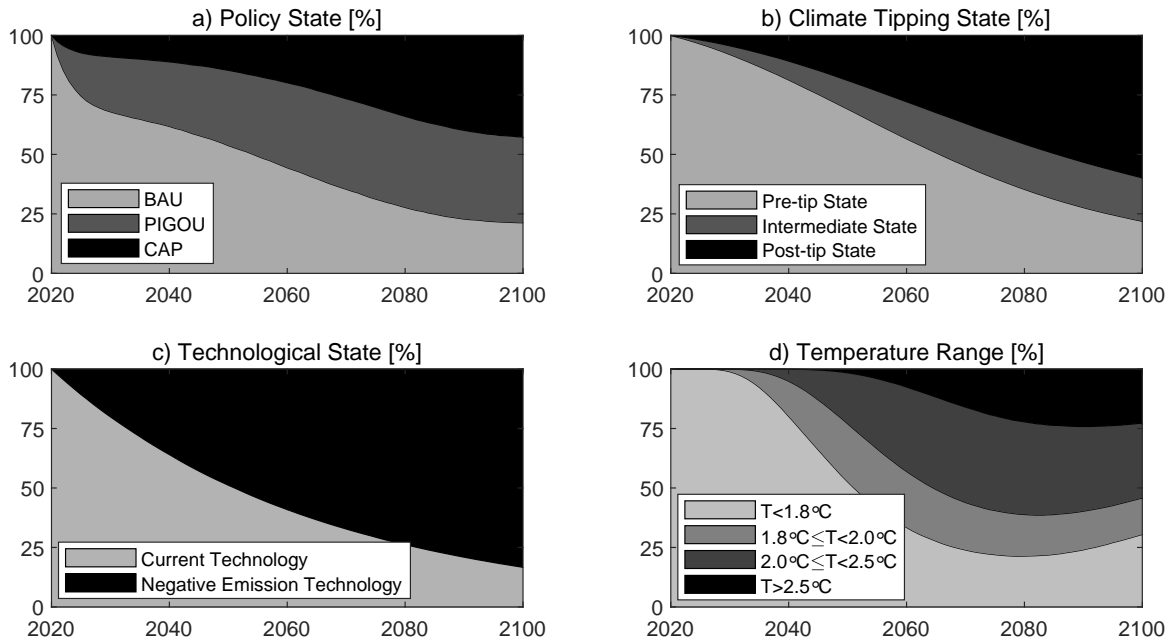


Figure 3: Markov Chains and Temperature Scenarios (starting from BAU with transition risks). In Panel a) the light area (■) is the proportion of simulations in the BAU state, the dark gray area (■) the proportion in the PIGOU state, and the black area (■) the proportion in the CAP state. In Panel b) the light area (■) is the proportion of simulations in the pre-tip state, the dark gray area (■) the proportion in the intermediate state, and the black area (■) the proportion in the post-tip state. In Panel c) the light area (■) is the proportion of simulations in the pre-breakthrough state and the black area (■) the proportion where the negative emission technology has come into force. In Panel d) the light area (■) is the proportion of simulations with temperature less than 1.8°C, the gray area (■) with temperature between 1.8°C and 2°C, the dark gray area (■) with temperature between 2°C and 2.5°C, and the black area (■) that with temperature above 2.5°C.

About 29% of the paths lead to a temperature lower than 1.8°C by the end of the century as shown by the light area (■) and 47% of the paths lead to a temperature increase between 1.8°C and 2.5°C, as shown by the aggregated gray and dark gray areas (■ and ■) (Panel d)). The remaining paths suffer from little or ineffective climate action and lead to a significant temperature increase of more than 2.5°C, as shown by the black area (■). These figures roughly correspond to the scenarios in Moore et al. (2022). The 2°C cap is violated for many paths from 2040 onwards, with the number of violations increasing sharply around 2050. About 46% of the sample paths up to 2100 adhere to the 2°C cap, but a greater proportion of paths temporarily violate the target. These paths are represented by the aggregated light and gray areas (■ and ■). These temporary violations are compensated by negative emissions. This underlines the importance of negative emissions technologies for the transition to a low-carbon economy.

Energy Transition and Global Output Figure 4 illustrates the transition towards a low-carbon economy until the year 2100. Due to political tipping the share of brown capital and the share of fossil

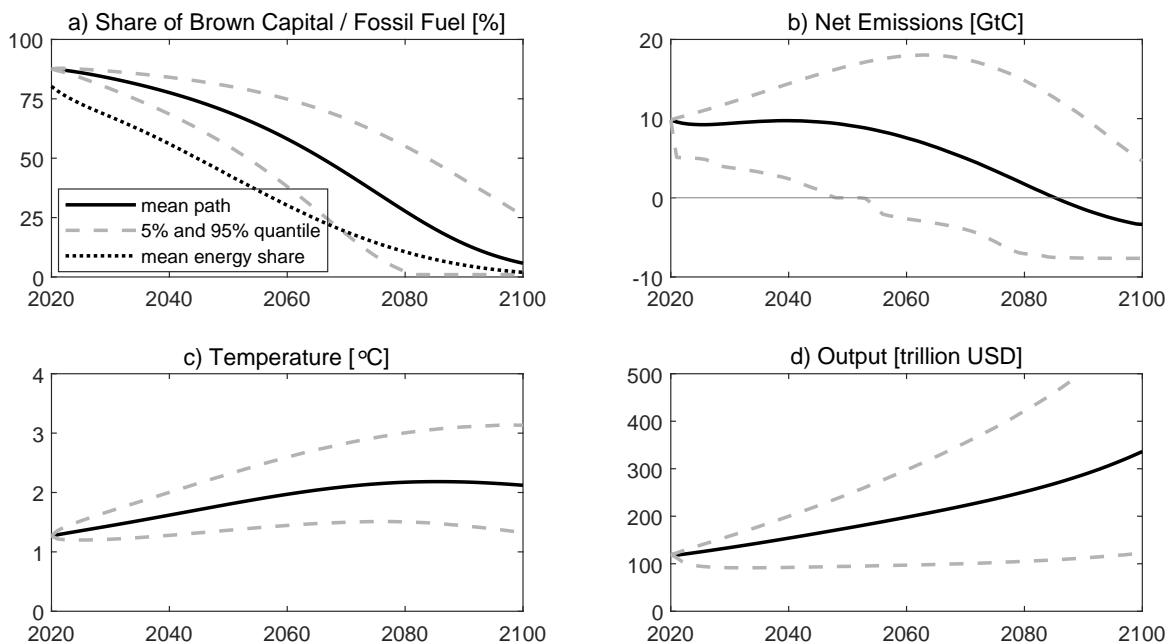


Figure 4: Transition of the Real Economy (starting from BAU with transition risks). Mean paths are depicted by solid lines (—) and dashed lines (---) show 5% and 95% quantiles. The dotted line (·····) in Panel a) shows the share of fossil fuel in the global energy mix.

fuel in the global energy mix decline much faster than in the pure BAU simulation (Panel a)). Still, the transition is plagued by substantial political uncertainty since in our policy tipping scenario policy makers can be replaced. In particular, in some paths already implemented carbon taxes are reversed by a new BAU-type government. Such political uncertainties explain the broad confidence bands of the share of brown capital and net emissions.

Mean temperature reaches a maximum around 2085 when the mean net emission path crosses the zero line (see Panel b and c)). Hereafter, mean temperature slowly falls due to the negative net emissions technology, which has become available in many paths. Global output increases at a slightly higher rate as society internalizes the negative externalities from emissions or imposes a temperature cap.

Carbon Tax Paths Starting from BAU The number of paths with active climate policies increases rapidly over time (Panel a) of Figure 3). Panel a) of Figure 5 shows unconditional means and quantiles of carbon taxes, and Panel b) shows means and quantiles of carbon taxes conditional on modest (PIGOU) or ambitious (CAP) climate policies being implemented. In about 8% of paths, the carbon tax is implemented in the year 2021 and then starts at an average of \$308/tC. The conditional distributions of the implemented carbon taxes are left-skewed in 2025 and become right-skewed in later years (see Figure D.3 and Table D.3). This negative skew is due to the negatively skewed distribution of the aggre-

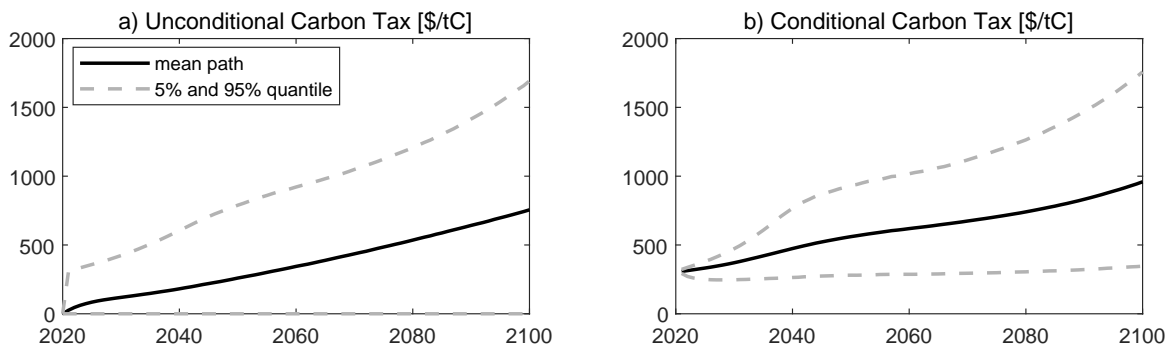


Figure 5: Carbon Taxes (starting from BAU with transition risks). The figure depicts the carbon taxes for the benchmark simulation until the year 2100. Mean paths are depicted by solid lines (—) and dashed lines (---) show 5% and 95% quantiles. Panel a) shows unconditional means and quantiles, and Panel b) shows means and quantiles conditional on being in the PIGOU or CAP state.

gate capital stock, which largely stems from rare economic disasters, and the optimal carbon tax being proportional to the capital stock (see (3.1)). As time goes by, climate risks (tipping points and climate disasters) and political shocks increase in intensity. These risks skew the carbon price to the right, hence gradually transforming the left-skewed into a right-skewed distribution (see Appendix D.1).

To analyze whether and how different political, technological, and tipping states affect the optimal carbon tax, we perform several Welch’s t -tests.³¹ We find three results that are statistically significant at the 1% level. First, optimal carbon taxes are consistently higher in the climate tipping state. This reflects that climate tipping leads to more pronounced economic damages (Panels d) – f) of Table D.3). Second average carbon taxes are slightly lower after a technological breakthrough. This is because negative emissions help reduce temperatures.³² Third, carbon taxes are consistently higher in the CAP state than in the PIGOU state but the differences are not very pronounced. Note that carbon taxes in the PIGOU state grow roughly in line with the growth rate of the economy while carbon taxes in the CAP state follow an average of such a Pigouvian path and a Hotelling path, where the carbon price in the latter path grows at a higher rate equal to the risk-adjusted interest rate (e.g. Olijslagers et al., 2023). This implies that the CAP state tilts the carbon path away from the present to the future relative to the carbon path in the PIGOU state, and thus the differences are not pronounced.

³¹A Welch’s t -test is a variant of a two-sample t -test which is used to test the null hypothesis that two populations have equal means. This test is more reliable than the classical Student’s t -test if both samples have unequal variances and possibly unequal sample sizes.

³²This finding is statistically significant for all years until 2100, but the difference is not always economically significant. E.g. in 2025 when this technology is too expensive to play a big role, the average carbon tax before the technological breakthrough is 333 \$/tC and 331 \$/tC after the technological breakthrough.

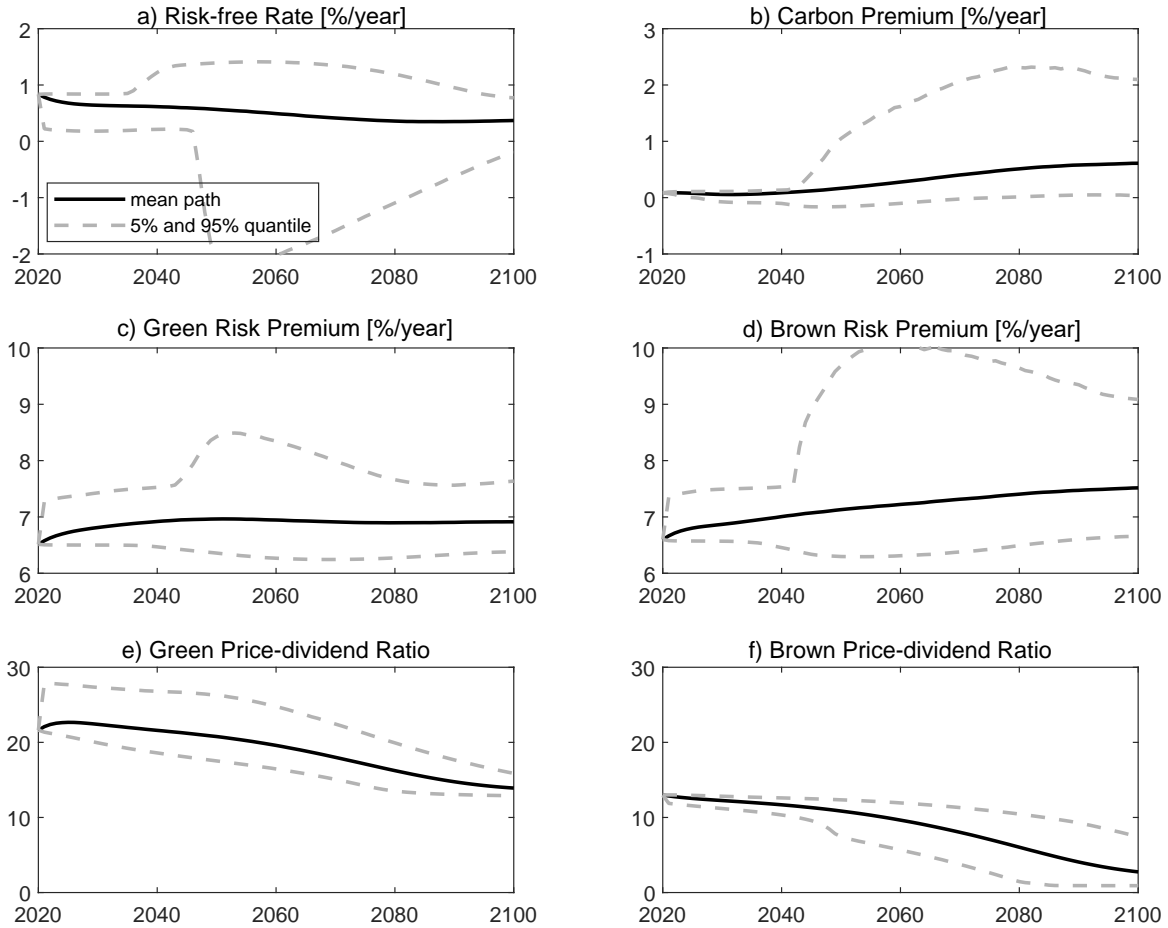


Figure 6: Asset Pricing Moments (starting from BAU with transition risks). This figure depicts the simulation of several asset pricing moments for benchmark simulation until the year 2100. Mean paths are depicted by solid lines (—) and dashed lines (---) show 5% and 95% quantiles.

5.3 Asset Pricing Paths with Transition Risks

Figure 6 illustrates the mean path as well as 5% and 95% quantiles of the risk-free rate, the green and brown risk premium, and the carbon premium until the year 2100. Equation (3.3) implies that sudden shocks to the political landscape, the climate system, and the technological state affect the risk-free rate, and thus also the price-dividend ratios and risk premiums of the risky assets. Moreover, the asset pricing moments depend in a non-linear manner on temperature, especially as the impact of a policy transition to CAP becomes potentially devastating when the 2°C cap is exceeded. This is reflected in the large extent of variation of the key variables shown in Figure 6. Although the effects of temperature and the share of brown capital on those asset pricing moments have extensively been discussed in Hambel et al. (2024), we want to stress that our model generates a *temperature risk premium* as empirically documented by Bansal et al. (2017), Donadelli et al. (2017), and Hong et al. (2019), which consistently

increases in temperature and can be interpreted as compensation for physical climate risk. In the remainder of this section, we focus on the novel implications of transition risks.

Risk-free Interest Rate The mean risk-free interest rate (—) starts at 0.8% and slowly decreases over time in response to growing climate-related risks (see Panel a)). The 5% quantile of the interest rate reflects extreme transition risks and starts to fall rapidly around 2045. This happens especially in paths with temperatures close to the 2°C cap while being in the CAP state. Under these circumstances only a small amount of carbon may be released and exceeding this would massively affect the productivity in the brown sector when fossil fuels can no longer be burned. This risk is priced in by financial markets and the corresponding precautionary savings reduce the risk-free interest rate considerably, up to -3% in some extreme paths. When the transition continues and the brown capital stock becomes smaller, the impact of ambitious policies to phase out fossil fuels diminishes, which is why demand for precautionary savings will fall again and the 5% quantile eventually returns to 0% in 2100.

Green and Brown Asset Returns In contrast to Hambel et al. (2024), which ignores climate transition risk, we consistently have a positive carbon premium even in the PIGOU state and the CAP state (see Panel b) of Figure 6).³³ This carbon premium is initially small and not economically significant (about 0.1%), in line with the empirical findings of Aswani et al. (2024) and Zhang (2024). Still, our model offers a mechanism to explain sizable carbon premiums when political transition risks prevail. The effect of transition risk is particularly strong if temperatures are close to the 2°C cap and society is already in the CAP state. The 95% quantiles in Panels c) and d) indicate that then the risk premiums for both assets go up considerably. This finding can be interpreted as a *transition risk premium* in the spirit of Engle et al. (2020) and Faccini et al. (2023). Moreover, transition risk has a larger effect on the brown asset. Consequently and in line with the empirical findings of Hsu et al. (2023) and Bolton and Kacperczyk (2021, 2023), a sizable *carbon premium* emerges that reflects the asymmetric impact of political transition risk (see Panel b)).³⁴

The green and brown price-dividend ratios tend to decline over time (see Panels e) and f)). The green asset's price-dividend ratio is initially relatively high reflecting the scarcity of this asset. A transition to active climate policies (either PIGOU or CAP) boosts demand for the green asset and thus sizably increases its price-dividend ratio (see the 95% quantile). The brown asset becomes worthless when the transition has come to an end and the brown capital stock has been run down completely.

³³Although Hambel et al. (2024) find a small positive carbon premium in their pure BAU scenario, this premium becomes negative if policy makers implement the first-best optimal Pigouvian carbon tax.

³⁴Further insights are given in Appendix D.1 and Figure D.4 by considering the effects on macroeconomics and financial variables if the carbon premium exceeds 1%.

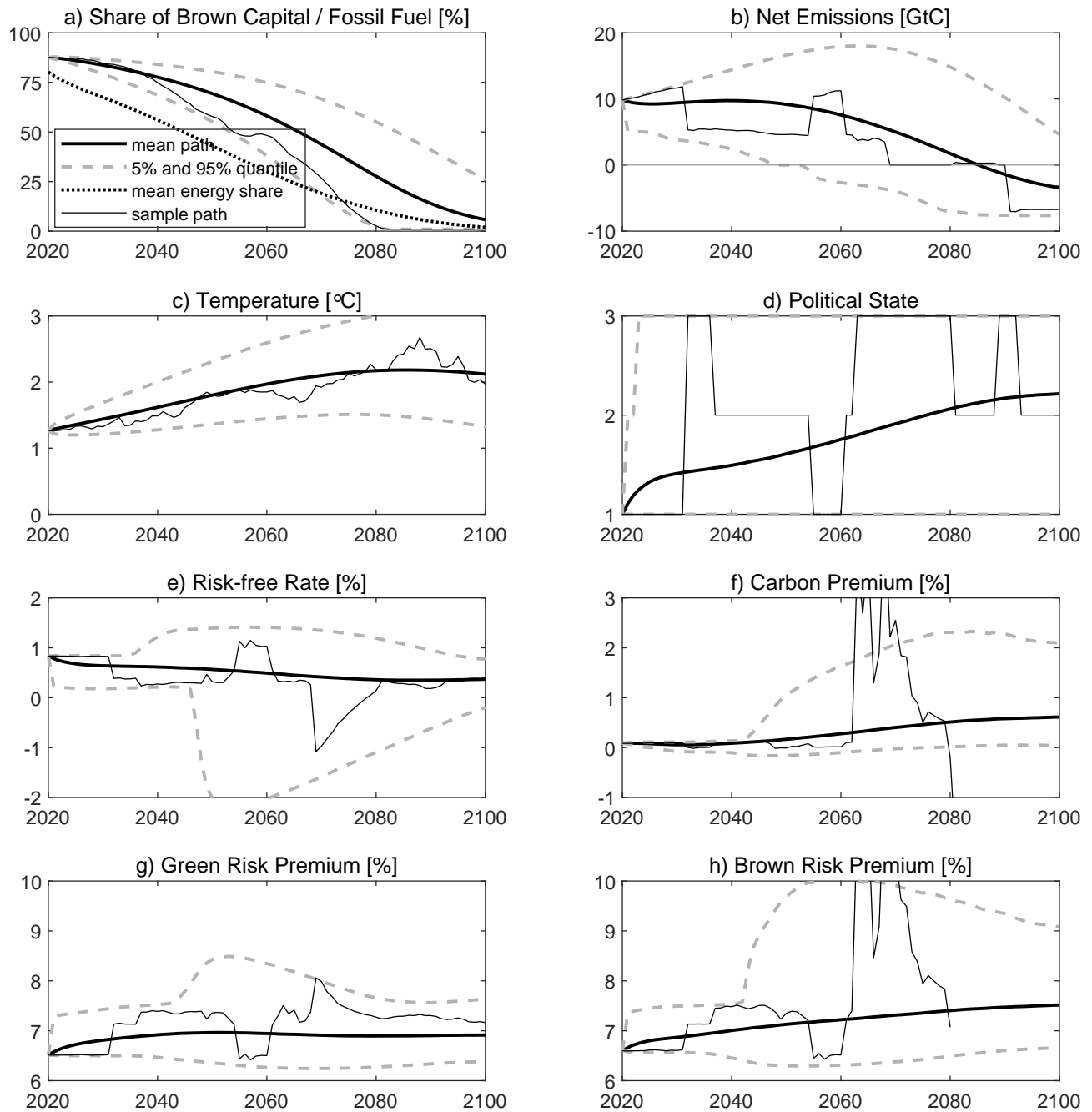


Figure 7: Illustrative Sample Path for BAU Scenario with Transition Risks. Average values are depicted by solid lines (—) and 5% and 95% quantiles by dashed lines (---). The dotted line (····) in Panel a) depicts the mean path of the share of fossil fuel in the global energy mix. The thin black line (—) shows one exemplary sample path.

An Exemplary Sample Path Figure 7 illustrates the mechanisms for generating the various climate-related risk premiums along one selected sample path shown by the thin black lines (—). Along this

path the economy is in the BAU state until the year 2030 when it transitions to the most climate ambitious policy, the CAP state (Panel d)). This transition leads to a drastic emission cut (Panel b)) and suddenly increases the risk premium of both risky assets by about 0.5 %-points as now the political risk of phasing out fossil fuels has increased substantially (Panels g and h)). At the same time, demand for precautionary savings is rising sharply and the risk-free interest rate is falling accordingly by around 0.5 %-points (Panel e)).

After a few years, the economy jumps to modest climate action, the PIGOU state, which further increases risk premiums and demand for precautionary savings. This shows that the transition risk in the PIGOU state is more pronounced than in the CAP state as in the PIGOU state policy transitions are possible in both directions, i.e. to more stringent climate action and to BAU. The return to BAU in 2055 is accompanied by increased emissions and a decline in risk premiums and demand for precautionary savings. This can be explained by the fact that a transition away from BAU is not considered a risk but a chance by market participants since the negative externality is not internalized in this state.

After 2060, the economy transitions back to ambitious climate action (CAP), thus lifting again risk premiums and curbing the risk-free rate. This effect is particularly pronounced when temperatures are close to the 2°C cap, hence transition risks are asymmetric as the brown sector faces the risk that fossil fuels could be phased out. This asymmetry leads then to a sizable carbon premium of about 3 %-points that reacts sensitively to small temperature fluctuations (see Panels c) and f)). Moreover, this carbon premium rapidly declines and becomes meaningless when the brown capital stock has been run down completely around 2080. Then, political transition risk plays a minor role and risk premium of the green asset and the demand for precautionary savings eventually get back to a level which is slightly higher than at the beginning. This additional risk premium is due to physical climate risk.

Finally, a competitive negative emission technology becomes available around 2090 (Panel b)) but this has a negligible effect on asset pricing moments.

5.4 Robustness

Pure PIGOU Scenario To test if the carbon premium emerges due to political transition risks, we have simulated a pure PIGOU scenario with no policy transitions to the BAU or CAP state (see Appendix D.2). Compared to the benchmark simulation, the carbon premium is initially very small and negative (0.08%) due to the absence of political transition risk, and turns positive when physical risks become sizable. Still, the magnitude of the carbon premium is small and economically not significant. This confirms that transition risk is the root of a sizable positive carbon premium and to a much lesser extent physical risk.

No negative emission technology To test if technological transition risk carries a risk premium, we have also simulated a scenario without the possibility of technological breakthroughs and obtain virtually unchanged results for the risk premiums as in the benchmark case (see Appendix D.3). This confirms that our results are robust to different assumptions about the existence and likelihood of competitive negative emissions technologies. Moreover, they support the empirical results of Engle et al. (2020), whose WSJ Climate Change index primarily reacts to climate-related political shocks and climate summits.

Tighter Carbon Budget We also consider a scenario where policy makers phase out fossil fuels in the CAP state if temperature exceeds 1.5°C instead of 2°C . Carbon pricing is then more ambitious to avoid the potentially devastating effects of overshooting the carbon budget. Figure D.7 shows that the carbon premium becomes earlier economically relevant than in the benchmark case when the economy is in the CAP state and the temperature is close to 1.5°C .

6 Transition Risk and Stranded Assets

To investigate the interplay between climate transition risk and stranded assets, we now adopt an alternative calibration where the brown sector only uses fossil fuel and the green sector uses both energy types (see Appendix C.3).³⁵ We still reproduce the emission and temperature paths of the pure BAU simulation of Section 5.1 but things become different once the political Markov chain is switched on. To ensure a consistent comparison with the benchmark results of Section 5, we keep the calibration of the Markov chains unchanged.³⁶

Energy Transition and Carbon Taxes In this alternative calibration it is no longer possible to replace fossil fuels with renewable energy in the brown sector. Thus, the transition to a green economy must necessarily take place through the development of the green sector. If this does not happen quickly enough before society jumps to the state with the most ambitious climate policies (the CAP state), the brown asset may become stranded. This hazard and the costs of stranding are priced in by policy makers, who thus implement higher carbon taxes compared to our benchmark calibration (in both the PIGOU state and the CAP state). Conditional on being implemented, the average carbon tax in the year 2021 is 366 \$/tC, which is about 19% higher than the 308 \$/tC in our benchmark simulation. This markup is sizable and solely driven by the transition risk of policy-related stranding of financial assets.

³⁵To test how sensitive our results are with respect to this assumption, Appendix C.3 provides two more alternative calibrations. The qualitative conclusions for those alternatives are unaltered and available upon request.

³⁶Results for a modified calibration that matches the temperature ranges in Moore et al. (2022) are available.

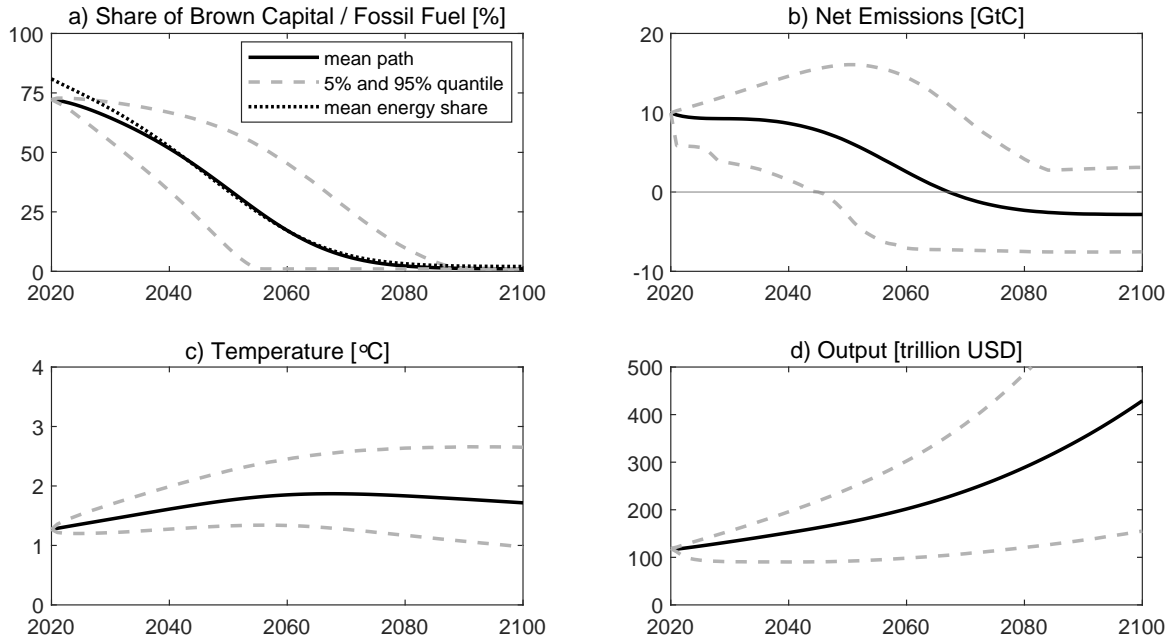


Figure 8: Transition of the Real Economy (Stranded Assets Scenario). Mean paths are depicted by solid lines (—) and dashed lines (---) show 5% and 95% quantiles. The dotted line (·····) in Panel a) shows the share of fossil fuel in the global energy mix.

Consequently, the transition to a low-carbon economy takes place at a much faster pace as policy makers aim to avoid the economic costs of stranded assets.

Figure 8 illustrates the transition towards a low-carbon economy until the year 2100. The hazard of stranded assets accelerates the green transition a lot relative to our benchmark scenario (see Panels a) and b)). Mean temperature reaches its maximum around 2065, about 20 years earlier than in our benchmark simulation (see Panel c)). The acceleration of the green transition is also reflected in Figure D.9 in Appendix D.5, which shows that the number of paths keeping global mean temperature below the 2°C cap in the year 2100 is 75% and thus much higher than the 45% in our benchmark (see Panel d)). This stems from the much more stringent climate policies in paths that entered the PIGOU or CAP state compared to our benchmark scenario even though slightly less paths than in our benchmark scenario have left the BAU state in the year 2100 (see Panel a)).

Economic Costs of Stranded Assets Panel a) of Figure 9 indicates that the share of sample paths with stranded assets increases rapidly from 2035 on, and peaks in the year 2080 at 15% of paths. Then this share starts to decline slowly. In our framework, the risk of stranded assets can be reverted if either policy makers switch back from the CAP state to less ambitious or no climate policies or if temperature falls below 2°C so that brown production can start up again. Negative emission technologies curb the

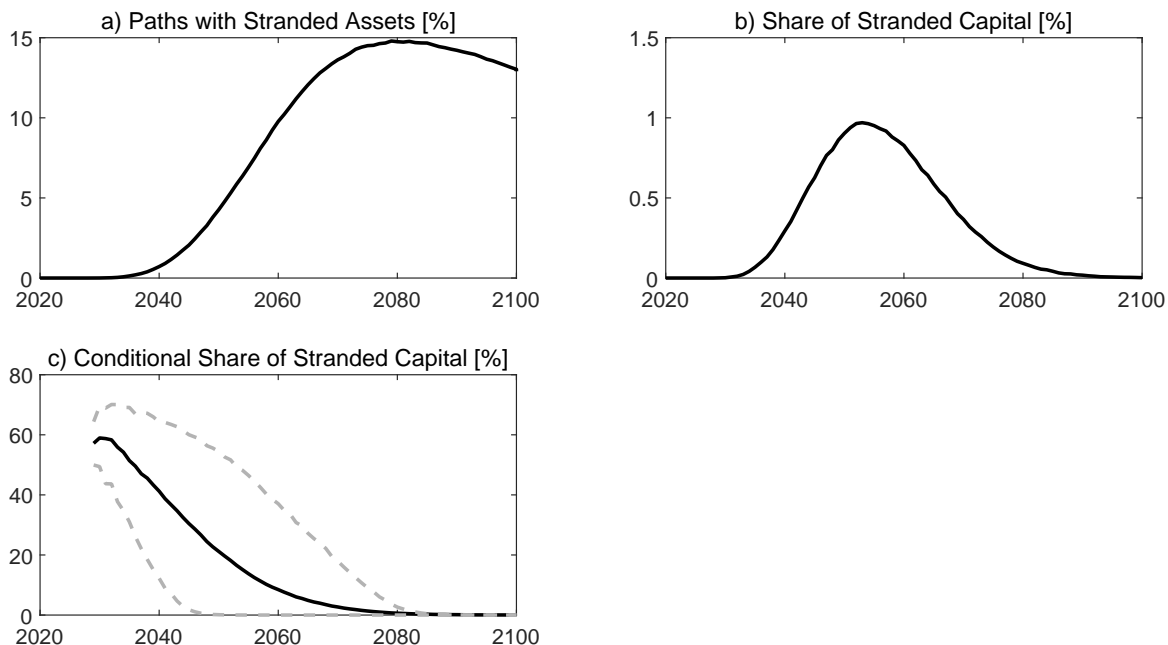


Figure 9: Risk of Stranded Assets. Panel a) shows the share of sample paths with stranded assets in simulations with our alternative calibration. Panel b) depicts the share of stranded capital by calculating the sample mean of $1_{\{T \geq 2, X^p = 3\}} S$ over all paths. Panel c) depicts the share of stranded capital conditional on those paths in which stranded asset occur by calculating the sample mean and quantiles of $1_{\{T \geq 2, X^p = 3\}} S$ over all paths in which stranded assets occur.

likelihood of stranded assets and increase the likelihood that the brown technology may eventually be operated again.

Panel b) of Figure 9 depicts the economic costs of stranded assets expressed as the average share of stranded capital. It peaks around 2055 at 1% of total capital. Conditioning this figure on those paths in which stranded assets occur, the economic costs are much higher and amount to up to around 75% of total capital if stranded assets occur before 2030 (see Panel c)). Although this happens in less than 0.2% of the paths, the probability of stranded assets sharply increases around 2040 while its economic costs decline gradually as the brown capital stock is cut back. Still, the economic impact of stranded assets can be devastating and its magnitude is comparable to the risk of recurring macroeconomic disasters.

Asset Pricing Implications of Stranded Assets Figure 10 that a policy transition to a 2°C temperature cap now has much more severe impacts on asset prices than in our benchmark simulations. Demand for precautionary savings and the risk-free rate are more strongly affected (see Panel a)). The risk premiums for both assets are significantly boosted by the risk of stranded assets and rises to 15% per year in some extreme cases (see Panels c) and d)). The effect is more pronounced for the brown asset, because of the enormous economic impact of stranded assets discussed in the previous paragraph. This

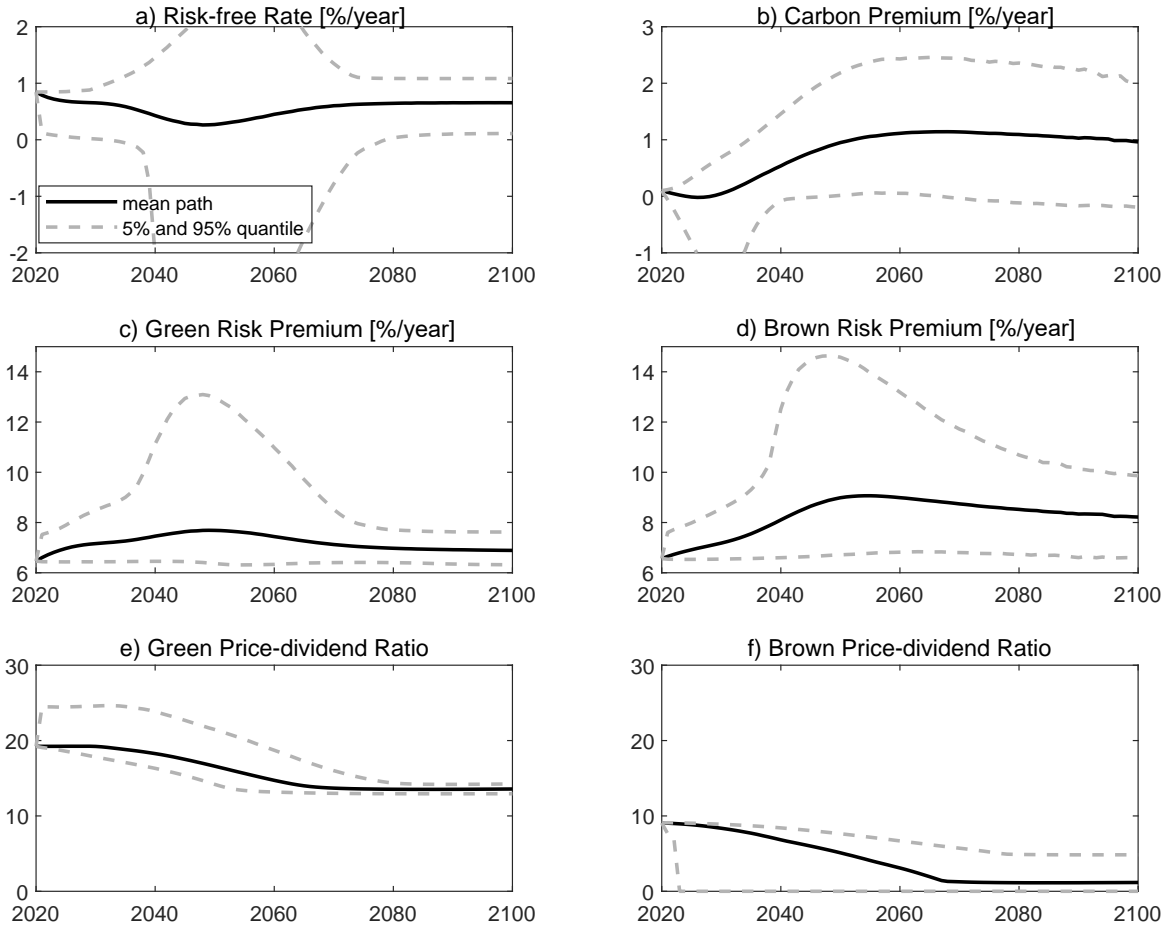


Figure 10: Asset Pricing Moments (Stranded Assets). This figure depicts the simulation of several asset pricing moments for simulations based on our alternative calibration until the year 2100. Mean paths are depicted by solid lines (—) and dashed lines (---) show 5% and 95% quantiles.

effect is much stronger than in our benchmark simulation without stranded assets. This leads to quite a high carbon premium of up to 2.5% per year (see Panel b)). Moreover, when the brown asset becomes stranded, it loses almost its whole value (see Panel f)).³⁷

7 Concluding Remarks

Our aim has been to better understand how transition risks (uncertainty about future policy regimes and breakthroughs in negative emissions technologies) and physical risks (temperature-related risks

³⁷Its value remains strictly positive as there is always a strictly positive probability that this policy transition will be reversed eventually or temperature falls again below 2°C because of use of the negative emission technology. Our framework does generate a brown asset price of zero if we model CAP as an absorbing state, there is no negative emissions technology, and the temperature evolution is deterministic.

of recurring climate disasters and climate tipping points) affect carbon pricing, asset returns, carbon premiums, and the risk of stranded assets. For this purpose, we have formulated and calibrated a two-sector DSGE model of the economy and the climate with a wide range of uncertainties affecting the economy, the climate, and global warming damages. We have distinguished three different political states: (i) no carbon pricing (business as usual), (ii) modest carbon pricing with the carbon tax set to the social cost of carbon, and (iii) ambitious climate carbon pricing with in addition a temperature gap of 2°C . Under (ii) and (iii) policy makers take account of the risks of future policy, technological, and climate tipping as well as the risk of regular macroeconomic disasters and temperature-related risk of climate disasters. Financial markets always takes account of all these risks.

If policy makers do not price carbon and negative emissions technology is excluded, the green transition takes place at a slow pace. In this business-as-usual scenario, emissions are high and global mean temperatures reach 4.2°C by the end of the century. Climate tipping points occurs in almost 90% of paths. This fuels global warming and leads to additional economic damages. Financial markets price in the adverse effects of global warming on output, the frequency of climate-related disasters, and the probability of climate tipping. This gives rise to a tiny carbon risk premium, since transition risks are absent. The risk-free rate falls due to precautionary saving. Global output is quite volatile due to growing physical risks.

However, if political and technological tipping are allowed for, carbon taxes are implemented by 2060 in about half of simulated pathways. Emissions and temperature are lower than in the absence of transition risks, which delays activation of climate tipping points. Now a little less than a third of paths lead to temperatures of less than 1.8°C by the end of this century, about half of paths lead to temperatures between 1.8°C and 2.5°C , and remaining paths lead to temperatures of more than 2.5°C . This is a lot better than in the scenario without transition risks. But the greening of the economy is plagued by substantial political uncertainty and thus temperatures are still a lot higher than if policy makers did not face such risks and could impose the first-best optimal climate policies.

The risk-free rate slowly decreases over time in response to growing climate-related risks. If the temperature cap kicks in, markets respond with precautionary savings and rapid falls in the risk-free interest rate. As the green transition continues and the brown capital stock falls, precautionary savings will fall again. We consistently find a positive carbon premium even when policy makers set carbon taxes or enforce a cap. This carbon premium reflects transition risks, especially political risk, and is particularly large if temperatures are close to or exceed the 2°C cap. This premium incentivizes firms to accelerate the green transition. In contrast, if policy makers ignore political transition risk and implement first-best carbon taxes, there is a slightly negative carbon premium. The green asset's price-dividend ratio is initially relatively high reflecting the scarcity of this asset. The brown asset becomes worthless when the transition has come to an end and the brown capital stock has run down completely.

To highlight the risk of stranded assets, we have also considered an alternative calibration in which the brown sector only uses fossil fuel energy and the green sector uses both energies. If it takes too long before society jumps into climate action, the brown asset may now become stranded. Policy makers want to avoid this by implementing higher carbon taxes and thus the green transition occurs more quickly. Policy makers now find themselves more often in a state where they take ambitious climate action. The risk of stranded assets can be reverted if policy makers switch back to less ambitious or no climate policies or if temperature falls below its cap in which case brown capital comes into operation again. Also, negative emission technologies curb the risk of stranded assets and make it more likely that brown technology may some time be operated again. Up to three quarters of total capital can become stranded before 2030 in all paths where stranded assets occur. The economic impact of stranding is comparable to that of the risk of macroeconomic disasters. The financial impacts are also more pronounced. For example, the risk premium on both green and brown assets and the carbon premium rise more sharply due to the risk of stranded assets. The carbon premium can be as much as 2.5% per year. Once the brown assets strand they lose almost their whole value, but not all as there is always a chance that brown capital comes into operation again.

Summing up, we have provided a mechanism for the carbon premium and stranded assets and have shown how these and carbon prices are qualitatively affected by political and technological tipping (transition risks) and by climate tipping and the risk of climate-related disasters such as extreme weather events (physical risks). In further research we aim to extend our framework to allow for credit market constraints, monetary policy, and systemic financial risk, and to study empirically the mechanisms underlying carbon premiums and stranded assets.

Acknowledgements We thank Ton van den Bremer, Carina Fleischer, Reyer Gerlagh, Ivan Jaccard, Holger Kraft, Armon Rezai, Sjak Smulders, Gerhard Stahl, Luca Taschini, and the participants of seminars the CCC Green Seminar Series at the Climate Change Centre of the ECB, the research department of the Bundesbank, the Environmental Economics Seminar, Tilburg University, University of Rome (Tor Vergata), CREST-CMAP, Paris, McGill University, and participants of the T2M 2024 conference, Amsterdam, and the SURED 2024 conference, Ascona, for very helpful comments and suggestions.

References

- Acemoglu, D., P. Aghion, L. Bursztyn, and D. Hemous, 2012, The environment and directed technical change, *American Economic Review* 102, 131–166.
- Allen, M. R., D. J. Frame, C. Huntingford, C. D. Jones, J. A. Lowe, M. Meinshausen, and N. Meinshausen, 2009, Warming caused by cumulative carbon emissions towards the trillionth tonne, *Nature* 458,

1163–1166.

- Ardia, D., K. Bluteau, K. Boudt, and K. Inghelbrecht, 2023, Climate change concerns and the performance of green vs. brown stocks, *Management Science* 69, 7151–7882.
- Aswani, J., A. Raghunandan, and S. Rajgopal, 2024, Are carbon emissions associated with stock returns?, *Review of Finance*, 28, 75–106.
- Bansal, R., D. Kiku, and M. Ochoa, 2017, Price of long-run temperature shifts in capital markets, *Working Paper*, Duke University.
- Bansal, R., and A. Yaron, 2004, Risks for the long run: A potential resolution of asset pricing puzzles, *Journal of Finance* 59, 1481–1509.
- Barnett, M., 2023, A run on fossil fuel? Climate change and transition risk, *Working Paper*, Arizona State University.
- Barro, R. J., 2006, Rare disasters and asset markets in the twentieth century, *Quarterly Journal of Economics* 121, 823–866.
- Barro, R. J., 2009, Rare disasters, asset prices, and welfare costs, *American Economic Review* 99, 243–264.
- Barro, R. J., and T. Jin, 2011, On the size distribution of macroeconomic disasters, *Econometrica* 79, 1567–1589.
- Bauer, M. D., D. Huber, G. D. Rudebusch, and O. Wilms, 2022, Where is the carbon premium? global performance of green and brown stocks, *Journal of Climate Finance* 1, 100006.
- Bolton, P., and M. Kacperczyk, 2021, Do investors care about carbon risk?, *Journal of Financial Economics* 142, 517–549.
- Bolton, P., and M. Kacperczyk, 2023, Global pricing of carbon-transition risk, *Journal of Finance*, 87, 3677–3754.
- Bolton, P., and M. Kacperczyk, 2024, Are carbon emissions associated with stock returns? Comment, *Review of Finance* 28, 107–109.
- Bouman, S., 2023, The asset pricing and risk management implications of climate transition risks, *Master Thesis* (Tilburg University).
- Bovenberg, A. L., and S. A. Smulders, 1996, Transitional impacts of environmental policy in an endogenous growth model, *International Economic Review* 37, 861–893.
- Cai, Y., T. M. Lenton, and T. S. Lontzek, 2016, Risk of multiple interacting tipping points should encourage rapid CO₂ emission reduction, *Nature Climate Change* 6, 520–525.

- Cai, Y., and T. S. Lontzek, 2019, The social cost of carbon with economic and climate risks, *Journal of Political Economy* 127, 2684–2734.
- Caldecott, B., 2018, *Stranded Assets and the Environment (1st ed.)* (Routledge).
- Caldecott, B., A. Clark, K. Koskelo, E. Mulholland, and C. Hickey, 2021, Stranded assets: environmental drivers, societal challenges, and supervisory responses, *Annual Review of Environment and Resources* 46, 417–447.
- Caldecott, B., E. Harnett, T. Cojoianu, I. Kok, and A. Pfeiffer, 2016, Stranded assets: a climate risk challenge, *Technical Report*, Inter-American Development Bank.
- Campiglio, E., and F. van der Ploeg, 2022, Macrofinancial risks of the transition to a low-carbon economy, *Review of Environmental Economics and Policy* 16, 173–195.
- Campos-Martins, S., and D. F. Hendry, 2023, Common volatility shocks driven by the global carbon transition, *Journal of Econometrics* 105472.
- Carney, M., 2015, Breaking the tragedy of the horizon – climate change and financial stability, *Speech*, Bank of England.
- Casey, G., 2023, Energy efficiency and directed technical change: Implications for climate change mitigation, *Review of Economic Studies* 90, 0034–6527.
- Cochrane, J. H., F. A. Longstaff, and P. Santa-Clara, 2007, Two trees, *Review of Financial Studies* 21, 347–385.
- Delis, M. D., K. de Greiff, M. Iosifidi, and S. Ongena, 2019, Being stranded with fossil fuel reserves? climate policy risk and the pricing of bank loans, *Working Paper*, Swiss Finance Institute.
- Dietz, S., and F. Venmans, 2019, Cumulative carbon emissions and economic policy: In search of general principles, *Journal of Environmental Economics and Management* 96, 108–129.
- Donadelli, M., M. Jueppner, M. Riedel, and C. Schlag, 2017, Temperature shocks and welfare costs, *Journal of Economic Dynamics and Control* 82, 331–355.
- Duffie, D., and L. G. Epstein, 1992a, Asset pricing with stochastic differential utility, *Review of Financial Studies* 5, 411–36.
- Duffie, D., and L. G. Epstein, 1992b, Stochastic differential utility, *Econometrica* 60, 353–394.
- Engle, R. F., S. Giglio, B. Kelly, H. Lee, and J. Stroebel, 2020, Hedging climate change news, *Review of Financial Studies* 33, 1184–1216.
- Epstein, L. G., and S. E. Zin, 1989, Substitution, risk aversion, and the temporal behavior of consumption and asset returns: A theoretical framework, *Econometrica* 57, 937–969.

- Faccini, R., R. Matin, and G. Skiadopoulos, 2023, Dissecting climate risks: Are they reflected in stock prices?, *Journal of Banking & Finance* 155, 106948.
- Fuss, S., W. F. Lamb, M. W. Callaghan, J. Hilaire, F. Creutzig, T. Amann, T. Beringer, W. de Oliveira Garcia, J. Hartmann, T. Khanna, G. Luderer, G. F. Nemet, J. Rogelj, P. Smith, J. L. Vicente, J. Wilcox, M. del Mar Zamora Dominguez, and J. C. Minx, 2018, Negative emissions—part 2: Costs, potentials and side effects, *Environmental Research Letters* 13, 063002.
- Gerlagh, R., and M. Liski, 2018, Carbon prices for the next hundred years, *Economic Journal* 128, 728–757.
- Golosov, M., J. Hassler, P. Krusell, and A. Tsyvinsky, 2014, Optimal taxes on fossil fuel in general equilibrium, *Econometrica* 82, 41–88.
- Gregory, R. P., 2024, Risk premiums from temperature trends, *International Review of Economics & Finance* 91, 505–525.
- Hambel, C., H. Kraft, and E. S. Schwartz, 2021a, Optimal carbon abatement in a stochastic equilibrium model with climate change, *European Economic Review* 132, 103642.
- Hambel, C., H. Kraft, and E. S. Schwartz, 2021b, The social cost of carbon in a non-cooperative world, *Journal of International Economics* 131, 103490.
- Hambel, C., H. Kraft, and F. van der Ploeg, 2024, Asset diversification versus climate action, *International Economic Review*, forthcoming.
- Hambel, C., and F. van der Sanden, 2024, Reevaluating the carbon premium: Evidence of green outperformance, *Working Paper*, Tilburg University.
- Hong, H., F. W. Li, and J. Xu, 2019, Climate risks and market efficiency, *Journal of Econometrics* 208, 265–281.
- Hsu, P.-H., K. Li, and C.-Y. Tsou, 2023, The pollution premium, *Journal of Finance* 78, 1343–1392.
- IPCC, 2014, *Fifth Assessment Report of the Intergovernmental Panel on Climate Change* (Cambridge University Press).
- IPCC, 2022, *Climate Change 2022 – Impacts, Adaptation and Vulnerability* (Cambridge University Press).
- Ivanov, I. T., M. S. Kruttli, and S. W. Watugala, 2023, Banking on carbon: Corporate lending and cap-and-trade policy, *Review of Financial Studies*, forthcoming.
- Karydas, C., and A. Xepapadeas, 2022, Climate change financial risks: Implications for asset pricing and interest rates, *Journal of Financial Stability* 63, 101061.

- Kelly, D. L., and C. D. Kolstad, 1999, Bayesian learning, growth, and pollution, *Journal of Economic Dynamics and Control* 23, 491–518.
- Kelly, D. L., and Z. Tan, 2015, Learning and climate feedbacks: optimal climate insurance and fat tails, *Journal of Environmental Economics and Management* 72, 98–122.
- Kreps, D. M., and E. L. Porteus, 1978, Temporal resolution of uncertainty and dynamic choice theory, *Econometrica* 46, 185–200.
- Lemoine, D., and C. P. Traeger, 2014, Watch your step: optimal policy in a tipping climate, *American Economic Journal: Economic Policy* 6, 137–166.
- Lemoine, D., and C. P. Traeger, 2016, Economics of tipping the climate dominoes, *Nature Climate Change* 6, 514–519.
- Longstaff, F. A., and M. Piazzesi, 2004, Corporate earnings and the equity premium, *Journal of Financial Economics* 74, 401–421.
- Matthews, H. D., N. P. Gillett, P. A. Stott, and K. Zickfeld, 2009, The proportionality of global warming to cumulative carbon emissions, *Nature* 459, 829–832.
- Matthews, H. D., K. Zickfeld, R. Knutti, and M. R. Allen, 2018, Focus on cumulative emissions, global carbon budgets and the implications for climate mitigation targets, *Environmental Research Letters* 13, 010201.
- McGlade, C., and P. Ekins, 2015, The geographical distribution of fossil fuels unused when limiting global warming to 2 °C, *Nature* 517, 187–190.
- Miftakhova, A., K. L. Judd, T. S. Lontzek, and K. Schmedders, 2020, Statistical approximation of high-dimensional climate models, *Journal of Econometrics* 214, 67–80, Annals Issue: Econometric Models of Climate Change.
- Moore, F. C., K. Lacasse, K. J. Mach, Y. A. Shin, L. J. Gross, and B. Beckage, 2022, Determinants of emissions pathways in the coupled climate–social system, *Nature* 603, 103–111.
- Munk, C., and C. Sørensen, 2010, Dynamic asset allocation with stochastic income and interest rates, *Journal of Financial Economics* 96, 433–462.
- Nordhaus, W. D., 1991, To slow or not to slow: the economics of the greenhouse effect, *Economic Journal* 101, 920–937.
- Nordhaus, W. D., 2017, Revisiting the social cost of carbon, *Proceedings of the National Academy of Sciences* 114, 1518–1523.

- Olijslagers, S., F. van der Ploeg, and S. van Wijnbergen, 2023, On current and future carbon prices in a risky world, *Journal of Economic Dynamics and Control* 146, 104569.
- Pastor, L., R. F. Stambaugh, and L. A. Taylor, 2021, Sustainable investing in equilibrium, *Journal of Financial Economics* 142, 550–571.
- Pastor, L., R. F. Stambaugh, and L. A. Taylor, 2022, Dissecting green returns, *Journal of Financial Economics* 146, 403–424.
- Pindyck, R. S., and N. Wang, 2013, The economic and policy consequences of catastrophes, *American Economic Journal: Economic Policy* 5, 306–339.
- Rebonato, R., D. Kainth, L. Melin, and D. O’Kane, 2023, Optimal climate policy with negative emissions, *Working Paper*, EDHEC-Risk Climate Impact Institute.
- Rezai, A., and F. van der Ploeg, 2016, Intergenerational inequality aversion, growth and the role of damages: Occam’s rule for the global carbon tax, *Journal of the Association of Environmental and Resource Economists* 3, 499–522.
- United Nations, 2015, Paris Agreement to the United Nations Framework Convention on Climate Change, *T.I.A.S.* 16-1104.
- van den Bijgaart, I., R. Gerlagh, and M. Liski, 2016, A simple formula for the social cost of carbon, *Journal of Environmental Economics and Management* 77, 75–96.
- van den Bremer, T. S., C. Hambel, and F. van der Ploeg, 2023, Three reasons to price carbon under uncertainty: Accuracy of simple rules, *Working Paper*, Tinbergen Institute.
- van den Bremer, T. S., and F. van der Ploeg, 2021, The risk-adjusted carbon price, *American Economic Review*, 111, 2782–2810.
- van der Ploeg, F., 2018, The safe carbon budget, *Climatic Change* 147, 47–59.
- van der Ploeg, F., and A. de Zeeuw, 2018, Climate tipping and economic growth: precautionary capital and the price of carbon, *Journal of the European Economic Association* 16, 1577–1617.
- van der Ploeg, F., and A. Rezai, 2020, Stranded assets in the transition to a carbon-free economy, *Annual Review of Resource Economics* 12, 1–18.
- Wachter, J. A., 2013, Can time-varying risk of rare disasters explain aggregate stock market volatility?, *The Journal of Finance* 68, 987–1035.
- Wetzer, T., R. Stuard-Smith, and A. Dibley, 2024, Climate risk assessments must engage with the law, *Science* 383, 152–154.
- Zhang, S., 2024, Carbon returns across the globe, *Journal of Finance*, forthcoming.

Online Appendix to

Pricing in Transition and Physical Risks:

Carbon Premiums and Stranded Assets

Current version: June 2024

Abstract: Here we present additional material such as proofs, a description of the numerical solution algorithm, calibration details, and further simulation results and robustness checks.

Table of Contents

A Solution Approach	A-1
A.1 Hamilton-Jacobi-Bellman Equation	A-1
A.2 Optimal Carbon Tax and Negative Emission Technology	A-1
A.3 Share of Brown Capital	A-2
A.4 Separation and Reduced-Form Value Function	A-3
A.5 Numerical Solution Approach	A-7
B Asset Pricing	A-9
B.1 Dynamics of the Stochastic Discount Factor	A-9
B.2 Dividend Dynamics	A-12
B.3 Price-dividend Ratios of Dividend Claims	A-13
B.4 Risk Premiums	A-15
C Details on the Calibration	A-15
C.1 Benchmark Calibration	A-15
C.2 Negative Emission Technology	A-20
C.3 Alternative Calibrations for Energy Substitutability	A-21
D Additional Simulation Results	A-22
D.1 Additional Material for the Benchmark Simulation	A-22
D.2 PIGOU Scenario without Policy Transition Risks	A-24
D.3 BAU Scenario with no Negative Emission Technology	A-24
D.4 BAU Scenario with a Tighter Carbon Budget	A-29
D.5 Additional Material for the Risk of Stranded Assets	A-29

A Solution Approach

A.1 Hamilton-Jacobi-Bellman Equation

Applying the Bellman principle in continuous time, the value function $J = J(t, K_1, K_2, T, \mathbf{X})$ solves a non-linear partial differential equation, which is typically referred to as Hamilton-Jacobi-Bellman equation (e.g., Duffie and Epstein 1992b). This equation is given by

$$\begin{aligned}
0 = \max_{D, F_n, G_n, I_n, R} & \left\{ J_t + \delta \theta J \left(\frac{(\sum_{n=1,2} [Y_n - I_n - b_g G_n - b_f F_n - \zeta_n b_d(S, \mathbf{X}, D, K)])^{1-1/\psi}}{[(1-\gamma)J]^{1-\gamma}} - 1 \right) \right. \\
& + J_T \vartheta(\mathbf{X}) (v_t [F_1 + F_2] - D) + \frac{1}{2} J_{TT} \sigma_T^2 + J_{K_1} \left(I_1 - \frac{1}{2} \phi_1 \frac{I_1^2}{K_1} + R - \frac{1}{2} \kappa \frac{R^2}{K_1} - \delta_1^k K_1 \right) \\
& + \frac{1}{2} J_{K_1 K_1} K_1^2 \sigma_1^2 + J_{K_2} \left(I_2 - \frac{1}{2} \phi_2 \frac{I_2^2}{K_2} - R - \delta_2^k K_2 \right) + \frac{1}{2} J_{K_2 K_2} K_2^2 \sigma_2^2 + J_{K_1 K_2} K_1 K_2 \sigma_1 \sigma_2 \rho_{12} \\
& \left. + \sum_{i=c,e} \lambda_i(T, \mathbf{X}) \mathbb{E}[J(K_1 Z_i, K_2 Z_i, T, \mathbf{X}) - J] + \sum_{x \neq \mathbf{X}} \lambda_x(\mathbf{S}, \mathbf{X}, x) [J(K_1, K_2, T, x) - J] \right\}, \tag{A.1}
\end{aligned}$$

subject to the constraints $D, F_n, G_n, I_n, R \geq 0$. Subscripts of J denote partial derivatives, e.g., $J_{K_1} = \frac{\partial J}{\partial K_1}$.

A.2 Optimal Carbon Tax and Negative Emission Technology

The first-order condition for optimal fossil fuel use is

$$f_C(C, J) \left(\frac{\partial Y_n}{\partial F_n} - b_f \right) = -J_T \vartheta(\mathbf{X}) v_t.$$

Setting the marginal product of fossil fuel equal its marginal cost b_f plus the external costs of emitting greenhouse gases into the atmosphere,

$$\frac{\partial Y_n}{\partial F_n} = b_f + \tau_f.$$

The optimal Pigouvian social cost for using one unit of fossil fuel is thus

$$\tau_f = - \frac{\vartheta(\mathbf{X}) v_t J_T C^{1/\psi}}{\delta [(1-\gamma)J]^{1-1/\theta}}.$$

Taking the different units between fossil fuel and carbon emissions into account, the SCC is

$$\tau = - \frac{\vartheta(\mathbf{X}) J_T C^{1/\psi}}{\delta [(1-\gamma)J]^{1-1/\theta}}. \tag{A.2}$$

Since $\varsigma_1 + \varsigma_2 = 1$, the first-order conditions for optimal carbon removal give

$$f_C(C, J) \frac{\partial b_d(S, \mathbf{X}, D, K)}{\partial D} = -J_T \vartheta(\mathbf{X}).$$

A.3 Share of Brown Capital

To solve the Hamilton-Jacobi-Bellman equation (A.1), we first transform it by expressing the decision variables in relative terms and reducing the number of state variables by one. Let $g_n = G_n/K_n$, $f_n = F_n/K_n$, $i_n = I_n/K_n$, $r = R/K_1$ denote the relative control variables. Exploiting the homogeneity property of b_d , we use the notation $\tilde{b}_d(S, \mathbf{X}, D) = b_d(S, \mathbf{X}, D, K)/K$. We express the value function in terms of total capital $K = K_1 + K_2$ and share of brown capital $S = K_2/(K_1 + K_2)$ (instead of K_1 and K_2). Besides, we set $c = C/K$. Using the notation $S_1 = 1 - S$, $S_2 = S$, the production functions can then be expressed as

$$Y_n = A_n S_n K (\kappa_{1,n} g_n^{\rho_n} + \kappa_{2,n} f_n^{\rho_n})^{\frac{\eta_n}{\rho_n}} \Lambda_n(T).$$

The amounts of consumption goods produced by each sector are

$$C_n = S_n K \left[A_n (\kappa_{1,n} g_n^{\rho_n} + \kappa_{2,n} f_n^{\rho_n})^{\frac{\eta_n}{\rho_n}} \Lambda_n(T, \mathbf{X}) - i_n - b_g(S) g_n - b_f(S) f_n - \frac{\varsigma_n(S)}{S_n} \tilde{b}_d(S, \mathbf{X}, D) \right].$$

Therefore,

$$c = A_1(1-S) (\kappa_{1,1} g_1^{\rho_1} + \kappa_{2,1} f_1^{\rho_1})^{\frac{\eta_1}{\rho_1}} \Lambda_1(T, \mathbf{X}) + A_2 S (\kappa_{1,2} g_2^{\rho_2} + \kappa_{2,2} f_2^{\rho_2})^{\frac{\eta_2}{\rho_2}} \Lambda_2(T, \mathbf{X}) - i_1(1-S) - i_2 S - b_g(S) [g_1(1-S) + g_2 S] - b_f(S) [f_1(1-S) + f_2 S] - \tilde{b}_d(S, \mathbf{X}, D).$$

The dynamics of the state variables can be written as

$$\begin{aligned} dK_1 &= K_1 - \left[\left(i_1 - \frac{1}{2} \varphi_1 i_1^2 + r - \frac{1}{2} \kappa r^2 - \delta_1^k \right) dt + \sigma_1 dW_1 - \sum_{i=c,e} \ell_i dN_i \right], \\ dK_2 &= K_2 - \left[\left(i_2 - \frac{1}{2} \varphi_2 i_2^2 - r \frac{1-S}{S} - \delta_2^k \right) dt + \sigma_2 \left(\rho_{12} dW_1 + \sqrt{1-\rho_{12}^2} dW_2 \right) - \sum_{i=c,e} \ell_i dN_i \right], \\ dT &= \hat{\vartheta}(t, \mathbf{X}) [f_1(1-S) + f_2 S] dt - \vartheta(\mathbf{X}) D dt + \sigma_T dW_3 + \kappa_T - dX^c, \end{aligned}$$

where $\hat{\vartheta}(t, \mathbf{X}) = \vartheta(\mathbf{X}) K_0 e^{\int_0^t g_v(s) ds}$. To shorten the notation, we write $W = (W_1, W_2, W_3)^\top$ and denote the drift of the capital stocks and temperature by μ_{K_i} and μ_T , respectively. The dynamics of K and S can be calculated using Ito's lemma:

$$dS = S(1-S) \left[\mu_S(i_1, i_2, r, S) dt + (\sigma_2 \rho_{12} - \sigma_1) dW_1 + \sigma_2 \sqrt{1-\rho_{12}^2} dW_2 \right],$$

$$dK = K_- \left[\mu_K(i_1, i_2, r, S) dt + [(1-S)\sigma_1 + S\sigma_2\rho_{12}] dW_1 + S\sigma_2 \sqrt{1-\rho_{12}^2} dW_2 - \sum_{i=c,e} \ell_i dN_i \right],$$

where the drift rates are given by

$$\begin{aligned} \mu_S(i_1, i_2, r, S) &= \mu_{K_1} - \mu_{K_2} + S(\sigma_1\sigma_2\rho_{12} - \sigma_2^2) + (1-S)(\sigma_1^2 - \sigma_1\sigma_2\rho_{12}), \\ \mu_K(i_1, i_2, r, S) &= (1-S)\mu_{K_1} + S\mu_{K_2}. \end{aligned}$$

A.4 Separation and Reduced-Form Value Function

We solve a modified HJB equation with finite differences in terms of only three (S, T, \mathbf{X}) instead of four state variables $(K_1, K_2, T, \mathbf{X})$. For this to be possible, we must assume that the transition intensities $\lambda_\ell(\mathbf{S}, i, j)$ depend on S and T but not explicitly on K_1 and K_2 . The following proposition summarizes our findings for the PIGOU state. The situation for the CAP state is discussed in Corollary A.3.

Proposition A.1 (Value Function and Optimal Controls in the PIGOU state). *Let $\hat{\vartheta}(t, \mathbf{X}) = \vartheta(\mathbf{X})K_0 e^{\int_0^t g_v(s) ds}$. Suppose that there is no temperature cap in the current state. The value function (2.6) then has the form*

$$J(t, K_1, K_2, T, \mathbf{X}) = \frac{1}{1-\gamma} (K_1 + K_2)^{1-\gamma} V(t, T, S(K_1, K_2), \mathbf{X}). \quad (\text{A.3})$$

where V satisfies a certain HJB equation which is given in (A.12) below. Optimal consumption is

$$c = \sum_{n=1,2} S_n \left[A_n (\kappa_{1,n} g_n^{\rho_n} + \kappa_{2,n} f_n^{\rho_n})^{\frac{\eta_n}{\rho_n}} \Lambda_n(T, \mathbf{X}) - i_n - b_g(S) g_n - b_f(S) f_n - \frac{\zeta_n}{S_n} \tilde{b}_a(S, \mathbf{X}, D) \right]. \quad (\text{A.4})$$

Optimal energy use is

$$g_1 = \left(\frac{b_g(S)}{\eta_1 A_1 (\kappa_{1,1} + \kappa_{2,1} z^{\rho_1})^{\frac{\eta_1}{\rho_1} - 1} \Lambda_1(T, \mathbf{X}) \kappa_{1,1}} \right)^{\frac{1}{\eta_1 - 1}}, \quad f_1 = g_1 z_1, \quad (\text{A.5})$$

$$g_2 = \left(\frac{b_g(S)}{\eta_2 A_2 (\kappa_{1,2} + \kappa_{2,2} z^{\rho_2})^{\frac{\eta_2}{\rho_2} - 1} \Lambda_2(T, \mathbf{X}) \kappa_{1,2}} \right)^{\frac{1}{\eta_2 - 1}} \quad f_2 = g_2 z_2, \quad (\text{A.6})$$

where

$$\begin{aligned} z_1 &= \left(\frac{\kappa_{1,1}}{\kappa_{2,1} b_g(S)} \right)^{\frac{1}{\rho_1 - 1}} \left[b_f(S) - \frac{V_T \hat{\vartheta}(t, \mathbf{X}) (1-S)}{[(1-\gamma)V - V_S S][1 - \varphi_1 i_1]} \right]^{\frac{1}{\rho_1 - 1}}, \\ z_2 &= \left(\frac{\kappa_{1,2}}{\kappa_{2,2} b_g(S)} \right)^{\frac{1}{\rho_2 - 1}} \left[b_f(S) - \frac{V_T \hat{\vartheta}(t, \mathbf{X}) S}{[(1-\gamma)V - V_S S][1 - \varphi_1 i_1]} \right]^{\frac{1}{\rho_2 - 1}} \end{aligned}$$

The condition for the optimal reallocation strategy is

$$r = \frac{1}{\kappa} \left(\frac{V_S}{V_S S + (\gamma - 1)V} \right) \quad (\text{A.7})$$

and optimal investment and carbon removal solves the nonlinear system

$$\delta(1 - \gamma)V^{1-1/\theta} c^{-1/\psi} = [(1 - \gamma)V - V_S S][1 - \varphi_1 i_1], \quad (\text{A.8})$$

$$\delta(1 - \gamma)V^{1-1/\theta} c^{-1/\psi} = [(1 - \gamma)V + V_S(1 - S)][1 - \varphi_2 i_2], \quad (\text{A.9})$$

$$\delta(1 - \gamma)V^{1-1/\theta} c^{-1/\psi} = -V_T \vartheta(\mathbf{X}) \left(\frac{\partial \tilde{b}_d(S, \mathbf{X}, D)}{\partial D} \right)^{-1}, \quad (\text{A.10})$$

The optimal carbon tax is

$$\tau = \frac{\vartheta(\mathbf{X}) c^{1/\psi}}{\delta(\gamma - 1)} \frac{V_T}{V^{1-1/\theta}} K. \quad (\text{A.11})$$

Proof. Let $i_n = I_n/K_n$, $f_n = F_n/K_n$, $g_n = G_n/K_n$, $r = R/K_1$ denote the control variables in relative terms. Substituting these relative controls into (A.1) leads to the HJB equation:

$$\begin{aligned} 0 = & \sup_{D, i_n, f_n, g_n, r} \left\{ J_t + \frac{\delta}{1-1/\psi} [(1-\gamma)J]^{1-1/\theta} \left(\sum_{n=1,2} [Y_n - I_n - b_g G_n - b_f F_n - c_n b_d(S, \mathbf{X}, D, K)] \right)^{1-1/\psi} \right. \\ & - \delta \theta J + J_{K_1} K_1 \left(i_1 - \frac{1}{2} \varphi_1 i_1^2 + r - \frac{1}{2} \kappa r^2 - \delta_1^k \right) + J_{K_2} K_2 \left(i_2 - \frac{1}{2} \varphi_2 i_2^2 - r \frac{K_1}{K_2} - \delta_2^k \right) \\ & + \frac{1}{2} J_{K_1 K_1} K_1^2 \sigma_1^2 + \frac{1}{2} J_{K_2 K_2} K_2^2 \sigma_2^2 + J_{K_1 K_2} K_1 K_2 \sigma_1 \sigma_2 \rho_{12} + J_T [\hat{\vartheta}(f_1 S_1 + f_2 S_2) - \vartheta D] + J_{TT} \frac{1}{2} \sigma_T^2 \\ & \left. + \sum_{i=c,e} \lambda_i(T) \mathbb{E}[J(K_1 Z_i, K_2 Z_i, T, \mathbf{X}) - J] + \sum_{x \neq X} \lambda_x(\mathbf{S}, \mathbf{X}, x) [J(K_1, K_2, T, x) - J] \right\} \end{aligned}$$

We conjecture that the value function has the form

$$J(t, K_1, K_2, T, \mathbf{X}) = \frac{1}{1-\gamma} (K_1 + K_2)^{1-\gamma} V(t, T, S(K_1, K_2), \mathbf{X}).$$

The partial derivatives of S are $S_{K_1} = -\frac{S}{K}$, $S_{K_2} = \frac{1-S}{K}$. This specification implies³⁸

$$V(t, T, S, \mathbf{X}) > 0, \quad V_T(t, T, S, \mathbf{X}) > 0.$$

³⁸The sign of $V_S(t, T, S, \mathbf{X})$ is ambiguous because S indicates how CO₂ intensive the economy is but also how much the economy is diversified, see Hambel et al. (2024) for an extensive discussion about the interaction of abatement and diversification motives.

The relevant partial derivatives of the value function J are

$$\begin{aligned}
J_{K_1} &= K^{-\gamma}V + \frac{1}{1-\gamma}K^{1-\gamma}V_S \frac{-S}{K}, \\
J_{K_1K_1} &= -\gamma K^{-\gamma-1}V + 2K^{-\gamma}V_S \frac{-S}{K} + \frac{1}{1-\gamma}K^{1-\gamma} \left[V_{SS} \frac{S^2}{K^2} + 2V_S \frac{S}{K^2} \right], \\
J_{K_2} &= K^{-\gamma}V + \frac{1}{1-\gamma}K^{1-\gamma}V_S \frac{1-S}{K}, \\
J_{K_2K_2} &= -\gamma K^{-\gamma-1}V + 2K^{-\gamma}V_S \frac{1-S}{K} + \frac{1}{1-\gamma}K^{1-\gamma} \left[V_{SS} \frac{(1-S)^2}{K^2} - 2V_S \frac{1-S}{K^2} \right], \\
J_{K_1K_2} &= -\gamma K^{-1-\gamma}V + K^{-\gamma}V_S \frac{1-2S}{K} + \frac{1}{1-\gamma}K^{1-\gamma} \left[V_{SS} \frac{-(1-S)S}{K^2} + V_S \frac{2S-1}{K^2} \right], \\
J_T &= \frac{1}{1-\gamma}K^{1-\gamma}V_T.
\end{aligned}$$

The aggregator is given by $f(C, J) = K^{1-\gamma}[\delta\theta V^{1-1/\theta} c^{1-1/\psi} - \delta\theta V]$. Substituting the conjecture and its partial derivatives into the HJB equation leads to the following reduced-form HJB equation

$$0 = \sup_{D, f_n, g_n, i_n, r} \left\{ V_t + M_0 + M_1V + M_2V_S + M_3V_{SS} + M_4V_T + M_5V_{TT} \right\} \quad (\text{A.12})$$

We introduce the three-dimensional volatility vectors

$$\sigma_k(S) = \left((1-S)\sigma_1 + S\sigma_2\rho_{12}, S\sigma_2\sqrt{1-\rho_{12}^2}, 0 \right)^\top, \quad (\text{A.13})$$

$$\sigma_s = \left(\sigma_2\rho_{12} - \sigma_1, \sigma_2\sqrt{1-\rho_{12}^2}, 0 \right)^\top. \quad (\text{A.14})$$

The coefficients M_ℓ ($\ell = 1, \dots, 5$) are given by

$$\begin{aligned}
M_0 &= \delta\theta V^{1-1/\theta} c^{1-1/\psi} + \sum_{x \neq \mathbf{X}} \lambda_x(\mathbf{S}, \mathbf{X}, x) V(t, T, \mathbf{S}, x), \\
M_1 &= (1-\gamma) \left[\underbrace{(1-S)\mu_1 + S\mu_2}_{=\mu_k} - \frac{1}{2}\gamma \underbrace{[(1-S)^2\sigma_1^2 + S^2\sigma_2^2 + 2S(1-S)\sigma_1\sigma_2\rho_{12}]}_{=\|\sigma_k\|^2} \right] \\
&\quad + \sum_{i=c,e} \lambda_i(T) \mathbb{E}[(1-\ell_i)^{1-\gamma} - 1] - \sum_{x \neq \mathbf{X}} \lambda_x(\mathbf{S}, \mathbf{X}, x) - \delta\theta, \\
M_2 &= S(1-S) \left(\mu_2 - \mu_1 - \gamma \underbrace{[S\sigma_2^2 - (1-S)\sigma_1^2 + (1-2S)\sigma_1\sigma_2\rho_{12}]}_{=\sigma_k^\top \sigma_s} \right), \\
M_3 &= \frac{1}{2}(1-S)^2 S^2 \underbrace{[\sigma_1^2 + \sigma_2^2 - 2\sigma_1\sigma_2\rho_{12}]}_{=\|\sigma_s\|^2}, \\
M_4 &= \hat{\vartheta}(t, \mathbf{X}) [f_1(1-S) + f_2S] - \vartheta(\mathbf{X})D,
\end{aligned}$$

$$M_5 = \frac{1}{2}\sigma_T^2,$$

where c is given in (A.4) and $\widehat{\vartheta}(t, \mathbf{X}) = \vartheta(\mathbf{X})K_0 e^{\int_0^t g_v(s) ds}$. Calculating the first-order conditions leads to the system of equations (A.5) – (A.9), which determine the optimal controls. The optimal SCC follows from substituting the value function (A.3) into (A.2). \square

We emphasize that the proposition is also valid in the BAU state. Policy makers ignore the negative externalities from emitting CO₂, so behave as if $\Lambda_n(T, \mathbf{X}) = 0$ and $\lambda_c(T) = 0$. This implies in particular $V_T = 0$, $D = 0$, and $\tau = 0$.

Corollary A.2 (Tobin's Q's). *Under the conditions of Proposition A.1, the Tobin's Q's of the green and brown asset, respectively, are given by*

$$q_1 = \frac{(1-\gamma)V - V_S S}{\delta(1-\gamma)V^{1-1/\theta} c^{-1/\psi}}, \quad q_2 = \frac{(1-\gamma)V + V_S(1-S)}{\delta(1-\gamma)V^{1-1/\theta} c^{-1/\psi}}.$$

Proof. This follows immediately from (A.8) and (A.9). \square

Now, we consider the case where a temperature cap is implemented in some state \mathbf{X} , i.e., carbon emissions are only allowed as long as $T_t \leq T_{cap}$. If the carbon budget has been maxed out, i.e. if temperature exceeds T_{cap} , society is not allowed anymore to release CO₂ into the atmosphere.

Corollary A.3 (Optimal Controls in the CAP state). *Suppose that in state \mathbf{X} , carbon emissions are prohibited if temperature exceeds its limit T_{cap} .*

- (i) *If temperature is below the cap, $T \leq T_{cap}$, the indirect utility function and the optimal controls are as stated in Proposition A.1.*
- (ii) *If temperature exceeds T_{cap} , the separation (A.3) still holds, but the release of CO₂ into the atmosphere is no longer allowed, i.e. $f_n = 0$. Then, the optimal energy composites are*

$$e_n = g_n \kappa_{1,n}^{\frac{1}{\rho_n}} = \begin{cases} \left[\frac{b_g(S)}{A_n \eta_n \kappa_{1,n}^{\eta_n/\rho_n} \Lambda_n(T)} \right]^{\frac{1}{\eta_n-1}} \kappa_{1,n}^{\frac{1}{\rho_n}}, & \text{if } \rho_n > 0 \\ 0, & \text{if } \rho_n \leq 0. \end{cases} \quad (\text{A.15})$$

Optimal consumption is

$$c = \sum_{n=1,2} \left(S_n \left[A_n e_n^{\eta_n} \Lambda_n(T) - i_n - b_g(S) g_n - \frac{\zeta_n}{S_n} \tilde{b}_d(S, \mathbf{X}, D) \right] \right). \quad (\text{A.16})$$

The optimal reallocation strategy is

$$r = \frac{1}{\kappa} \left(\frac{V_S}{V_S S + (\gamma - 1)V} \right) \quad (\text{A.17})$$

and optimal investment and optimal carbon removal solve the nonlinear system

$$\delta(1 - \gamma)V^{1-1/\theta}c^{-1/\psi} = [(1 - \gamma)V - V_S S][1 - \varphi_1 i_1], \quad (\text{A.18})$$

$$\delta(1 - \gamma)V^{1-1/\theta}c^{-1/\psi} = [(1 - \gamma)V + V_S(1 - S)][1 - \varphi_2 i_2], \quad (\text{A.19})$$

$$\delta(1 - \gamma)V^{1-1/\theta}c^{-1/\psi} = -V_T \vartheta(\mathbf{X}) \left(\frac{\partial \tilde{b}_d(S, \mathbf{X}, D)}{\partial D} \right)^{-1}. \quad (\text{A.20})$$

The optimal SCC is as stated in Proposition A.1 and the Tobin's Q 's are as stated in Corollary A.2.

Proof. Along the lines of the proof of Proposition A.1. □

Although the decomposition of the indirect utility function and the optimal controls in (i) are unaffected when the temperature cap kicks in, the values are different. This is because V has a different shape in states with and without temperature cap. In the latter scenario, the value function is much steeper as temperature approaches T_{cap} .

A.5 Numerical Solution Approach

Basic Idea We face a problem with an infinite time horizon. To solve this problem we first compute the steady state $\tilde{V}(T, S, \mathbf{X})$ on a grid (T, S, \mathbf{X}) assuming there is no exogenous time trend. Thus, we first have to solve a similar PDE as in (A.12) but without the time derivative. The resulting steady state $\tilde{V}(T, S, \mathbf{X})$ is then used as a terminal condition $V(t_{\max}, T, S, \mathbf{X}) = \tilde{V}(T, S, \mathbf{X})$ for the value function in the year 2400 corresponding to $t_{\max} = 380$. Starting with this terminal condition, we proceed backwards through the time grid to analyze the transition towards the steady state.

Definition of the Grid We use a grid-based solution approach to solve the non-linear PDE. We discretize the (t, T, S) -space using an equally-spaced lattice. Its grid points are defined by

$$\{(t_n, T_i, S_j) \mid n = 0, \dots, N_t, i = 0, \dots, N_T, j = 0, \dots, N_S\},$$

where $t_n = n\Delta_t$, $T_i = i\Delta_T$, and $S_j = j\Delta_S$ for some fixed grid size parameters Δ_t , Δ_T , and Δ_S that denote the distances between two grid points. The numerical results are based on a choice of $N_T = 50$, $N_S = 200$ and one time step per year. Our results hardly change if we use a finer grid or more time steps per year.

In the sequel, $V_{n,i,j,k}$ denotes the approximated value function at the grid point $(t_n, T_i, S_j, \mathbf{X} = k)$ and $\pi_{n,i,j,k}$ refers to the corresponding set of optimal controls. We apply an implicit finite-difference scheme.

Finite Differences Approach We now describe the numerical solution approach in more detail. We adapt the numerical solution approach used by Munk and Sørensen (2010). The numerical procedure works as follows. At any point in time, we make a conjecture for the optimal strategy $\pi_{n,i,j,k}^*$. A good guess is the value at the previous grid point since the abatement strategy varies only slightly over a small time interval, i.e. we set $\pi_{n-1,i,j,k} = \pi_{n,i,j,k}^*$. Substituting this guess into the HJB equation yields a semi-linear PDE:

$$0 = V_t + \delta\theta V^{1-1/\theta} c^{1-1/\psi} + \sum_{x \neq \mathbf{X}} \lambda_x(\mathbf{S}, \mathbf{X}, x) V(t, T, S, x) + M_1 V + M_2 V_T + M_3 V_{TT} + M_4 V_S + M_5 V_{SS}$$

with state-dependent coefficients $M_i = M_i(t, T, S, \mathbf{X})$ as stated in Appendix A.4. Due to the implicit approach, we approximate the time derivative by forward finite differences. In the approximation, we use the so-called *up-wind* scheme that stabilizes the finite differences approach. Therefore, the relevant finite differences at the grid point (n, i, j, k) are given by

$$\begin{aligned} D_T^+ V_{n,i,j,k} &= \frac{V_{n,i+1,j,k} - V_{n,i,j,k}}{\Delta_T}, & D_T^- V_{n,i,j,k} &= \frac{V_{n,i,j,k} - V_{n,i-1,j,k}}{\Delta_T}, \\ D_S^+ V_{n,i,j,k} &= \frac{V_{n,i,j+1,k} - V_{n,i,j,k}}{\Delta_S}, & D_S^- V_{n,i,j,k} &= \frac{V_{n,i,j,k} - V_{n,i,j-1,k}}{\Delta_S}, \\ D_{TT}^2 V_{n,i,j,k} &= \frac{V_{n,i+1,j,k} - 2V_{n,i,j,k} + V_{n,i-1,j,k}}{\Delta_T^2}, \\ D_{SS}^2 V_{n,i,j,k} &= \frac{V_{n,i,j+1,k} - 2V_{n,i,j,k} + V_{n,i,j-1,k}}{\Delta_S^2}, \\ D_t^+ V_{n,i,j,k} &= \frac{V_{n+1,i,j,k} - V_{n,i,j,k}}{\Delta_t}. \end{aligned}$$

Substituting these expressions into the PDE above yields the following semi-linear equation for the grid point (t_n, T_i, S_j, k) :

$$\begin{aligned} V_{n+1,i,j,k} \frac{1}{\Delta_t} &= V_{n,i,j,k} \left[-M_1 + \frac{1}{\Delta_t} + \text{abs}\left(\frac{M_2}{\Delta_T}\right) + \text{abs}\left(\frac{M_4}{\Delta_S}\right) + 2\frac{M_3}{\Delta_T^2} + 2\frac{M_5}{\Delta_S^2} \right] \\ &+ V_{n,i-1,j,k} \left[\frac{M_2^-}{\Delta_T} - \frac{M_3}{\Delta_T^2} \right] + V_{n,i+1,j,k} \left[-\frac{M_2^+}{\Delta_T} - \frac{M_3}{\Delta_T^2} \right] \\ &+ V_{n,i,j-1,k} \left[\frac{M_4^-}{\Delta_S} - \frac{M_5}{\Delta_S^2} \right] + V_{n,i,j+1,k} \left[-\frac{M_4^+}{\Delta_S} - \frac{M_5}{\Delta_S^2} \right] \\ &+ \delta\theta V_{n,i,j,k}^{1-1/\theta} c_{n,i,j,k}^{1-1/\psi} + \sum_{\hat{k} \neq k} \lambda(\mathbf{S}, k, \hat{k}) V_{n,i,j,\hat{k}}. \end{aligned}$$

Therefore, for a fixed point in time each grid point is determined by a non-linear equation. This results in a non-linear system of $(N_S + 1)(N_T + 1)$ equations for every state k of the Markov chain \mathbf{X} that can be solved for the vector

$$V_{n,k} = (V_{n,1,1,k}, \dots, V_{n,1,N_S,k}, V_{n,2,1,k}, \dots, V_{n,2,N_S,k}, \dots, V_{n,N_T,1,k}, \dots, V_{n,N_T,N_S,k}).$$

Using this solution we update our conjecture for the optimal controls at the current point in the time dimension. We apply the first-order conditions as stated in Proposition A.1 and determine the optimal strategies and the optimal SCC with the above-mentioned finite-difference approximations of the corresponding partial derivatives. After we have solved the model, we simulate all state and decision variables in a Monte-Carlo simulation. We simulate 200,000 paths and calculate quantiles, means, and other moments for all relevant variables.

B Asset Pricing

B.1 Dynamics of the Stochastic Discount Factor

Duffie and Epstein (1992a) show that the dynamics of the pricing kernel H are given by

$$\frac{dH}{H_-} = \frac{df_c(C, J)}{f_c(C, J)} + f_J(C, J)dt.$$

The relevant partial derivatives of the aggregator are

$$f_c(C, J) = \delta V^{1-1/\theta} K^{-\gamma} c^{-1/\psi}, \quad f_J(C, J) = \delta(\theta - 1)c^{1-1/\psi} V^{-1/\theta} - \delta\theta.$$

To calculate the dynamics of the SDF, we first compute

$$\frac{dK^{-\gamma}}{K_-^{-\gamma}} = \left(-\gamma\mu_k + \frac{1}{2}\gamma(\gamma+1)\|\sigma_k\|^2 \right) dt - \gamma\sigma_k^\top dW + \sum_{i=c,e} ((1-\ell_i)^{-\gamma} - 1)dN_i.$$

Secondly, we determine the dynamics of $V^{1-1/\theta}$. According to Ito's lemma, $V = V(t, S, T, \mathbf{X})$ satisfies

$$\frac{dV}{V_-} = \mu_v dt + \sigma_v^\top dW - \sum_{x \neq \mathbf{X}} j_v^x dN^x$$

where N^x is a point process that indicates a jump to state x , i.e.,

$$N_{\tau_x}^x = \begin{cases} N_{\tau_x^-}^x + 1: & \mathbf{X}_{\tau_x} = x, \mathbf{X}_{\tau_x^-} \neq x \\ N_{\tau_x^-}^x: & \text{else} \end{cases}$$

with

$$\mu_v = \frac{1}{V_-} \left(V_t + V_S S(1-S)\mu_s + V_T \partial v(f_1(1-S) + f_2 S) - V_T \partial D \right. \\ \left. + \frac{1}{2} V_{SS} S^2 (1-S)^2 \|\sigma_s\|^2 + \frac{1}{2} V_{TT} \sigma_T^2 \right), \quad (\text{B.1})$$

$$\sigma_v = \frac{1}{V_-} \left(V_S S(1-S)(-\sigma_1 + \sigma_2 \rho_{12}), V_S S(1-S)\sigma_2 \sqrt{1-\rho_{12}^2}, V_T \sigma_T \right)^\top, \quad (\text{B.2})$$

$$j_v^x = 1 - \frac{V(t, T, S, x)}{V(t, T, S, \mathbf{X})}. \quad (\text{B.3})$$

Another application of Ito's lemma yields

$$\frac{dV^{1-1/\theta}}{V_-^{1-1/\theta}} = \left[\frac{\theta-1}{\theta} \mu_v - \frac{\theta-1}{2\theta^2} \|\sigma_v\|^2 \right] dt + \frac{\theta-1}{\theta} \sigma_v^\top dW + \sum_{x \neq \mathbf{X}} \left((1-j_v^x)^{1-1/\theta} - 1 \right) dN^x.$$

Therefore, by Ito's product rule,

$$\frac{d(V^{1-1/\theta} K^{-\gamma})}{(V^{1-1/\theta} K^{-\gamma})_-} = \left(-\gamma \mu_k + \frac{1}{2} \gamma(\gamma+1) \|\sigma_k\|^2 \right) dt + \frac{\theta-1}{\theta} \left(\mu_v - \gamma \langle \sigma_k, \sigma_s \rangle \frac{V_S}{V} S(1-S) \right) dt \\ - \frac{\theta-1}{2\theta^2} \|\sigma_s\|^2 \frac{V_S^2}{V^2} S^2 (1-S)^2 dt + \left(\frac{\theta-1}{\theta} \sigma_v - \gamma \sigma_k \right)^\top dW + \sum_{i=c,e} \left((1-\ell_i)^{-\gamma} - 1 \right) dN_i \\ + \sum_{x \neq \mathbf{X}} \left((1-j_v^x)^{1-1/\theta} - 1 \right) dN^x. \quad (\text{B.4})$$

Notice that according to the simplified HJB equation (A.12),

$$\mu_v - \gamma \langle \sigma_k, \sigma_s \rangle \frac{V_S}{V} S(1-S) = (\gamma-1) \left(\mu_k - \frac{1}{2} \gamma \|\sigma_k\|^2 \right) + \delta\theta - \delta\theta V^{-1/\theta} c^{1-1/\psi} \\ - \sum_{i=c,e} \lambda_i \mathbb{E}[(1-\ell_i)^{1-\gamma} - 1] + \sum_{x \neq \mathbf{X}} \lambda_x j_v^x,$$

where we use the short-hand notation $\lambda_x = \lambda_x(\mathbf{S}, \mathbf{X}, x)$. Substituting this term into (B.4) yields

$$\frac{d(V^{1-1/\theta} K^{-\gamma})}{(V^{1-1/\theta} K^{-\gamma})_-} = \left(-\gamma \mu_k + \frac{1}{2} \gamma(\gamma+1) \|\sigma_k\|^2 \right) dt - \frac{\theta-1}{2\theta^2} \|\sigma_s\|^2 \frac{V_S^2}{V^2} S^2 (1-S)^2 dt \\ + \left(\frac{\theta-1}{\theta} \sigma_v - \gamma \sigma_k \right)^\top dW$$

$$\begin{aligned}
& + \frac{\theta-1}{\theta} \left((\gamma-1) \left(\mu_k - \frac{1}{2} \gamma \|\sigma_k\|^2 \right) + \delta\theta - \delta\theta V^{-1/\theta} c^{1-1/\psi} \right) dt + \sum_{i=c,e} \left((1-\ell_i)^{-\gamma} - 1 \right) dN_i \\
& + \sum_{x \neq \mathbf{X}} \left((1-j_v^x)^{1-1/\theta} - 1 \right) dN^x - \frac{\theta-1}{\theta} \left(\sum_{i=c,e} \lambda_i \mathbb{E} \left[(1-\ell_i)^{1-\gamma} - 1 \right] - \sum_{x \neq \mathbf{X}} \lambda_x j_v^x \right) dt.
\end{aligned}$$

Furthermore, the consumption-capital ratio $c = C/K$ has the following dynamics

$$\frac{dc}{c_-} = \mu_c dt + \sigma_c^\top dW - \sum_{x \neq \mathbf{X}} j_c^x dN^x$$

for auxiliary functions $\mu_c(t, T, S, \mathbf{X})$ and $\sigma_c(t, T, S, \mathbf{X})$, which can be determined numerically, and

$$j_c^x = 1 - \frac{c(t, T, S, x)}{c(t, T, S, \mathbf{X})}. \quad (\text{B.5})$$

In turn,

$$\frac{dc^{-1/\psi}}{c_-^{-1/\psi}} = -\frac{1}{\psi} (\mu_c dt + \sigma_c^\top dW) + \frac{1+\psi}{\psi^2} \|\sigma_c\|^2 dt + \sum_{x \neq \mathbf{X}} \left((1-j_c^x)^{-1/\psi} - 1 \right) dN^x$$

Consequently, the pricing kernel dynamics are given by

$$\begin{aligned}
\frac{dH_-}{H_-} & = -r_t^f dt + \left(-\gamma\sigma_k + \frac{\theta-1}{\theta}\sigma_v - \frac{1}{\psi}\sigma_c \right)^\top dW + \sum_{i=c,e} \left((1-\ell_i)^{-\gamma} - 1 \right) dN_i - \lambda_i \mathbb{E} \left[(1-\ell_i)^{-\gamma} - 1 \right] dt \\
& + \sum_{x \neq \mathbf{X}} \left[\left((1-j_v^x)^{1-1/\theta} (1-j_c^x)^{-1/\psi} - 1 \right) dN^x - \lambda_x \left((1-j_v^x)^{1-1/\theta} (1-j_c^x)^{-1/\psi} - 1 \right) dt \right], \quad (\text{B.6})
\end{aligned}$$

where the risk-free rate is given by

$$\begin{aligned}
r_t^f & = \delta + \frac{1}{\psi} \mu_k - \frac{1}{2} \gamma \left(1 + \frac{1}{\psi} \right) \|\sigma_k\|^2 - \left(\frac{1+\psi}{\psi^2} \|\sigma_c\|^2 - \frac{\theta-1}{2\theta^2} \|\sigma_v\|^2 - \frac{1}{\psi} \sigma_c^\top \left(\frac{\theta-1}{\theta} \sigma_v - \gamma\sigma_k \right) \right) \\
& - \sum_{i=c,e} \lambda_i \mathbb{E} \left[(1-\ell_i)^{-\gamma} - 1 + \frac{\psi^{-1}-\gamma}{1-\gamma} (1 - (1-\ell_i)^{1-\gamma}) \right] \\
& - \sum_{x \neq \mathbf{X}} \left[\lambda_x \left((1-j_v^x)^{1-1/\theta} (1-j_c^x)^{-1/\psi} - 1 \right) + \frac{\theta-1}{\theta} \lambda_x j_v^x \right].
\end{aligned}$$

An application of Itô's lemma gives the drift and volatility vector of optimal consumption as

$$\mu_C(t, T, S) = \mu_k(S) + \mu_c(t, T, S) + \langle \sigma_c(t, T, S), \sigma_k(S) \rangle, \quad (\text{B.7})$$

$$\sigma_C(t, T, S) = \sigma_k(S) + \sigma_c(t, T, S). \quad (\text{B.8})$$

Substituting (B.7) and (B.8) into the pricing kernel dynamics and some algebra completes the proof. \square

B.2 Dividend Dynamics

The amount of consumption goods produced by asset n are

$$C_n = Y_n - I_n - b_f F_n - b_g G_n - b_d(S, \mathbf{X}, D, K) = \chi_n K_n$$

with $\chi_n = [A_n (\kappa_{1,n} g_n^{\rho_n} + \kappa_{2,n} f_n^{\rho_n})^{\frac{1}{\rho_n}} \Lambda_n(T) - i_n - b_g(S) g_n - b_f(S) f_n - \tilde{b}_d(S, \mathbf{X}, D)]$. An application of Ito's lemma shows that χ_n evolves according to

$$\frac{d\chi_n}{\chi_n} = \mu_{\chi_n} dt + \sigma_{\chi_n}^\top dW - \sum_{x \neq \mathbf{X}} j_{\chi_n}^x dN^x$$

for auxiliary functions μ_{χ_n} , σ_{χ_n} , $j_{\chi_n}^x$ that can be determined numerically along the lines of (B.1) – (B.3). Notice that χ_n is unaffected when the economy is hit by an economic Barro-type disaster shock N^d .

Empirically, dividends are more volatile than consumption (e.g. Bansal and Yaron 2004) and dividends fall more than consumption when a disaster hits the economy (e.g. Longstaff and Piazzesi 2004). Following Wachter (2013), among others, we thus model dividends as levered consumption, i.e. $\mathcal{D}_n = C_n^\phi$ for $\phi \geq 1$.³⁹ An application of Ito's product rule yields the dividend dynamics

$$\frac{d\mathcal{D}_n}{\mathcal{D}_n} = \mu_{\mathcal{D}_n} dt + \sigma_{\mathcal{D}_n}^\top dW + \sum_{i=c,e} j_{\mathcal{D}_n}^i dN^i + \sum_{x \neq \mathbf{X}} j_{\mathcal{D}_n}^x dN^x$$

with

$$\begin{aligned} \mu_{\mathcal{D}_n} &= \phi(\mu_{K_n} + \mu_{\chi_n} + \sigma_{\chi_n}^\top \sigma_{K_n}) + \frac{1}{2} \phi(\phi - 1) \|\sigma_{K_n} + \sigma_{\chi_n}\|^2, \\ \sigma_{\mathcal{D}_n} &= \phi(\sigma_{K_n} + \sigma_{\chi_n}), \\ j_{\mathcal{D}_n}^i &= (1 - \ell_i)^\phi - 1, \\ j_{\mathcal{D}_n}^x &= (1 - j_{\chi_n}^x)^\phi - 1. \end{aligned}$$

In a next step, we determine the dynamics of discounted dividends, $\widehat{\mathcal{D}}_n = H\mathcal{D}_n$. Another application of Ito's product rule implies

$$\frac{d\widehat{\mathcal{D}}_n}{\widehat{\mathcal{D}}_n} = \mu_{\widehat{\mathcal{D}}_n} dt + \sigma_{\widehat{\mathcal{D}}_n}^\top dW + \sum_{i=c,e} j_{\widehat{\mathcal{D}}_n}^i dN^i + \sum_{x \neq \mathbf{X}} j_{\widehat{\mathcal{D}}_n}^x dN^x$$

³⁹A popular alternative to this approach is modelling the consumption-dividend ratio as a stationary but persistent process, as in Longstaff and Piazzesi (2004), among others. In order to focus on the novel implications of climate transition risk on asset prices, we keep the setting simple although following this approach would also be feasible in our setting.

with

$$\begin{aligned}\mu_{\widehat{\mathcal{D}}_n} &= \mu_H + \mu_{\mathcal{D}_n} + \sigma_H^\top \sigma_{\mathcal{D}_n}, \\ \sigma_{\widehat{\mathcal{D}}_n} &= \sigma_H + \sigma_{\mathcal{D}_n}, \\ j_{\widehat{\mathcal{D}}_n}^i &= (1 - \ell_i)^{\phi - \gamma} - 1, \\ j_{\widehat{\mathcal{D}}_n}^x &= (1 - j_{\chi_n}^x)^\phi (1 - j_v^x)^{1 - 1/\theta} (1 - j_c^x)^{-1/\psi} - 1.\end{aligned}$$

B.3 Price-dividend Ratios of Dividend Claims

Let $\Pi_n = \frac{P_n}{\mathcal{D}_n}$ denote the price-dividend ratio of asset n , and $\pi_n = \log\left(\frac{P_n}{\mathcal{D}_n}\right)$ the log price-dividend ratio. Due to the representation of the dividends, the dynamics of K_n , and the pricing equation, the price is linear in K_n and thus the price-dividend ratio is independent of K_n . Therefore, it is not driven by the disaster risk process N^d , and the dynamics of the log price-dividend ratio can be written as

$$\frac{d\pi_n}{\pi_{n-}} = \mu_{\pi_n} dt + \sigma_{\pi_n}^\top dW - \sum_{x \neq \mathbf{X}} j_{\pi_n}^x dN^x,$$

where the drift and the volatility vector are given by

$$\begin{aligned}\mu_{\pi_n} &= \frac{1}{\pi_n} \left[\pi_{n,t} + \pi_{n,S} S(1-S)\mu_S + \pi_{n,T} \mu_T + \frac{1}{2} \pi_{n,TT} \|\sigma_T\|^2 + \frac{1}{2} \pi_{n,SS} S^2(1-S)^2 \|\sigma_S\|^2 \right], \\ \sigma_{\pi_n} &= \frac{1}{\pi_n} \left[\pi_{n,T} \sigma_T + \pi_{n,S} S(1-S) \sigma_S \right], \\ j_{\pi_n}^x &= 1 - \frac{\pi_n(t, T, S, x)}{\pi_n(t, T, S, \mathbf{X})}.\end{aligned}$$

In particular, the price-dividend ratio $\Pi_n = e^{\pi_n}$ satisfies the following dynamics

$$\frac{d\Pi_n}{\Pi_{n-}} = \left(\pi_n \mu_{\pi_n} + \frac{1}{2} \pi_n^2 \|\sigma_{\pi_n}\|^2 \right) dt + \pi_n \sigma_{\pi_n}^\top dW - \sum_{x \neq \mathbf{X}} j_{\Pi_n}^x dN^x,$$

where

$$j_{\Pi_n}^x = 1 - \frac{\Pi_n(t, T, S, x)}{\Pi_n(t, T, S, \mathbf{X})}.$$

We rewrite the discounted asset price HP_n as $\widehat{P}_n(\widehat{\mathcal{D}}_n, \pi_n) = \widehat{\mathcal{D}}_n e^{\pi_n}$. An application of Itô's lemma implies

$$\frac{d\widehat{P}_n}{\widehat{P}_{n-}} = \left(\mu_{\widehat{\mathcal{D}}_n} + \pi_n \mu_{\pi_n} + \frac{1}{2} \pi_n^2 \|\sigma_{\pi_n}\|^2 + \pi_n \sigma_{\pi_n}^\top \sigma_{\widehat{\mathcal{D}}_n} \right) dt + (\pi_n \sigma_{\pi_n} + \sigma_{\widehat{\mathcal{D}}_n})^\top dW$$

$$+ \sum_{i=c,e} ((1-\ell_i)^{\phi-\gamma} - 1) dN_i + \sum_{x \neq \mathbf{X}} ((1-j_{\Pi_n}^x)(1+j_{\hat{\mathcal{D}}_n}^x) - 1) dN^x.$$

An application of the Feynman-Kač Theorem yields

$$\mathcal{L}\hat{P}_n + e^{-\pi_n}\hat{P}_n = 0, \quad (\text{B.9})$$

where $\mathcal{L}\hat{P}_n$ denotes the infinitesimal generator. The no-arbitrage condition implies

$$\begin{aligned} \frac{\mathcal{L}\hat{P}_n}{\hat{P}_n} &= \mu_{\hat{\mathcal{D}}_n} + \pi_n \mu_{\pi_n} + \frac{1}{2} \pi_n^2 \|\sigma_{\pi_n}\|^2 + \pi_n \sigma_{\pi_n}^\top \sigma_{\hat{\mathcal{D}}_n} + \sum_{i=c,e} \lambda_i(T) \mathbb{E}[(1-\ell_i)^{\phi-\gamma} - 1] \\ &+ \sum_{x \neq \mathbf{X}} \lambda_x((1-j_{\Pi_n}^x)(1+j_{\hat{\mathcal{D}}_n}^x) - 1). \end{aligned} \quad (\text{B.10})$$

Substituting (B.10) into (B.9) yields

$$\begin{aligned} 0 &= \mu_{\hat{\mathcal{D}}_n} + \pi_n \mu_{\pi_n} + \frac{1}{2} \pi_n^2 \|\sigma_{\pi_n}\|^2 + \pi_n \sigma_{\pi_n}^\top \sigma_{\hat{\mathcal{D}}_n} + \sum_{i=c,e} \lambda_i(T) \mathbb{E}[(1-\ell_i)^{\phi-\gamma} - 1] + e^{-\pi} \\ &+ \sum_{x \neq \mathbf{X}} \lambda_x((1-j_{\Pi_n}^x)(1+j_{\hat{\mathcal{D}}_n}^x) - 1). \end{aligned}$$

Consequently, we obtain the following partial differential equation for the log price-dividend ratio π_n :

$$\begin{aligned} 0 &= e^{-\pi_n} + \mu_{\hat{\mathcal{D}}_n} + \pi_{n,t} + \pi_{n,S} S(1-S) \mu_S + \pi_{n,T} \mu_T + \frac{1}{2} (\pi_{n,TT} + \pi_{n,T}^2) \|\sigma_T\|^2 \\ &+ \frac{1}{2} (\pi_{n,SS} + \pi_{n,S}^2) S^2 (1-S)^2 \|\sigma_S\|^2 + (\pi_{n,T} \sigma_T + \pi_{n,S} S(1-S) \sigma_S)^\top \sigma_{\hat{\mathcal{D}}_n} \\ &+ \sum_{i=c,e} \lambda_i(T) \mathbb{E}[(1-\ell_i)^{\phi-\gamma} - 1] + \sum_{x \neq \mathbf{X}} \lambda_x((1-j_{\Pi_n}^x)(1+j_{\hat{\mathcal{D}}_n}^x) - 1). \end{aligned}$$

Notice that this PDE is nonlinear since it involves squared partial derivatives of π_n . To simplify the numerical solution approach, we transform this PDE into a linear, parabolic PDE that can be solved using finite differences. We substitute $\Pi_n = e^{\pi_n}$ and end up with

$$\begin{aligned} 0 &= 1 + \sum_{x \neq \mathbf{X}} \lambda_x \Pi_n(t, T, S, x) (1 + j_{\hat{\mathcal{D}}_n}^x) + \Pi_n \left(\mu_{\hat{\mathcal{D}}_n} + \sum_{i=c,e} \lambda_i(T) \mathbb{E}[(1-\ell_i)^{\phi-\gamma} - 1] - \sum_{x \neq \mathbf{X}} \lambda_x \right) \\ &+ \Pi_{n,t} + \Pi_{n,S} S(1-S) \mu_S + \Pi_{n,T} \mu_T + \frac{1}{2} \Pi_{n,TT} \|\sigma_T\|^2 + \frac{1}{2} \Pi_{n,SS} S^2 (1-S)^2 \|\sigma_S\|^2 \\ &+ (\Pi_{n,T} \sigma_T + \Pi_{n,S} S(1-S) \sigma_S)^\top \sigma_{\hat{\mathcal{D}}_n} \end{aligned} \quad (\text{B.11})$$

B.4 Risk Premiums

The dynamics of the asset price $P_n = e^{\pi_n} \mathcal{D}_n$ follow by Itô's lemma. We obtain the following asset price dynamics

$$\begin{aligned} \frac{dP_n}{P_{n-}} &= \mu_n^p dt + (\sigma_{\pi_n} + \sigma_{\mathcal{D}_n})^\top dW + \sum_{i=c,e} ((1 - \ell_i)^\phi - 1) dN_i - \lambda_i(T) \mathbb{E}[(1 - \ell_i)^\phi - 1] dt \\ &\quad + \sum_{x \neq \mathbf{X}} \left[((1 - j_{\Pi_n}^x)(1 + j_{\mathcal{D}_n}^x) - 1) dN^x - \lambda_x((1 - j_{\Pi_n}^x)(1 + j_{\mathcal{D}_n}^x) - 1) \right], \end{aligned}$$

where the expected stock return and the volatility vector are given by

$$\mu_n^p = \mu_{\pi_n} + \mu_{\mathcal{D}_n} + \sigma_{\mathcal{D}_n}^\top \sigma_{\pi_n} + \frac{1}{2} \|\sigma_{\pi_n}\|^2 + \sum_{i=c,e} \lambda_i(T) \mathbb{E}[(1 - \ell_i)^\phi - 1] + \sum_{x \neq \mathbf{X}} \lambda_x((1 - j_{\Pi_n}^x)(1 + j_{\mathcal{D}_n}^x) - 1).$$

Now, the risk premium of asset n can be computed as the sum of its expected stock return, μ_{P_n} , and its dividend yield, $y_n^d = e^{-\pi_n}$, minus the risk-free interest rate, r^f , i.e.

$$r_n^p = \mu_n^p + y_n^d - r^f.$$

C Details on the Calibration

Here we provide further calibration details for all relevant parts of the model. We also present alternative calibrations used for sensitivity analyses and robustness checks.

C.1 Benchmark Calibration

Macroeconomic Uncertainty We set annual volatility of capital diffusion risk to $\sigma_1 = \sigma_2 = 2\%$ matching the observed volatility of consumption or output (e.g., Wachter 2013). We assume a zero *instantaneous correlation* between the two capital stocks, $\rho_{12} = 0$ (cf. Cochrane et al., 2007). The total correlation between capital stocks is much higher than indicated by the value of ρ_{12} due to joint macroeconomic disaster shocks and common state variables that affect both sectors (cf. Hambel et al., 2024).

The recovery rates of macroeconomic and climate-related disasters, respectively, $Z_i = 1 - \ell_i$, $i \in \{c, e\}$, have a power distribution over $(0, 1)$ with parameter $\alpha_i > 0$ and density functions $\zeta_i(Z_i) = \alpha_i Z_i^{\alpha_i - 1}$, $Z_i \in (0, 1)$ (Pindyck and Wang, 2013). The n^{th} moment of the recovery rate is $\mathbb{E}[Z_i^n] = \frac{\alpha_i}{\alpha_i + n}$. To calibrate the macroeconomic disaster-size distribution, we follow Wachter (2013) and define a disaster as an event destroying more than $\bar{\ell} = 10\%$ of GDP or aggregate consumption. She uses historical consumption data

to estimate an annual disaster probability of 3.55% and an average consumption loss of 25% when a disaster strikes: $\lambda_e \int_0^{1-\bar{\ell}} \zeta_e(Z) dZ = 0.0355$ and $\mathbb{E}[\ell_e | \ell_e > \bar{\ell}] = 0.25$. This pins down $\alpha_e = 5$ and $\lambda_e = 0.06$.

Economic Growth To jointly calibrate the production and preference parameters, we follow Hambel et al. (2024) and firstly consider a model with only one capital share in the spirit of Pindyck and Wang (2013). Their model also abstracts from climate change, but it is nested in our two-sector model. The model is well-suited to explain *historical* asset returns, since dirty capital dominated the world economy in the past, while the influence of climate change on asset markets was modest. We assume that the single-capital stock evolves according to

$$dK = \left(I - \frac{1}{2} \phi \frac{I^2}{K} - \delta_k K \right) dt + K \sigma dW - K \ell_e dN_e.$$

Besides, output is produced by capital K and energy E by a Cobb-Douglas production technology, $Y = AK^{1-\eta}E^\eta = I + C + bE$, where b is the price of one unit of the energy composite E . In the optimum, the model becomes a simple AK -technology with linear production function $Y = A^*K$ where productivity is

$$A^* = A \left(\frac{b}{\eta A} \right)^{\frac{\eta}{\eta-1}}.$$

This aggregate model closely follows Pindyck and Wang (2013), but involves an energy input E . We solve this model for a representative investor with Epstein-Zin-preferences and obtain a set of non-linear equations that pin down the model parameters.

Fixing the leverage parameter at $\phi = 2.6$ (Wachter 2013) and the elasticity of intertemporal substitution at $\psi = 1.5$ (Bansal and Yaron 2004), we calibrate the remaining parameters to match an expected GDP growth rate of $\bar{\mu} = 2.52\%$ in normal times, i.e. in the absence of a disaster (Wachter 2013), an average consumption rate of $\frac{C}{Y} = 63\%$ of GDP, a risk-free interest rate of $r^f = 0.8\%$, an equity premium of $r^p = 6.6\%$, and a Tobin's Q of 1.548 (Pindyck and Wang 2013). Following the calculations in Pindyck and Wang (2013) but taking leverage into account one obtains a non-linear system that involves five equations and five unknowns $A^*, \phi, \delta_k, \delta, \gamma$. For the risk-free rate and the risk premium, one obtains

$$r^f = \delta + \frac{\bar{\mu}}{\psi} - \frac{1}{2} \gamma \left(1 + \frac{1}{\psi} \right) \sigma^2 - \lambda_e \left(\frac{\alpha_e}{\alpha_e - \gamma + 1} \frac{1/\psi - \gamma}{1 - \gamma} - \frac{\alpha_e}{\alpha_e - \gamma} \right), \quad (\text{C.1})$$

$$r^p = \phi \gamma \sigma^2 + \lambda_e \gamma \left[\frac{\alpha_e}{\alpha_e - \gamma} - \frac{\alpha_e}{\alpha_e - \gamma + \phi} + \frac{\alpha_e}{\alpha_e + \phi} - 1 \right]. \quad (\text{C.2})$$

Given the values of σ , λ_e , and α_e , (C.2) pins down the degree of relative risk aversion γ . Then, (C.1) can be solved for the time preference rate δ . Then, we determine the productivity by

$$A^* = \frac{q}{\chi} \left[\delta + \left(\frac{1}{\psi} - 1 \right) \left(\bar{\mu} - \frac{1}{2} \gamma \sigma^2 - \frac{\lambda_e}{1 - \gamma} \frac{\alpha_e}{\alpha_e - \gamma + 1} \right) \right]. \quad (\text{C.3})$$

In equilibrium, the model generates an investment-capital ratio of $i = A^*(1 - \chi - \eta)$ and Tobin's Q is $q = \frac{1}{1 - \varphi i}$. Hence, the adjustment cost parameter φ is given by

$$\varphi = \frac{1 - 1/q}{i}. \quad (\text{C.4})$$

Finally, the capital depreciation rate δ_k is given by

$$\delta_k = i - 0.5\varphi i^2 - \bar{\mu}. \quad (\text{C.5})$$

We use the above equations to calibrate the remaining preference parameters, the depreciation rate, the investment adjustment cost parameters, and the total factor productivities given in Table 1 to match an expected GDP growth rate of $\bar{\mu} = 2.52\%$ in normal times without disasters (Wachter, 2013), a consumption share of $\frac{C}{Y} = 63\%$ of GDP, a risk-free interest rate of $r^f = 0.8\%$, an equity risk premium of $r^p = 6.6\%$, and a Tobin's Q of 1.548 (Pindyck and Wang, 2013).

Energy Consumption We set the energy shares in the production functions to $\eta_i = 0.043$ (van den Bremer and van der Ploeg, 2021).⁴⁰ We set the initial cost of fossil fuel to $b_f(S_0) = \$540/\text{tC}$ (cf. van den Bremer and van der Ploeg, 2021), but use a significantly higher initial cost of green energy, $b_g(S_0) = \$810/\text{etC}$, in line with production costs in developed countries. We suppose that the cost parameter for green energy gradually declines over time as the green transition progresses by setting $b_g(S_t) = b_g(S_0)k_0(1 - S_t)^{-k_1}$ with $k_0 > 0$ and $k_1 > 0$. We calibrate so that costs for renewable energy drop by 20% for every doubling of cumulative installed volume in accordance with Swanson's law.⁴¹ This gives $k_0 = 0.5107$ and $k_1 = 0.3219$.

The green sector only uses renewable energy, so $\kappa_{1,1} = 1$, $\kappa_{2,1} = 0$, and ρ_1 can be chosen arbitrarily. The brown sector can be fueled by both energy sources. To calibrate the energy composite of the brown sector and the CES weights, we set the elasticity of intratemporal substitution to $\zeta_2 = 2$ corresponding to $\rho_2 = 0.5$ and the CES weights to $\kappa_{1,2} = 0.356$, $\kappa_{2,2} = 0.644$ (Goloso et al., 2014). With this calibration it is possible to fully replace fossil fuel by green energy within this sector even though moving capital

⁴⁰This assumption is in line with Goloso et al. (2014) who use an energy share of 4%.

⁴¹Swanson's law is the solar industry specific application of Wright's Law which states there will be a fixed cost reduction for each doubling of manufacturing volume. More specifically, Swanson's law states that the price of solar panels drops by 20 percent every time the volume of panels shipped doubles, see <https://www.economist.com/news/2012/11/21/sunny-uplands>.

to the green sector may be more efficient.⁴² Given those parameter choices, we determine the share of brown capital such that the model generates 19.77% of renewable energy in total energy demand in the BAU-scenario in 2020.⁴³ This gives an initial share of brown capital of $S_0 = 0.876$. We can thus back out the initial green and brown capital stocks (74.3 and 1353.9 trillion US \$, respectively).

Emission Intensity Since the emission intensity v follows equation (2.8), industrial emissions are given by $E_t^{ind} = (f_{1t}(1 - S_t) + f_{2t}S_t)K_0e^{\int_0^t g_v(s)ds}$. In the BAU state, the social planner does not take account of the negative externalities caused by emissions but reallocates capital from the brown to the green sector for other reasons such as diversification purposes (e.g. Hambel et al. (2024) and the references therein). We now solve and simulate the pure BAU scenario over the next 100 years assuming a reallocation cost parameter of $\kappa = 2$. This parameter choice yields a BAU simulation of temperature, emissions, and energy that is well in line with the adjusted RCP8.5 scenario. Given the adjusted RCP8.5 emission data E_t and the simulated share of brown capital S_t , we approximate $p(t) = \frac{E_t}{\mathbb{E}[f_{1t}(1 - S_t) + f_{2t}S_t]}$ by a cubic polynomial function of time, $p(t) = p_0 + p_1t + p_2t^2 + p_3t^3$, with $p_0 = 2.08 \cdot 10^{15}$, $p_1 = 4.22 \cdot 10^{13}$, $p_2 = 1.01 \cdot 10^{12}$, $p_3 = -9.76 \cdot 10^9$, and $R^2 > 99\%$. The corresponding growth rate g_v is then given by $g_v(t) = \frac{d}{dt} \ln p(t)$. Figure C.1 depicts the adjusted RCP8.5 emission data and the model fit. Panel (a) shows the simulated data $p(t)$ (o) determining the emission intensity and its cubic fit. Panel (b) depicts the median evolution of the BAU emissions (—) and compares it to the RCP8.5 emission predictions (o). It also shows the corresponding 5% and 95% quantile of BAU emissions (- - -). This calibration implies that the emission intensity v_t tends to decline over time although it is exposed to stochastic shocks.

We thus calibrate the emission intensity such that the pure BAU simulation mimics the modified RCP8.5 scenario of IPCC (2014). RCP8.5 is characterized by high emissions leading to a temperature increase of about 4.3°C relative to the pre-industrial level by the end of this century.⁴⁴ We slightly modify the emission data to take account of the lower emissions in reality compared to the RCP8.5 scenario. While the scenario predicts emissions of 12.44 GtC in 2020, emissions were only 10 GtC. Thus, we calibrate the emission intensity (2.8) to adjusted RCP8.5 emission data that is 20% lower than the original data.

⁴²Alternative calibrations for when the two energy forms are complements within the brown sector (e.g. the benchmark calibration of Golosov et al. 2014 with $\zeta_2 = 0.95$ and $\rho_2 = -0.058$) or when the brown sector only takes fossil fuel as input (e.g., Hambel et al. 2024 with $\kappa_{1,2} = 0$ and $\kappa_{2,2} = 1$) are discussed in Appendix C.3. With those calibrations, it is not possible to completely replace fossil fuels with renewable energies within the brown sector. This may cause stranded assets if the carbon budget is exceeded and the CAP scenario enforced.

⁴³We use world bank data on the share of renewable energy of total final energy consumption, see <https://data.worldbank.org/indicator/EG.FEC.RNEW.ZS>.

⁴⁴The data is available from the RCP database, see <http://tntcat.iiasa.ac.at/RcpDb>.

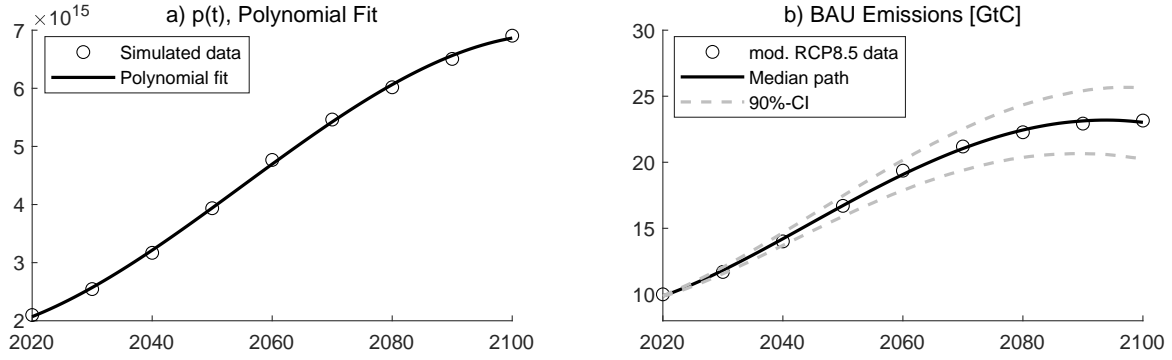


Figure C.1: Calibration of Emission Intensity. Panel (a) shows the simulated data $p(t)$ (o) determining the emission intensity and its cubic fit. Panel (b) depicts the median evolution of the BAU emissions (—) and compares it to the adjusted RCP8.5 emission data (o). It also shows the 5% and 95% quantiles of BAU emissions (---).

Temperature Dynamics Estimates of the transient climate response to cumulative emissions range from 0.8 to 2.4°C/TtC (e.g. Allen et al., 2009; Matthews et al., 2009, 2018). We take an initial value of the TCRE of $\vartheta(\mathbf{X}_0) = 1.8^\circ\text{C}/\text{TtC}$, which is in line with the temperature evolution in DICE-2016R and other climate-economic models such as Dietz and Venmans (2019) or the econometric approach in Miftakhova et al. (2020). Moreover, we choose a constant temperature volatility of $\sigma_T = 0.033$ to match the temperature range of global mean temperature increase in the RCP scenarios.⁴⁵ The effect of climate tipping risk on the transient climate response to cumulative emissions is shown in Panel (a) of Figure 1.

Climate Tipping Risks Given the initial value of the TCRE in the pre-tip state, $\vartheta(X_0^c = 1) = 1.8^\circ\text{C}/\text{TtC}$, and the range of estimates up to 2.4°C/TtC for the TRCE, we choose a TCRE of $\vartheta(X^c = 2) = 2.1^\circ\text{C}/\text{TtC}$ for the intermediate state and $\vartheta(X^c = 3) = 2.4^\circ\text{C}/\text{TtC}$ for the post-tip state (see Figure 1). From the pre-tip state, the transition intensity to the intermediate and post-tip state is $\lambda_c(\mathbf{S}, 1, j) = \hat{\lambda}_c^{1,j}(T - 1)$ with $\hat{\lambda}_c^{1,j} = 0.012$ (cf. Cai and Lontzek, 2019).⁴⁶ This implies an annual initial tipping intensity of 0.324% at $T_0 = 1.27^\circ\text{C}$ corresponding to an expected duration of 309 years and a tipping intensity of 1.2% at $T = 2^\circ\text{C}$ corresponding to an expected duration of 83 years. The transition intensity for the post-tip state conditional on being in the intermediate state is $\lambda_c(\mathbf{S}, 2, 3) = \hat{\lambda}_c^{2,3} = 0.02$ corresponding to an average duration of 50 years between the intermediate and the final climate tipping state. The climate can also jump directly from state 1 to state 3, so the total tipping intensity at the initial temperature

⁴⁵The temperature range in the year 2100 of the various RCP scenarios varies between 0.8°C around its mean in RCP2.6 to 1.1°C in RCP8.5.

⁴⁶Climate tipping is only possible if temperature exceeds 1°C, which given our initial temperature is the case.

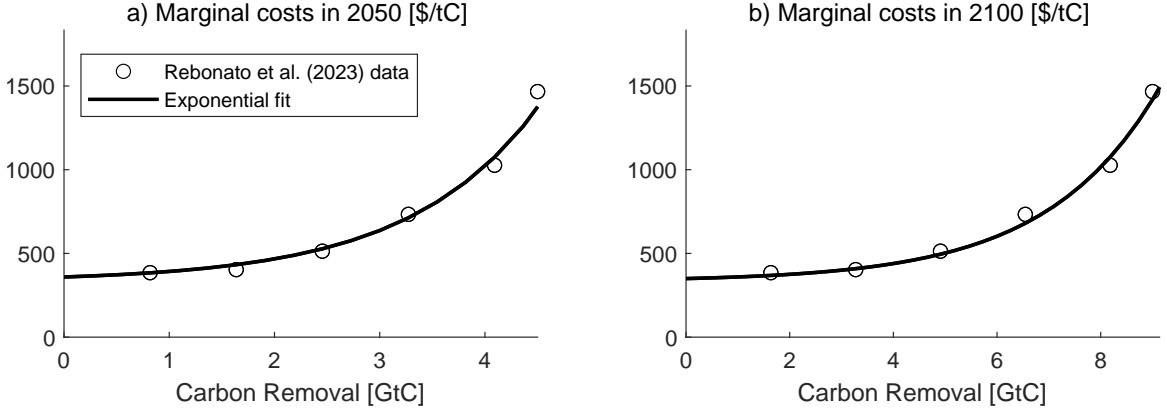


Figure C.2: Calibration of the Marginal Cost Function for NET. The figure shows the averaged data from the two scenarios in Rebonato et al. (2023) (o). Panel (a) shows the resulting marginal costs function for the year 2050 and Panel (b) for the year 2100, respectively. We fit an exponential function of the form $\frac{\partial b_d(S, X^t=2, D, K)}{\partial D} = K[a_1(S) + a_2(S)a_3(S)\exp(a_3(S)D)]$ to this data as shown by the black line (—), where $a_j(S) = b_j \max(\zeta, S)^{c_j}$ are truncated power functions of the share of brown capital.

$T_0 = 1.27^\circ\text{C}$ is 0.648% (cf. van den Bremer et al., 2023). Finally, we have irreversible climate tipping, so $\lambda_c(\mathbf{S}, i, j) = 0$ for $j < i$.

C.2 Negative Emission Technology

For the calibration of the parameters of the marginal cost function for the negative emission technology $\frac{\partial b_d(S, X^t=2, D, K)}{\partial D} = K[a_1(S) + a_2(S)a_3(S)\exp(a_3(S)D)]$, we first average the data from the two scenarios described in Rebonato et al. (2023) and shown in their Figure 5. We neglect the very small share with low but steep marginal costs for removal that is close to zero. The averaged data—expressed in GtC—is depicted in Figure C.2 for the year 2050 (Panel a) and 2100 (Panel b). Then, we calibrate the truncated power functions of the form $a_j(S) = b_j \max(\zeta, S)^{c_j}$, $j \in \{1, 2, 3\}$ jointly to both curves by assuming that the time dependencies are only driven by variations in S . In this sense, S models technological progress towards a low-carbon economy. We simulate S and K for the optimal scenario (PIGOU) and calibrate the power functions a_1, a_2, a_3 such that the expected marginal costs at $\tau \in \{31, 81\}$, i.e., in the years 2050 and 2100, respectively, match the marginal cost curves as closely as possible in a least-squares sense. The parameters obtained are all strictly positive so that in particular $\frac{\partial^2 b_d(S, X^t=2, D, K)}{\partial D \partial S} > 0$, i.e., the greater the proportion of brown capital, the greater the marginal removal costs. The fit is visualized by the black line (—). The exponential marginal cost function performs very well with an R^2 exceeding 99%.

Benchmark: Substitutes within the brown sector			
S_0	initial share of brown capital	from World Bank data (Footnote 43)	0.876
k_0	cost function parameter	calibrated in accordance with Swanson's law	0.5107
κ	capital reallocation cost parameter	calibrated to modified RCP8.5, see Section 4	2
ζ_n	elasticity of energy substitution	Golosov et al. (2014)	2
$\kappa_{2,2}$	fossil fuel weight in brown sector	Golosov et al. (2014)	0.644
$\kappa_{1,1}$	renewable energy weight in green sector	assumption	1
p_0	emission intensity parameter	calibrated to modified RCP8.5, see Section 4	$2.08 \cdot 10^{15}$
p_1	emission intensity parameter	calibrated to modified RCP8.5, see Section 4	$4.22 \cdot 10^{13}$
p_2	emission intensity parameter	calibrated to modified RCP8.5, see Section 4	$1.01 \cdot 10^{12}$
p_3	emission intensity parameter	calibrated to modified RCP8.5, see Section 4	$-9.76 \cdot 10^9$
Alternative I: Brown sector takes fossil fuel only; green sector takes both energy forms			
S_0	initial share of brown capital	from World Bank data (Footnote 43)	0.712
k_0	cost function parameter	from Swanson's law (Footnote 41)	0.6586
κ	capital reallocation cost parameter	from benchmark	2
ζ_n	elasticity of energy substitution	from benchmark	2
$\kappa_{1,1}$	renewable energy weight in green sector	assumption	0.9
$\kappa_{2,2}$	fossil fuel weight in brown sector	Hambel et al. (2024)	1
p_0	emission intensity parameter	calibrated to modified RCP8.5, see Section 4	$2.10 \cdot 10^{15}$
p_1	emission intensity parameter	calibrated to modified RCP8.5, see Section 4	$4.18 \cdot 10^{13}$
p_2	emission intensity parameter	calibrated to modified RCP8.5, see Section 4	$1.15 \cdot 10^{12}$
p_3	emission intensity parameter	calibrated to modified RCP8.5, see Section 4	$-9.34 \cdot 10^9$
Alternative II: Both sectors take only one energy type			
S_0	initial share of brown capital	from World Bank data (Footnote 43)	0.726
k_0	cost function parameter	from Swanson's law (Footnote 41)	0.6592
κ	capital reallocation cost parameter	from benchmark	2
ζ_n	elasticity of energy substitution	from benchmark / has no influence	2
$\kappa_{2,2}$	fossil fuel weight in brown sector	Hambel et al. (2024)	1
$\kappa_{1,1}$	renewable energy weight in green sector	Hambel et al. (2024)	1
p_0	emission intensity parameter	calibrated to modified RCP8.5, see Section 4	$2.09 \cdot 10^{15}$
p_1	emission intensity parameter	calibrated to modified RCP8.5, see Section 4	$4.08 \cdot 10^{13}$
p_2	emission intensity parameter	calibrated to modified RCP8.5, see Section 4	$8.26 \cdot 10^{11}$
p_3	emission intensity parameter	calibrated to modified RCP8.5, see Section 4	$-9.08 \cdot 10^9$
Alternative III: Complements within the brown sector			
S_0	initial share of brown capital	from benchmark	0.876
k_0	cost function parameter	from benchmark	0.5107
κ	capital reallocation cost parameter	calibrated to modified RCP8.5, see Section 4	10
ζ_n	elasticity of energy substitution	Golosov et al. (2014)	0.95
$\kappa_{2,2}$	fossil fuel weight in brown sector	calibrated to World Bank data (Footnote 43)	0.862
$\kappa_{1,1}$	renewable energy weight in green sector	assumption	1
p_0	emission intensity parameter	calibrated to modified RCP8.5, see Section 4	$2.69 \cdot 10^{15}$
p_1	emission intensity parameter	calibrated to modified RCP8.5, see Section 4	$5.18 \cdot 10^{13}$
p_2	emission intensity parameter	calibrated to modified RCP8.5, see Section 4	$1.17 \cdot 10^{12}$
p_3	emission intensity parameter	calibrated to modified RCP8.5, see Section 4	$-9.97 \cdot 10^9$

Table C.1: Alternative Calibrations. This table summarizes the three alternative calibrations for stranded assets.

C.3 Alternative Calibrations for Energy Substitutability

In the benchmark calibration, fossil fuel and renewable energy within the brown sector are substitutes with a substitution elasticity of $\zeta_2 = 2$ (i.e., $\rho_2 = 0.5$). This means in particular that the brown sector

can always operate because it is able to shift its energy demand away from fossil fuel and to renewable energies. Therefore, this calibration cannot generate stranded assets. We thus offer three alternative calibrations that address this issue.

First, we consider a calibration, where the brown sector takes only fossil fuel as an input factor, but the green sector can take both energy forms but with limited substitutability and high weight on renewable energy (Alternative I). In addition, we consider a variant in which both sectors take only one energy sources as an input factor as in Hambel et al. (2024) (Alternative II). In these cases, the elasticity of substitution within the brown sector becomes irrelevant. Finally, we offer a calibration in which the brown sector takes both energy forms complementarily (Alternative III). For this we follow Golosov et al. (2014) and choose a elasticity of substitution of $\zeta_2 = 0.95$ (i.e., $\rho_2 = -0.058$) within this sector.

Notice that with these alternative calibrations, it is not possible to (fully) replace fossil fuels with renewables within the brown sector, which is why the transition to a green economy must necessarily take place through the development of the green sector. If this does not happen quickly enough and the CO₂ budget is exceeded when society jumps to CAP, the brown asset may be stranded. This hazard is priced in by financial markets through higher risk premiums, especially for the brown asset, and by the social planner, who may implement higher carbon taxes. We discuss the results for Alternative I in detail in Section 6. Simulations for Alternatives II and III confirm those findings and are available upon request.

The calibration strategy follows the same steps as for the benchmark calibration. However, a number of parameters have to be recalibrated in order to match the calibration targets outlined in the main text, i.e. the 19.77% share of green energy in the energy mix in 2020, the initial energy price ratio of 1.5, and the emissions in the adjusted RCP8.5 scenario. As we sometimes have more degrees of freedom in the calibration than calibration targets, we choose the parameters so that we have to recalibrate as few parameters as possible. Table C.1 summarizes the changed parameters. All other parameters are as in the benchmark calibration shown in Table 1. Variants of Figures C.1 and C.2 for these alternative calibrations are available upon request.

D Additional Simulation Results

D.1 Additional Material for the Benchmark Simulation

This section provides additional material for the benchmark simulation such as additional tables and figures.

Optimal Carbon Taxes Table D.2 reports the unconditional moments of the implemented carbon tax for the years 2025, 2050, 2075, and 2100. Since the carbon tax is implemented in only about 25% of the

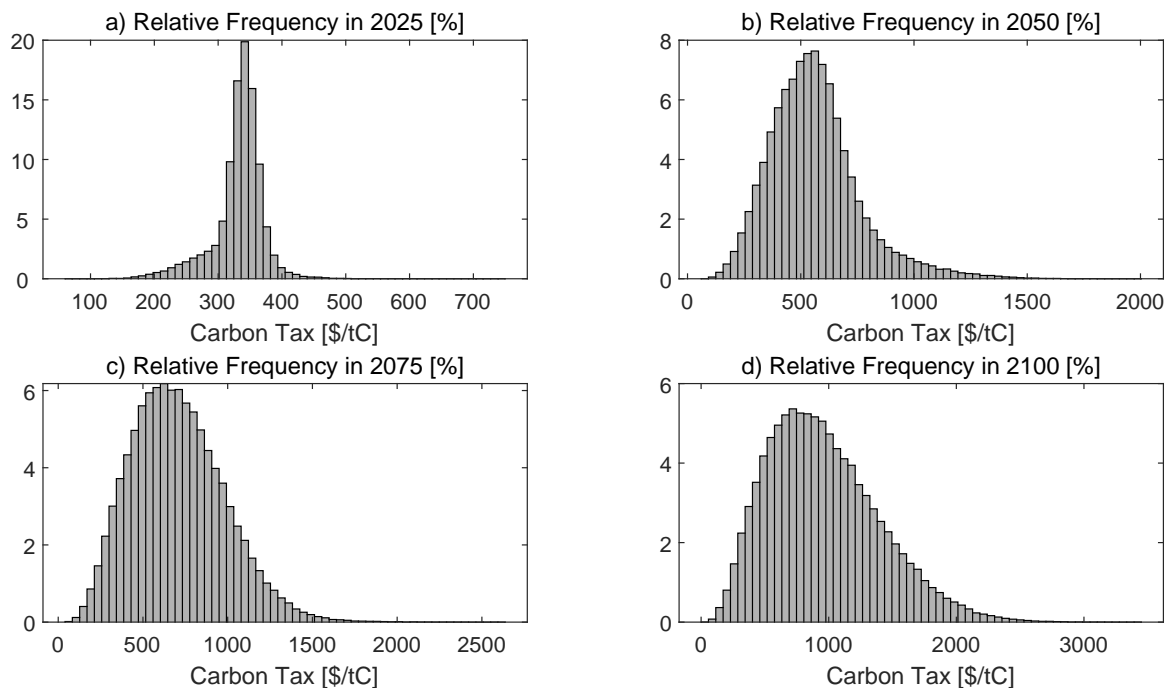


Figure D.3: Carbon Taxes. The figure shows histograms for the implemented carbon tax, i.e., conditional on being in the PIGOU or CAP state, in the years a) 2025, b) 2050, b) 2075, and d) 2100.

Unconditional moments						
	$E[\tau]$	$\text{Med}(\tau)$	$\sigma(\tau)$	$q_{5\%}(\tau)$	$q_{95\%}(\tau)$	$\text{Skew}(\tau)$
2025	85	0	146	0	358	1.19
2050	260	0	311	0	789	0.79
2075	485	521	398	0	1124	0.22
2100	755	756	551	0	1692	0.30

Table D.2: Unconditional Optimal Carbon Tax. The table reports summary statistics of the unconditional optimal carbon tax for the years 2025, 2050, 2075, and 2100.

paths in 2025, its unconditional distribution is obviously right-skewed. Its skewness tends to decline over time as carbon taxes are implemented in more and more paths. Figure D.3 shows histograms for implemented carbon taxes for the years 2025, 2050, 2075, and 2100, respectively, conditional on being in the TAX or LIM state. Those histograms are generated with 200,000 paths, of which around 25% have a tax implemented in 2025, 46% in 2050, 69% in 2075, and 79% in 2100. Panel a) illustrates the negative skewness of the implemented carbon tax, as reported in Table D.3, in the year 2025. This negative skewness of the conditional distribution can be explained by a negatively skewed distribution of global output, which is largely generated by the economic disasters. Since the optimal carbon tax is proportional to the capital stock, see (3.1), this left-skewed distribution carries over to the carbon tax.

As time progresses and climate risks such as tipping points or climate disasters, as well as political shocks, increase in intensity, the SCC will be skewed to the right by these risks, gradually transforming the left-skewed distribution into a right-skewed distribution. This can be seen from Panels b) to d).

Driver of the Carbon and Transition Risk Premiums We now present simulation results conditional on an annual carbon premium of at least 1%. These results are reported in Figure D.4. It is evident that the model generates a high carbon premium if climate transition risk is most pronounced, that is if temperatures are close to but slightly below two degrees and society is already in the CAP state. Under those circumstances, a small temperature shock could make policy makers phase out fossil fuel use, which has potentially devastating consequences if the stock of brown capital is still relatively large. The high carbon premium is accompanied by a large demand for precautionary savings leading to negative interest rates. Besides, both risky assets have significantly higher risk premiums than they would have in the absence of transition risk (cf., Figure D.5 below). These results confirm the earlier findings on the emergence of transition risk and carbon premiums from Section 5.3. We also find a sizable carbon premium in some paths where society is still in the PIGOU state, temperatures are close to two degrees, and the share of brown capital is still sizable. Then, a transition to the CAP state could lead to the same effect as outlined above explaining the sizable carbon premium and the large demand for precautionary savings.

D.2 PIGOU Scenario without Policy Transition Risks

Figure D.5 provides the results for the first-best optimal outcomes (the pure PIGOU scenario), which excludes policy transition to the BAU or CAP state (with the political Markov chain switched off). Compared to the benchmark simulation, the carbon premium is initially small and negative (-0.08%) due to the absence of political transition risk, and turns positive when physical risks become sizable. Still the magnitude of the carbon premium is small. Moreover, the carbon taxes are on average slightly higher in this scenario than in the benchmark scenario with political transition risk. In 2021, the average carbon tax is 326 $\$/tC$, which is about 6% higher than the average carbon tax in paths of the benchmark scenario where carbon taxes are implemented or the temperature cap is enforced (308 $\$/tC$). Since there are many paths where policy makers have not tipped into climate action yet in the benchmark scenario, the transition towards a low-carbon economy takes place much faster than in the benchmark.

D.3 BAU Scenario with no Negative Emission Technology

Figure D.6 provides the results for a scenario which excludes negative emission technologies (with the technological Markov chain switched off). Compared to the benchmark scenario, temperatures are a

Moments conditional on carbon tax being implemented ($X^P \neq 1$)						
(a)	$\mathbb{E}[\tau X^P \neq 1]$	$\text{Med}(\tau X^P \neq 1)$	$\sigma(\tau X^P \neq 1)$	$q_{5\%}(\tau X^P \neq 1)$	$q_{95\%}(\tau X^P \neq 1)$	$\text{Skew}(\tau X^P \neq 1)$
2025	332	338	39	250	380	-1.01
2050	561	542	199	280	933	1.02
2075	705	683	275	298	1187	0.54
2100	959	905	436	346	1757	0.66
Moments conditional on the political state						
(b)	$\mathbb{E}[\tau X^P = 2]$	$\text{Med}(\tau X^P = 2)$	$\sigma(\tau X^P = 2)$	$q_{5\%}(\tau X^P = 2)$	$q_{95\%}(\tau X^P = 2)$	$\text{Skew}(\tau X^P = 2)$
2025	331	338	38	249	376	-1.29
2050	511	513	146	272	750	0.07
2075	689	671	259	295	1141	0.37
2100	957	901	438	344	1764	0.67
(c)	$\mathbb{E}[\tau X^P = 3]$	$\text{Med}(\tau X^P = 3)$	$\sigma(\tau X^P = 3)$	$q_{5\%}(\tau X^P = 3)$	$q_{95\%}(\tau X^P = 3)$	$\text{Skew}(\tau X^P = 3)$
2025	336	341	41	254	391	-0.51
2050	667	630	251	312	1138	0.68
2075	726	698	292	302	1244	0.65
2100	961	908	434	347	1751	0.65
Moments conditional on the climate tipping state and on $X^P \neq 1$						
(d)	$\mathbb{E}[\tau X^c = 1]$	$\text{Med}(\tau X^c = 1)$	$\sigma(\tau X^c = 1)$	$q_{5\%}(\tau X^c = 1)$	$q_{95\%}(\tau X^c = 1)$	$\text{Skew}(\tau X^c = 1)$
2025	331	338	38	250	375	-1.33
2050	531	518	181	272	864	0.98
2075	660	641	254	280	1100	0.51
2100	899	849	402	328	1634	0.61
(e)	$\mathbb{E}[\tau X^c = 2]$	$\text{Med}(\tau X^c = 2)$	$\sigma(\tau X^c = 2)$	$q_{5\%}(\tau X^c = 2)$	$q_{95\%}(\tau X^c = 2)$	$\text{Skew}(\tau X^c = 2)$
2025	343	349	40	260	398	-1.13
2050	566	552	196	284	937	0.95
2075	664	644	254	289	1098	0.53
2100	882	833	397	320	1609	0.62
(f)	$\mathbb{E}[\tau X^c = 3]$	$\text{Med}(\tau X^c = 3)$	$\sigma(\tau X^c = 3)$	$q_{5\%}(\tau X^c = 3)$	$q_{95\%}(\tau X^c = 3)$	$\text{Skew}(\tau X^c = 3)$
2025	403	406	50	304	475	-0.63
2050	659	643	227	331	1080	0.85
2075	763	741	290	326	1266	0.46
2100	1003	947	453	364	1834	0.64
Moments conditional on the technological state and on $X^P \neq 1$						
(g)	$\mathbb{E}[\tau X^t = 1]$	$\text{Med}(\tau X^t = 1)$	$\sigma(\tau X^t = 1)$	$q_{5\%}(\tau X^t = 1)$	$q_{95\%}(\tau X^t = 1)$	$\text{Skew}(\tau X^t = 1)$
2025	333	339	39	251	380	-1.00
2050	564	544	201	281	941	1.01
2075	706	684	275	298	1189	0.53
2100	978	923	442	356	1784	0.66
(h)	$\mathbb{E}[\tau X^t = 1]$	$\text{Med}(\tau X^t = 1)$	$\sigma(\tau X^t = 1)$	$q_{5\%}(\tau X^t = 1)$	$q_{95\%}(\tau X^t = 1)$	$\text{Skew}(\tau X^t = 1)$
2025	331	337	39	249	379	-1.12
2050	557	539	198	280	923	1.02
2075	705	683	275	298	1186	0.54
2100	955	901	435	344	1752	0.66

Table D.3: Carbon Taxes, U.S. \$/tC (starting from BAU with Transition Risks). Summary statistics of the carbon taxes for the years 2025, 2050, 2075, and 2100 are reported. All reported moments are at least conditional on being in the PIGOU or CAP state, i.e., on $X^P \neq 1$. These summary statistics are generated with 200,000 sample paths, of which around 25% have a carbon tax implemented in 2025, 46% in 2050, 69% in 2075, and 79% in 2100. Unconditional moments are reported in Table D.2.

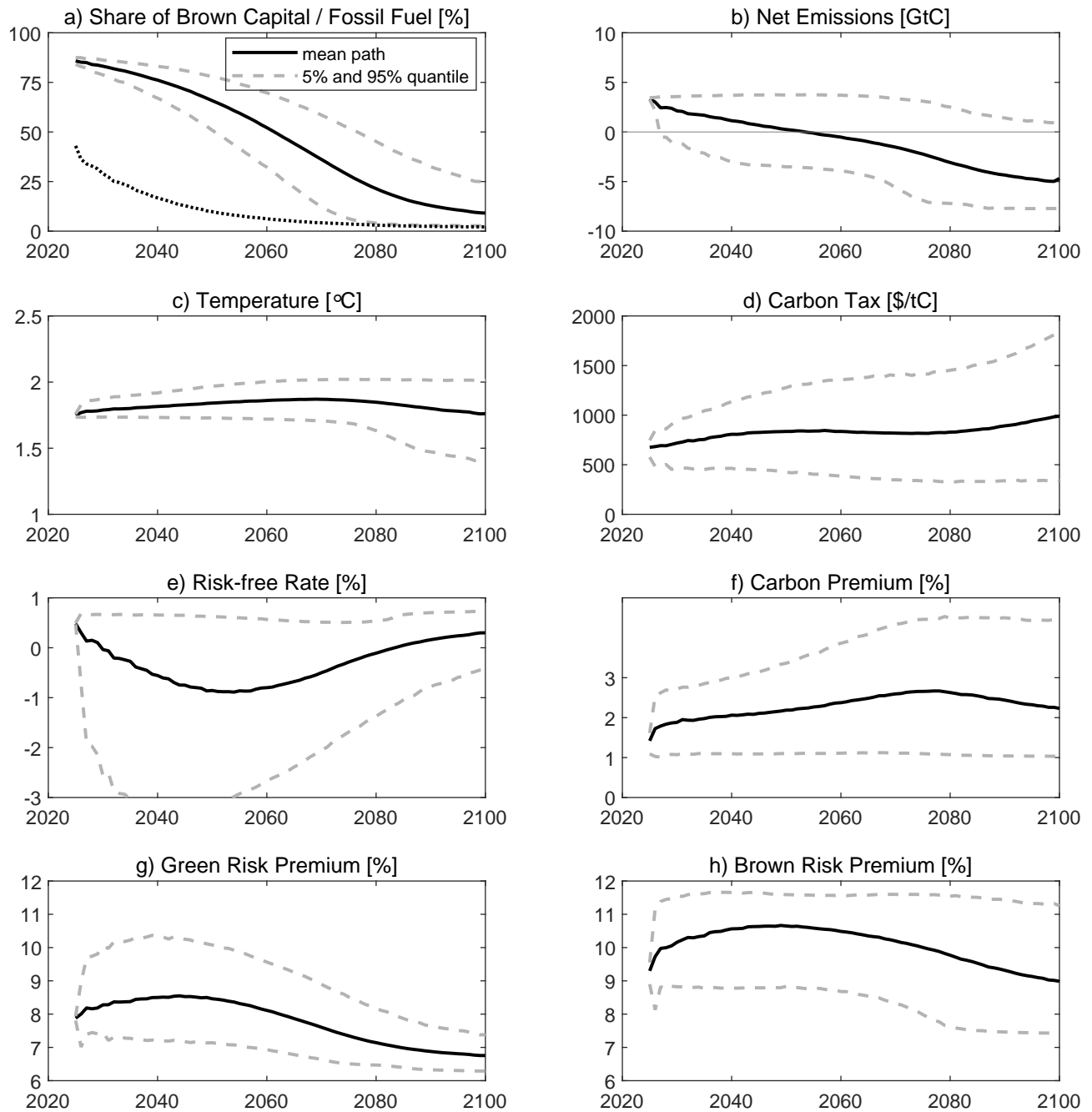


Figure D.4: BAU Scenario with Transition Risks Conditional on a High Carbon Premium. The figure shows the simulation results conditional on the carbon premium exceeding 1% annually. Average values are depicted by solid lines (—) and 5% and 95% quantiles by dashed lines (---). The dotted line (····) in Panel a) depicts the mean path of the share of fossil fuel in the global energy mix.

bit higher as society cannot curb them with a negative emission technology. The results for the risk-free rate and the risk premiums are virtually unchanged compared to the benchmark scenario. This

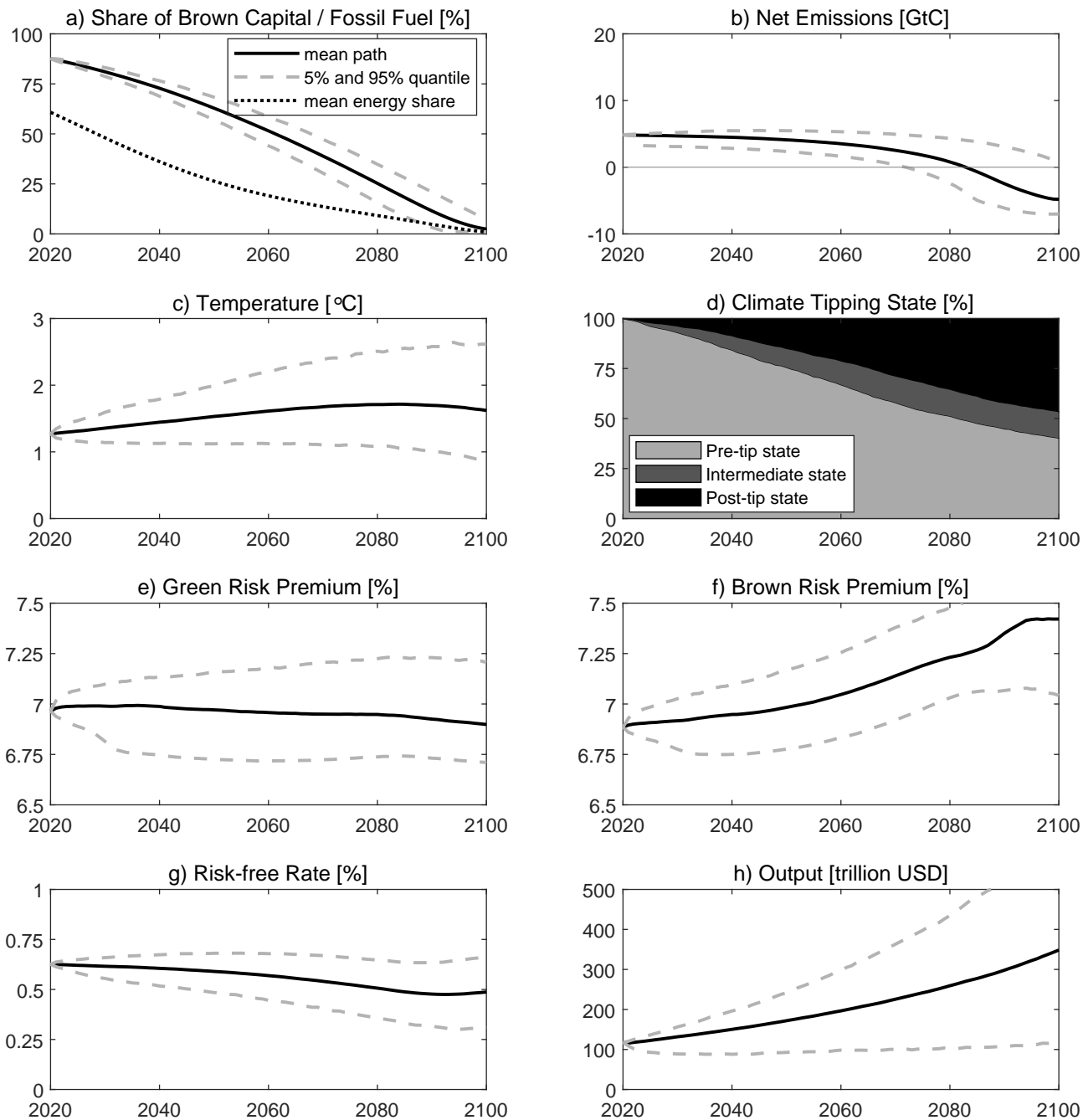


Figure D.5: PIGOU Scenario with no Transition Risks (Optimal Carbon Taxes). Average values are depicted by solid lines (—) and 5% and 95% quantiles by dashed lines (---). The dotted line (·····) in Panel a) depicts the mean path of the share of fossil fuel in the global energy mix. The light (■), dark gray (■), and black (■) areas in Panel d) depict the proportion of simulations in the pre-tip ($X^c = 1$), intermediate ($X^c = 2$), and post-tip ($X^c = 3$) climate state, respectively.

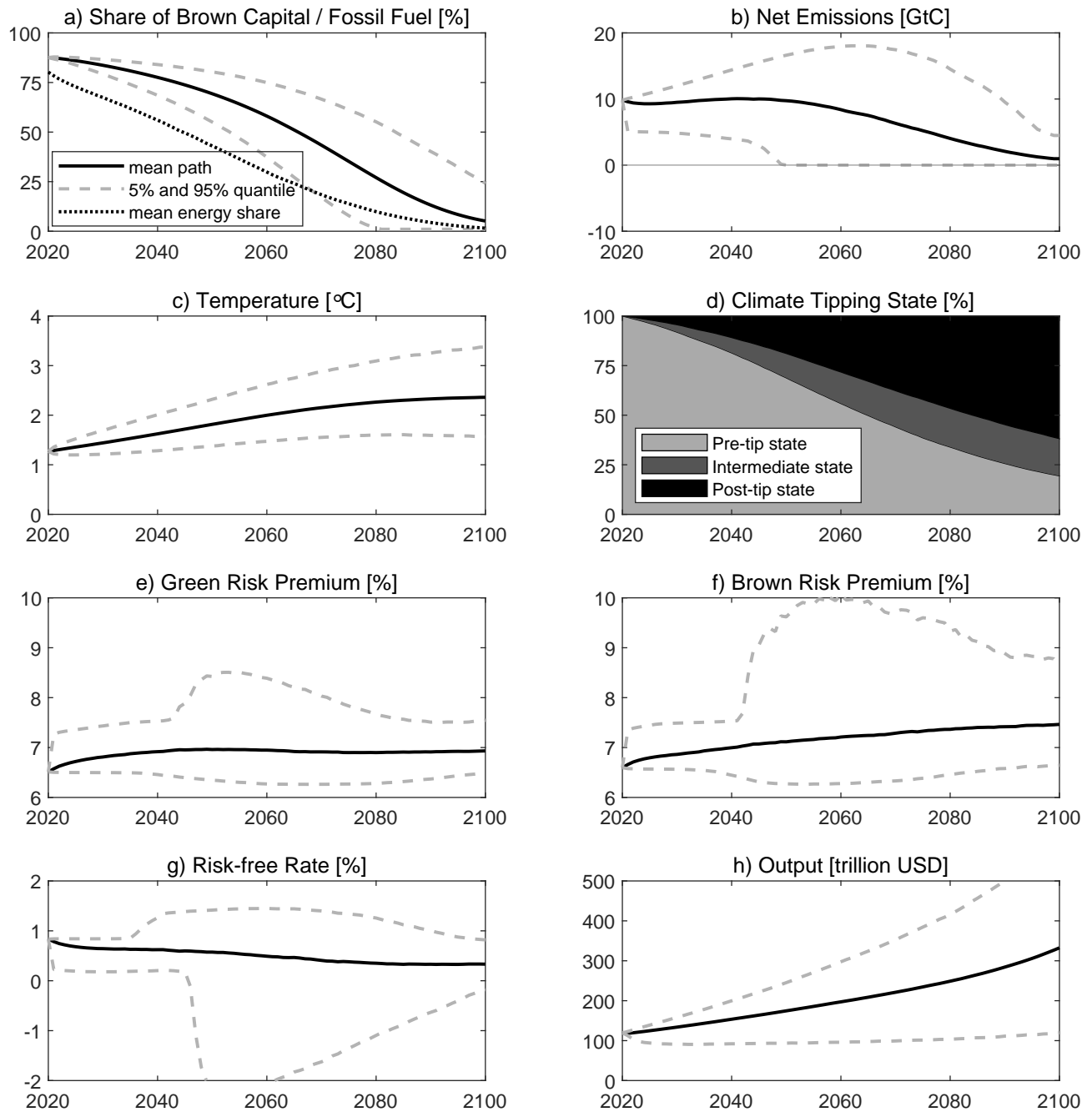


Figure D.6: BAU Scenario with no Negative Emission Technology. Average values are depicted by solid lines (—) and 5% and 95% quantiles by dashed lines (---). The dotted line (····) in Panel a) depicts the mean path of the share of fossil fuel in the global energy mix. The light (■), dark gray (■), and black (■) areas in Panel d) depict the proportion of simulations in the pre-tip ($X^c = 1$), intermediate ($X^c = 2$), and post-tip ($X^c = 3$) climate state, respectively.

indicates that the transition risk premium and the carbon premium are mainly driven by political

transition risk rather than technological transition risk. This confirms that our results are robust to different assumptions about the existence and likelihood of competitive NET technologies. Moreover, those results support the empirical findings of Engle et al. (2020), whose WSJ Climate Change index primarily reacts to climate-related political shocks and climate summits.

D.4 BAU Scenario with a Tighter Carbon Budget

Figure D.7 provides the results for a scenario with a significantly tighter carbon budget. For this purpose, we assume that in the CAP state the social planner abolishes fossil fuels if temperature exceeds $T_{cap} = 1.5^\circ\text{C}$ instead of $T_{cap} = 2^\circ\text{C}$. This leads to more ambitious climate policy in the CAP state because the potentially devastating consequences of exceeding the budget and abolishing fossil fuels are now more likely to occur. Consequently, the transition risk is more pronounced in this scenario.

D.5 Additional Material for the Risk of Stranded Assets

This section provides additional simulation results for the interplay between climate transition risk and stranded assets. Figure D.8 is the counterpart to Figure 5 and shows the evolution of the optimal carbon taxes both unconditional and conditional on being implemented. Figure D.9 is the counterpart to Figure 3 and depicts the evolution of the three-dimensional Markov chain \mathbf{X} .

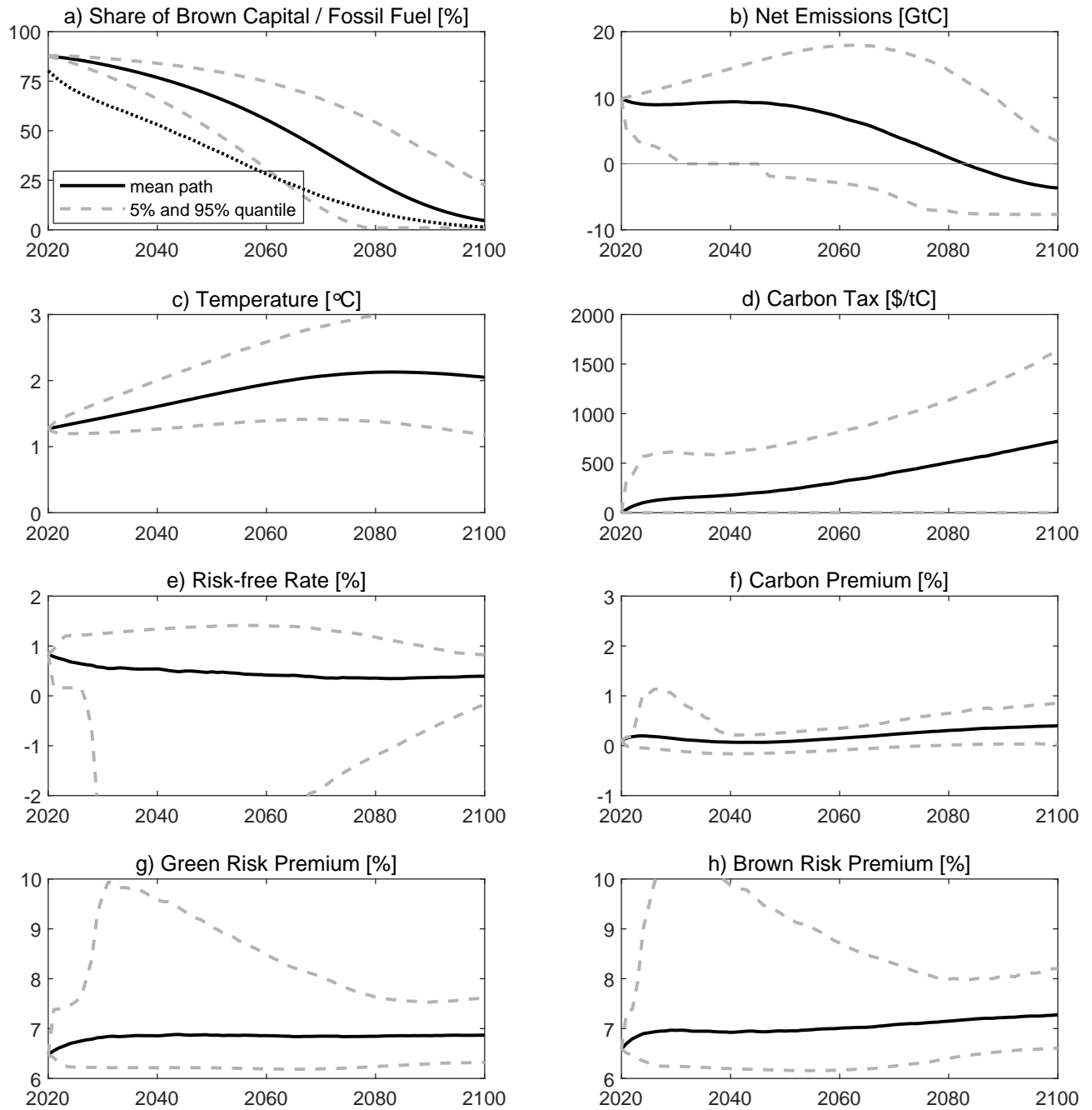


Figure D.7: BAU Scenario with a Tighter Carbon Budget. Average values are depicted by solid lines (—) and 5% and 95% quantiles by dashed lines (- - -). The dotted line (·····) in Panel a) depicts the mean path of the share of fossil fuel in the global energy mix.

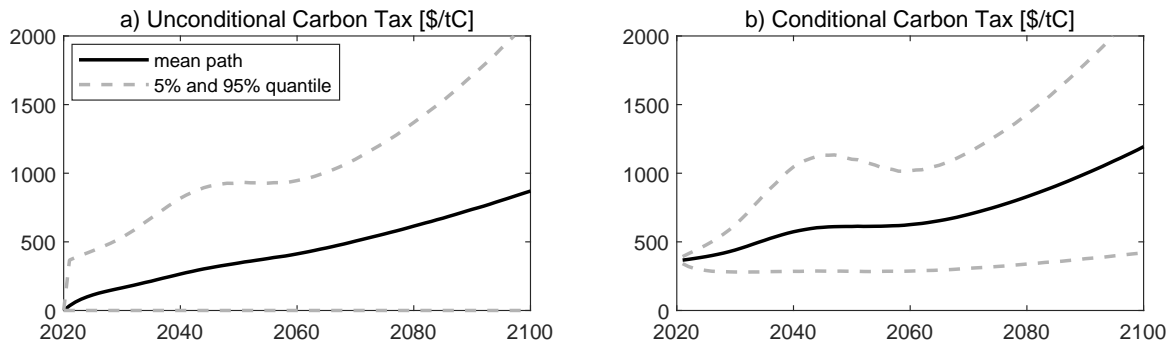


Figure D.8: Carbon Tax Simulation (Stranded Assets). The figure depicts the carbon tax for the benchmark simulation until the year 2100. Mean paths are depicted by solid lines (—) and dashed lines (---) show 5% and 95% quantiles. Panel a) shows unconditional means and quantiles, and Panel b) shows means and quantiles conditional on being in the PIGOU or CAP state.

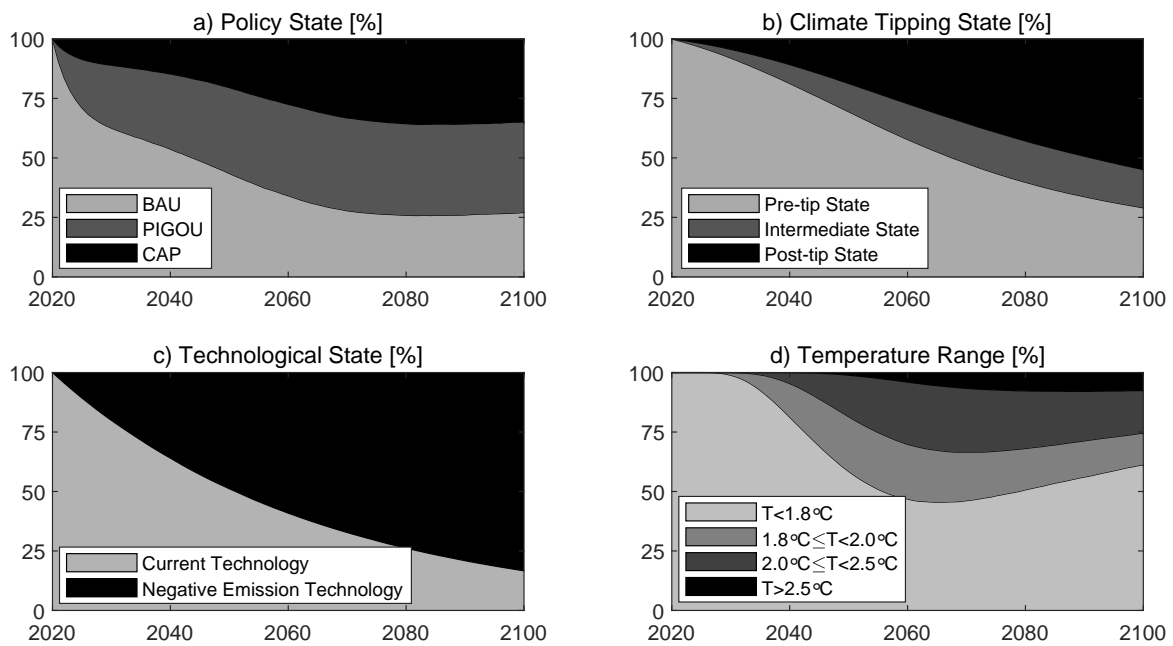


Figure D.9: Markov Chains and Temperature Scenarios (Stranded Assets). In Panel a) the light area (■) is the proportion of simulations in the BAU state, the dark gray area (■) the proportion in the PIGOU state, and the black area (■) the proportion in the CAP state. In Panel b) the light area (■) is the proportion of simulations in the pre-tip state, the dark gray area (■) the proportion in the intermediate state, and the black area (■) the proportion in the post-tip state. In Panel c) the light area (■) is the proportion of simulations in the pre-breakthrough state and the black area (■) the proportion where the negative emission technology has come into force. In Panel d) the light area (■) is the proportion of simulations with temperature less than 1.8°C, the gray area (■) the proportion with temperature between 1.8°C and 2.0°C, the dark gray area (■) the proportion with temperature between 2.0°C and 2.5°C, and the black area (■) the proportion with temperature above 2.5°C.